HIGH-RESOLUTION CONTACTLESS SURFACE ACOUSTIC WAVE CELL PATTERNING FOR TISSUE ENGINEERING

Karina Martinez Villegas

Biomat'X Laboratories

Department of Biomedical Engineering

Biological and Biomedical Engineering

McGill University, Montreal, Canada

A Thesis Submitted to McGill University in Partial Fulfillment of the Requirements of the Degree of Master of Engineering

Abstract

The design and fabrication of functional tissues are critical in clinical applications such as regenerative medicine. Cell patterns induced by native tissue architectures coupled with mechanical and environmental cues play fundamental roles in regulating cellular functions. Despite the interest in inducing cell spatial patterns for building tissue-relevant cell architectures, conventional patterning methods suffer from numerous drawbacks. Heterogeneous constructs, lack of dynamic geometric arrangements, long fabrication times, and reliance on high-energy or contact-based mechanisms which hinder cell viability remain to be addressed. Acoustofluidics, the combination of acoustics and microfluidics, has shown a great potential for patterning single and multiple cells in a label-free and contactless nature within seconds with high biocompatibility. This study first presents an overview of acoustofluidics, with an emphasis on surface acoustic waves, for cell patterning and cell functionality modulation. We then present preliminary work using standing surface acoustic waves (SSAWs) for rapid and reproducible cell patterning of different cell lines. SSAWs guided cells towards pressure nodal lines via acoustic radiation forces, with a reproducible spacing of ~150μm, creating contactless linear cell patterns in < 5s in culture media. The acoustic platform was validated using adipose-derived mesenchymal stem cells in a methacrylated collagen type I hydrogel, with consistent patterning in < 1 min in the hydrogel. After 3 minutes of ultra-violet light exposure, the acoustically patterned cells in hydrogel were successfully crosslinked and could be retrieved from the platform for potential implantation. Furthermore, the cell viability was preserved for acoustically patterned cells for up to 48hr, confirming the gentle nature of high-frequency waves for cell manipulation. The metabolic and alkaline phosphatase activities were also evaluated, in differentiation and growth media. Our results confirmed higher metabolic and alkaline phosphatase activities for acoustically patterned cells in hydrogel after 14 days in culture, suggesting higher proliferation rates and differentiation potential. Conversely, preliminary results demonstrated the capacity of our platform to pattern cell cocultures with an even nodal distribution, which could be suitable to study angiogenesis. The results presented in this study suggest the vast potential of acoustofluidics as a rapid and contactless method for creating functional *in vitro* tissue patches, which opens a new avenue of opportunities to investigate their use in stem cell-based regenerative medicine.

Keywords: *acoustofluidics, standing surface acoustic waves, cell patterning, adipose-derived mesenchymal stem cells, cell differentiation, tissue engineering.*

Résumé

Le design et la fabrication de tissus fonctionnels sont essentielles pour les applications cliniques telles que la médecine régénérative. Les modèles cellulaires induits par les architectures tissulaires natives en répondant à des signaux mécaniques et environnementaux, jouent un rôle fondamental dans la régulation des fonctions cellulaires. Malgré l'intérêt pour l'induction d'arrangements spatio-temporel cellulaires pour le génie tissulaire, les méthodes conventionnelles souffrent de l'hétérogénéité du tissue régénérés, l'absence d'arrangements géométriques dynamiques, de la long-durée de fabrication et de la nécessité d'application d'une énergie élevée, ou encore un manque d'interaction intracellulaire qui pourraient ainsi entraver la viabilité cellulaire ou la performance tissulaires. L'acoustofluidique qui est une combinaison de l'acoustique et de la microfluidique, a montré un grand potentiel pour sa compatibilité élevée avec les cellules et pour sa capacité de manipulation rapide, l'ordre de quelques secondes, et ceci sans marquage. Ce travail présente d'abord une vue d'ensemble de l'acoustofluidique, en particulier les ondes acoustiques de surface, et sa capacité pour l'arrangements spatio-temporel des cellules avec une haute résolution spatiale et la modulation de leur fonctionnalité. Nous présentons ensuite les travaux préliminaires utilisant les ondes acoustiques de surface stationnaires pour une alignement rapide et reproductible des cellules en forme des lignes parallèles dans le milieu de culture. Des ondes acoustiques propagées à la surface ont guidé les cellules vers les lignes de nœuds de pression, avec une distance nodale reproductible de ~150μm. Ainsi les forces acoustiques radiales générées permettent un arrangement linéaire des cellulaires, sans contact dans un temps inférieur à 5s dans le milieu de culture. Cette plateforme acoustique a été validée en utilisant des cellules souches mésenchymateuses dérivées du tissu adipeux. Nous avons obtenu un arrangement linéaire des cellules dans un temps inférieur à une minute dans un hydrogel composé de méthacrylate-collagène de type I. Une fois cet arrangement cellulaire attient, une exposition de 3 minutes à la lumière ultraviolette, permet de confiner les cellules dans l'hydrogel, obtenir un film mince contenant des cellules, le décoller et l'utilise comme un patch, par exemple à fin d'implantation et la régénération tissulaire. Nous avons démontré qu'une viabilité cellulaire supérieur à 90% a été préservée après l'application des ondes acoustiques, confirmant la nature douce des ondes à haute fréquence pour la manipulation des cellules. Les activités métaboliques et de phosphatase alcaline ont également été évaluées, dans des milieux de différenciation et de croissance. Nos résultats ont confirmé des activités métaboliques et de phosphatase alcaline plus élevées pour les cellules

arrangées avec forces acoustiques dans l'hydrogel après 14 jours de culture, ce qui suggère des taux de prolifération et un potentiel de différenciation plus élevés. Inversement, les résultats préliminaires ont démontré la capacité de notre plateforme à structurer des cocultures cellulaires avec une distribution nodale uniforme, ce qui pourrait convenir à l'étude de l'angiogenèse. Par conséquent, les résultats présentés dans cette étude suggèrent le vaste potentiel de l'acoustofluidique en tant que plateforme rapide et sans contact pour créer des patchs de tissus fonctionnels in vitro, ce qui ouvre une nouvelle voie pour étudier leur utilisation en médecine régénérative à base de cellules souches.

Mots clés : *acoustofluidique, ondes acoustiques de surface stationnaires, modelage cellulaire, cellules souches mésenchymateuses dérivées du tissu adipeux, différenciation cellulaire, ingénierie tissulaire.*

Acknowledgments

I would like to start by thanking my supervisor Professor Maryam Tabrizian for her help and support throughout my degree, as well for her great mentorship, guidance, and encouragement throughout the completion of my master's degree. I would also like to thank my fellow lab mates and friends in Biomat'X Research Laboratories, for their immense support, mentorship, and guidance with equipment and cell culture training. Thank you, Christian Moya, James Porter, Celine Agnes, Radu Alex Paun, Antoine Karoichan, Michael Yitayew, Mariam Saad, Dr. Luanda Lins, and Dr. Karla Oliveira for being amazing coworkers, and being like family throughout this degree. My deepest appreciation to my acoustofluidics mentor, Reza Rasouli, for his advice, support, mentorship, and friendship. I want to also acknowledge James Porter and Reza Rasouli for proofreading sections of my thesis and manuscript. Thank you, Dr. Ling Li and Christine Walker for their help in managing the laboratory and ordering materials and equipment for my project, and the Biological and Biomedical Engineering Student Council 2020-2021 members for their friendship and for making my master's experience very special.

I would like to extend my gratitude to the Program of Biological and Biomedical Engineering, the program coordinator Dr. Brandon Xia, and the program's administrative staff, Pina Sorrini and Sabrina Teoli. Thank you for always answering my questions and for your support during the completion of my degree. I want to also acknowledge the Microfabrication facility team, especially, Dr. Zhao Lu and Mcolisi Dlamini for training me and for their help in the Clean Room.

Last, but certainly not least, I would like to thank my brother, my mom, my dad, my family, and my amazing friends for their continued love, support, encouragement, and motivation, especially, during the pandemic. You're my backbone and I am truly lucky to have you in my life.

Table of Contents

Abstract II
Résumé III
Acknowledgments V
Table of Contents VI
Contribution of Authors VIII
List of Figures IX
List of Tables XIII
List of Abbreviations XIV
CHAPTER 1: INTRODUCTION AND RESEARCH OBJECTIVES 1
1.1 Introduction and Research Rationale 1
1.2 Hypothesis and Research Objectives 3
1.3 Thesis outline 4
CHAPTER 2: LITERATURE REVIEW 5
2.1. Acoustofluidics and Acoustic Cell Patterning 5
2.1.1 Acoustic Manipulation Phenomena 5
2.1.2 SAW acoustic principles 6
2.1.3 SAW operating mechanisms 8
2.2. SAW PATTERNING FOR TISSUE ENGINEERING AND ITS EFFECTS ON CELL FUNCTIONALITY 10
2.2.1 SAW Cell Manipulation at a Single Level 10
2.2.2 SAW Cell-Cell Patterning and Tissue Engineering 11
2.2.3 SAWs Modulate Cell Functionality 16
CHAPTER 3: OPTIMIZATION OF DESIGN AND EXPERIMENTAL PARAMETERS OF THE SSAW PLATFORM FOR CELL PATTERNING 19
3.1 Introduction 19
3.2 Materials and Methods 19
3.2.1 Materials 19
3.2.2 SSAW Device Fabrication 20
3.2.3 Cell culture and sample preparation 21
3.2.4 Cell Agglomerate Patterning Experimental Setup 21
3.2.5 Parallel-Lines Cell Patterning Experimental Setup 22
3.2.5 Live Dead Assay 22
3.3 Results and Discussion 22
3.3.1 Cell Agglomerate Patterning using Orthogonal IDTs 22

3.3.2 Formation of Cell Agglomerates in Different Culture Chambers 23
3.3.3 Linear Cell Patterning using Parallel IDTs 25
3.3.4 Cell viability and Co-Culture Cell Patterning 29
CHAPTER 4: ORIGINAL PUBLICATION – MANUSCRIPT ARTICLE 32
4.1 Abstract 34
4.2 Introduction 35
4.3 Results and Discussion 38
4.3.1 Parameters Optimization of SSAW Platform Using PS particles and MC3T3-E1 Cells 38
4.3.2 SSAW patterning of Stem Cells Enhances Cell Viability, Metabolic Activity and Osteogenic Differentiation 45
4.4 Conclusion 50
4.5 Materials and Methods 51
4.5.1 Materials 51
4.5.2 Fabrication of the SSAW platform 52
4.5.3 Cell Culture 52
4.5.4 Experimental setup for cell patterning platform 52
4.5.5 Live Dead Cell Evaluation 53
4.5.6 Metabolic activity of encapsulated ASCs 54
4.5.8 Alkaline phosphatase (ALP) activity for osteogenic differentiation 54
4.5.9 Immunofluorescence 55
4.5.10 TrackMate Analysis 55
4.5.11 Statistical analysis 55
4.6 References 58
4.7 Supplementary Information 62
CHAPTER 5: GENERAL DISCUSSION 66
CHAPTER 6: CONCLUSIONS AND FUTURE PERSPECTIVE 70
CHAPTER 7: REFERENCES FROM MASTER'S THESIS 72
APPENDIX THESIS 82

Contribution of Authors

All work and experiments conducted in this thesis were done by the author, Karina Martinez Villegas, at the Biomat'X Research Laboratory under the direct supervision of Professor Maryam Tabrizian. All experimental figures and data analysis presented herein were completed by the author. Reza Rasouli contributed to the submitted manuscript by advising experimental methods and reviewing the manuscript. Harvesting of adipose tissue from rats was performed by Antoine Karoichan and Dr. Hadil Al-Jallad at the Shriners Children's Hospital affiliated with McGill University.

List of Figures

Figure 1: Acoustic schematic of forces exerted on cells upon an acoustic field. A) Acoustic mechanism of cell-cell agglomerate formation in pressure nodes showing forces experienced by a cell suspended in a medium and a cell near the piezoelectric substrate, where F_D is the drag force, F_R is the primary acoustic radiation force, F_B is the buoyant force, and G is the force of gravity. B) Simulation of the acoustic radiation pressure distribution around a pressure and microstreaming phenomena.[36] Reprinted with permission. 7

Figure 2: SSAW Patterning Schematic. A) One directional patterning using one pair of mirrored IDTs thus creating parallel linear arrangements. B) Two directional patterning using two pairs of IDTs in an orthogonal position creating cell agglomerates. 8

Figure 3: Acoustic linear patterning. A) SSAW-induced vascularization of HUVECs, stained with CD31 , and hADSCs, stained with CD44 at different HUVEC/hADSC ratios (1:0, 5:1, 2:1) (Scale bar = 100μm).[21] B) SSAW-patterned cardiac cells forming interconnected cellular networks after 7 days of culture with evidence of spontaneous beating rates over time.[44] C) 3D fibroblasts patterned in fibrin gels using SAWs with different cellular structures: a network, cages with different sizes, and unidirectional bundles with different diameters after 30 hours. The tissues are acoustically patterned with fibroblasts and then cultured for 30 hours.[41] Reprinted with permission. 13

Figure 4: Cell spheroid formation using SSAWs with preserved viability over time. A) SSAW-based spheroid formation platform using orthogonal IDT configuration (top) for HepG2 cells after 7 days. Live cells were labelled with calcein AM (green) and dead cells with propidium iodide (red) (Scale bar = 50μm).[36] B) SSAW-based spheroid formation platform consisting of a capillary tube coupled to a parallel IDT setup for mouse embryonic carcinoma (P19) cells spheroid formation. Acoustically-assembled cell clusters grow into spheroids on an ultralow attachment dish after two days in culture. (Scale bar = 200μm).[60] C) High throughput SSAW-based spheroid formation platform (top) for PAnc02, UN-KC-6141, EO771, A2780, A549, MCF-7 spheroids for 7 days (bottom) (Scale bar = 100μm).[62] Adapted and reprinted with permission. 16

Figure 5: SSAWs platforms and chambers design for cell agglomerate and linear patterning. A) Square PDMS coupled to orthogonal IDTs pairs for cell agglomerate formation, and B) Ibidi channel coupled to mirrored IDT pairs for linear patterning. 21

Figure 6: Cell agglomerate patterning module. A) Schematic of cell agglomerate formation upon two SAWs in orthogonal directions due to ARFs. B) Cell aggregate formation after <30s of SSAW induction. Scale bar is 50 μm. 23

Figure 7: Particle/Cell Aggregation using two pairs of IDTs at 45° from the X-propagation direction of the $LiNbO_3$. A) Effects of one and two IDT pairs activated for PS particles aggregation. B) Cell patterning upon activation of two pairs of IDTs in a PDMS Square Chamber bonded to a glass slide for MCF-7 and MDA-MB-231 cells, and capillary tube for MCF-7 and MDA-MB-231. Scale bar is 100 μm. 24

Figure 8: Linear patterning module. A) Linear-Patterning Schematic using one pair of IDTs opposite-facing each other with parallel PDMS channels. B) PS particles being patterned after SSAW was induced for 5 seconds. Scale bar is 200 µm. 26

Figure 9: Linear Patterning using Parallel channels. A) Before and after SAW patterning of MCF-7 (left) and MDA-MB-231 (right) showing cell pressure lines. B) Effects of thinner and wider channels for linear node patterning with better reproducibility for wider channels. 27

Figure 10: Linear Patterning Optimization. A) MDA-MB-231 cells contained in a square PDMS bonded to a glass slide. B) MDA-MB-231 cells contained in a hollow square PDMS bonded to two glass slides (top and bottom). C) MDA-MB-231 cells acoustically patterned in a µ-Slide channel (ibidi®). D) MDA-MB-231 cells showing pattern preservation in the µ-Slide 30 minutes after being acoustically patterned. Scale bar is 250 µm. 28

Figure 11: Platforms Validation via Cell Viability and Co-Culture Patterning. A) Calcein AM (green)/homodimer-III (red) stained MDA-MB-231 cells showing cell viability preservation after 30 min of SSAW activation at 40Vpp using a PDMS Square chamber bonded to a glass slide (Scale bar = 100µm), Capillary Tube (Scale bar = 100µm), PDMS Parallel Channel (Scale bar = 250µm), and 9 × 2 well µ-Slide (ibidi®) (Scale bar = 250µm). B) Cell viability for different chambers after 30 min of SSAW activation without significant changes in viability suggesting its high biocompatibility. C) Proof of concept of co-culture patterning prior (I) and after (II) SSAW induction using MCF-7 (blue) and MDA-MB-231 (red) (Scale bar = 500µm). 30

Figure 4.1: Graphical Abstract – Cell patterning working mechanism. A) Illustrative schematic of cell aggregation upon the activation of SAWs traveling in opposite directions to create standing waves. B) Working principle of cell patterning, showing cells getting guided into pressure nodes due to ARFs. C) LIVE/DEAD pictures of SSAW patterned cells (II) with defined location and high spatial resolution and control cells with no SSAW induced (I). Scale bar is 500µm. 34

Figure 4.2: SSAW patterning platform and workflow of patterning mechanism and retrievability. A) Schematic of SSAW platform. B) Cells-Hydrogel solution is seeded into the platform. B) SSAW waves are induced to the IDTs via a function generator to create cell patterns. D) UV light is applied to the patterned cells in the hydrogel to crosslink the scaffold. E) Short incubation of UV-crosslinked cells-hydrogel scaffold is done to complete the gelation of the cell-patch. F) Cell-Patch is retrieved from the platform for potential implantation. G) Cell analysis is performed at days 1, 7, and 14. 38

Figure 4.3: A) Cells prior SSAW activation and after SSAW activation with kymograph image showing nodal line distribution and distance. B) Velocity vs voltage plot. C) Velocity distribution of cells in culture media. Scale bar is 500µm. 42

Figure 4.4: Cell Patterning Sample Optimization. A) Retrievability of cell-hydrogel construct after 3 min of UV-exposure. B) Velocity distribution of different cell-suspension conditions. C) Cell patterning for various cell densities (I) 2.5 x 10^6, (II) 1.3 x 10^6, and (III) 0.6 x 10^6 cells/mL showing defined patterned lines. Scale bar is 250µm. 44

Figure 4.5: Cell viability and metabolic activity for patterned and non-patterned cells. A) Cell viability for patterned ASCs and MC3T3-E1 with and without PhotoCol® for up to 48hr after SSAW induction (n=3; *: $p < 0.05$; **: $p < 0.01$; ***: $p < 0.001$; ****: $p < 0.0001$). B) Live/Dead showing high cell viability after (I) 0hr and (II) 48hrs of SSAW induction. C) Acoustically patterned ASCs showing aligned nucleus (Hoechst 33342) and actin (Phalloidin-iFluor 594) fibers aligned after one week in growth media. D) ASCs cells-cell structure alignment of non-patterned (I) and patterned (II) cells in PhotoCol® at day 14. E) Metabolic activity of acoustically patterned and non-patterned ASCs cultured in growth media and differentiation media. Scale bar is 250 μm. 47

Figure 4.6: Osteogenic Differentiation Potential of Acoustically Patterned Cells. A) ALP Activity for non-patterned and patterned cells encapsulated in PhotoCol®-LAP hydrogel at days 1, 7 and 14 (n=3; *: $p < 0.05$; **: $p < 0.01$; ***: $p < 0.001$; ****: $p < 0.0001$). B). Confocal images of non-patterned (control) cells (I) and acoustically patterned cells (II) with an equal density of 2.5×10^6 cells/mL after 14 days of culture in differentiation media, where osteocalcin is shown in red and the nuclei in blue. C) Osteocalcin percentage difference between acoustically patterned and non patterned groups. Confocal images were analyzed using ImageJ to quantify the ratio of the osteocalcin signal area percentage versus the total stained area, (n=3; ****: $p < 0.0001$). Scale bar is 250 μm..... 49

Supplementary Figure 1: Brightfield images of high-resolution standing surface acoustic wave patterning of MC3T3-E1 cells showing 20 well-defined pressure nodal lines. A) Non-patterned cells showing random distribution of cells. B) Acoustically patterned cells showing defined lines of high-density cells (1.5×10^6 cells/mL) in growth media. Scale bar is 250μm. 62

Supplementary Figure 2: Metabolic activity as an indicator of cell proliferation of acoustically patterned and non-patterned (control) cells in PhotoCol®-LAP hydrogel cultured in growth and differentiation media. A) Acoustically patterned cells in PhotoCol®-LAP cultured in growth media show a significantly different increase in metabolic activity compared to control samples for days 7 and 14 (n=3; ****: $p < 0.001$). B) Metabolic activity of patterned and control samples, where acoustically patterned samples have an increase in showing a sign increase for acoustically patterned cells in PhotoCol®-LAP cultured in differentiation media with statistical significance for days 7 and 14 (n=3; ****: $p < 0.0001$). 62

Supplementary Figure 3: Alkaline Phosphatase Activity of acoustically patterned cells in PhotoCol®-LAP hydrogel cultured in growth and differentiation media. A) Alkaline Phosphatase activity showing slight upregulation of ALP activity at day 14 of acoustically patterned samples cultured in growth media with statistically significance for days 1 and 14 (n=3; *: $p < 0.05$; **: $p < 0.01$; ***: $p < 0.001$;****: $p < 0.0001$). B) Alkaline Phosphatase Activity of all groups combined showing significant difference between growth and differentiation media with an increase in ALP for cell-laden hydrogels cultured in differentiation media after days 1, 7, and 14 (n=3; *: $p < 0.05$; **: $p < 0.01$; ***: $p < 0.001$;****: $p < 0.0001$). 63

Supplementary Figure 4: Acoustically patterned adipose-derived stem cells (ASCs) showing nucleus (Hoechst 33342) in single pressure node cultured in growth media after (A) one week of culture and (B) two weeks of culture. Scale bar is 250µm. 63

Supplementary Figure 5: Cell morphology for control and acoustically patterned adipose-derived stem cells in PhotoCol®-LAP hydrogel after 14 days cultured in differentiation media. A) Random distribution of ASCs led to poor cellular interconnections with few cell membrane protrusions. B) Acoustically patterned cells showed high-levels of cellular interconnections with a dense spreading-like morphology suggesting strong cell-cell interconnections. Scale bar is 250µm.... 64

Supplementary Figure 6: Z-stack projection of acoustically patterned adipose-derived stem cells (ASCs) showing aligned nucleus (Hoechst 33342) and actin fibers (Phalloidin-iFluor 594) cultured in growth media after one week of culture from closer point to the piezoelectric substrate (A) to furthest point from the substrate (D). Scale bar is 250µm. 65

List of Tables

Table 1: Summary of published work on cell patterning and applications of cell patterning for tissue engineering using SAWs. 12

Table 2: Parameter selection for SSAW-patterning optimization 43

List of Abbreviations

Abbreviation	Definition
ASCs	Adipose-derived mesenchymal stem cells
MC3T3-E1	Murine Pre-Osteoblasts
MDA-MB-231	Human Breast Adenocarcinoma Cell
MCF-7	Human Breast Cancer Cell
PS	Polystyrene
PhotoCol®-LAP	Methacrylated Collagen with LAP Photoinitiator
SAW	Surface Acoustic Waves
SSAW	Standing Surface Acoustic Waves
TSAW	Travelling Surface Acoustic Waves
BAW	Bulk Acoustic Waves
SBAW	Standing Bulk Acoustic Waves
$LiNbO_3$	Lithium Niobate
ARF	Acoustic Radiation Force
F_r	Primary Acoustic Radiation Force
F_D	Stoke's Drag Force
p_0	Acoustic Pressure
V_p	Volume of the Particle
β_f	Compressibility of the Fluid
β_p	Compressibility of the Particle
ρ_f	Density of the Fluid
ρ_p	Density of the Particle
φ (β, ρ)	Acoustic Contrast Factor
x	Distance from a Pressure Node
v_p	Velocity of Particle
v_S	Velocity of Streaming Field
μ	Viscosity
r	Radius of Particle
f	Frequency
c_s	Speed of Sound
λ	Acoustic Wavelength
s	Seconds
min	Minutes
hr	Hours
Hz	Hertz
kHz	Kilo-Hertz
MHz	Mega-Hertz
GHz	Giga-Hertz

CHAPTER 1: INTRODUCTION AND RESEARCH OBJECTIVES

1.1 Introduction and Research Rationale

Arranging cells in a controlled and organized manner, while preserving their structure and functionality over time is one of the current challenges in tissue engineering and regenerative medicine. Biological tissues are composed of cellular architectures that rely on microenvironmental cues, including homotypic and heterotypic cell-cell contacts, extracellular matrix (ECM) stimuli, physical forces, and biochemical signaling.[1] During tissue development, cells organize in spatial and temporal patterns through cell growth, cell-cell adhesions and actomyosin-based contractility, cell migration, and differentiation, which contribute to the formation of a dynamic microenvironment.[2–4] Cell-cell signaling has been reported to be crucial in various biological processes, including the study of the kinetics of aggregation in new tissues, cell aggregation for spheroid formation, directed outgrowth of neuronal cluster networks, angiogenesis and organogenesis, wound healing and cell migration, and cell proliferation and differentiation.[5–11] Tissue engineering methods aim to recreate the native environment of biological samples by promoting external matrix stimuli, high cell density, growth factors, and by inducing cell communication via nano- and micro-scale technologies.[12]

Despite the interest in recapitulating the native tissue architecture, cell patterning techniques, including photolithography stamps, optical tweezers, magnetic patterning, electrophoresis, and 3D printing often suffer from limitations, including cell cytotoxicity, long fabrication times, lack of cell density control, require conductive media, cell pattern heterogeneity, have low spatial resolution, and/or lack of reproducibility.[13–17] Moreover, high-energy and contact-based cell patterning methods can potentially affect the cell phenotype, which may hinder cell viability and functionality. Acoustic-force integrated microfluidics, often termed as acoustofluidics, has been widely explored in the past two decades due to its high spatial and contactless control of biosamples, coupled with its rapid operating mechanism.[18] Acoustic-force manipulation has shown to offer a plethora of applications in biomedical sciences, from bioparticle manipulation, cell sorting, cell patterning, tissue engineering, and therapeutics.[19–22] The contactless and label-free nature of acoustofluidics and its ability to adjust its input energy and working frequency grant it as a highly biocompatible method. Moreover, its high-resolution, rapid manipulating nature, and

versatility with various media conditions including hydrogels, as opposed to electrophoresis and optical tweezers, allow this method to easily recreate cell-cell interactions in ECM-like hydrogels for more relevant *in vitro* tissues.

The working mechanism of acoustofluidics relies on the acoustic type used, the two most common being bulk acoustic waves (BAWs), where waves travel throughout the bulk body of the material, and surface acoustic waves (SAWs), where waves travel at the surface of the material. SAWs offer greater advantages over BAWs, due to their high working frequency in the megahertz (MHz) to gigahertz (GHz) region which allows for high-spatial resolution patterning.[23–25] SAWs propagate at the surface of the piezoelectric material and decay exponentially with respect to the thickness of the material. This characteristic allows SAW-based devices to minimize the power input and thus reduce the heating produced during cell patterning and cell manipulation.[26] In SAW platforms, the wavelength and resonant frequency are directly determined by the design of the interdigitated transducers (IDTs) sets. Moreover, the configuration of IDTs can create either traveling or standing waves. Standing surface acoustic waves (SSAWs), for instance, are often generated by two opposing pairs of IDTs patterned on a piezoelectric substrate. Upon the activation of two equal radiofrequency (RF) signals from each IDT set, two opposite traveling waves propagate at the surface of the piezoelectric creating maximum and minimum acoustic pressure regions, *i.e.*, antinodes and nodes. In the proximity of coupling fluid, waves leak and propagate throughout any secondary material coupled to the piezoelectric, thus allowing to manipulate cells or particles via mechanical vibrations.[27]

In this study, we investigated the use of SSAWs for the rapid and contactless patterning of cells with preserved viability and functionality. We designed a SSAW-based platform to arrange different cells, including MDA-MB-231, MCF-7, MC3T3-E1, and adipose-derived mesenchymal stem cells (ASCs) in various media conditions and a methacrylated collagen type I hydrogel (PhotoCol®-LAP). An experimental methodology was used to demonstrate that the proposed acoustofluidics platform can control the spatial alignment of cells in different geometrical configurations using culture media and a hydrogel solution, while preserving the cell viability. Microscopy techniques were used to study the nodal or linear geometric arrangements of cells and their structural preservation over time. We validated our platform using multipotent ASCs as a relevant cell model due to their self-renewal and differentiation potential into multiple lineages

including bone, cartilage, connective tissue, and muscle.[3,6,8] Live/dead, alamarBlue™, and alkaline phosphatase (ALP) enzymatic assays were used to investigate the effects of SSAW on viability, metabolic activity, and osteogenic differentiation of patterned ASCs in the PhotoCol®-LAP matrix up to day 14, respectively, cultured in differentiation and growth/culture media. Furthermore, the expression of osteocalcin in acoustically patterned cells was compared to the control group via confocal microscopy, to study the potential of the proposed SSAW-based platform for creating an *in vitro* biomimetic tissue construct.

1.2 Hypothesis and Research Objectives

The objective of this study is to design, fabricate, and validate a SSAW-based acoustofluidics platform for the manipulation and patterning of adipose-derived stem cells suspended in a methacrylated collagen type I hydrogel (PhotoCol®-LAP) and to study the effects of SSAWs on cell survival, metabolic activity, differentiation potential, and retrievability as a 3D biomimetic cell patch.

The aims of this study can be further divided into:

1. Design and optimization of a SSAW-based platform for controlled spatial patterning of particles and cells.
   1.1. Design and optimization of interdigitated transducers (IDTs) and culture chambers for rapid, easy, reproducible, and optimal cell patterning in grow media and hydrogels.
   1.2. Optimization of the amplitude, working frequency, and velocity of the SSAW-devices for the rapid and controlled formation of pressure nodes to guide and manipulate polystyrene (PS) particles.

2. Validation of the SSAW-based platform using MCF-7, MDA-MB-231, and MC3T3-E1 cells
   2.1. Validation of the functionality and performance of the acoustic patterning platform using MCF-7, MDA-MB-231, MC3T3-E1, and co-culture.
   2.2. Study of the velocity, cell density, culture media conditions, patterning time, nodal distance, and biocompatibility of the SSAW-platform.

3. Investigation of the potential of SSAWs-based patterning for enhanced metabolic activity and osteogenic differentiation of ASCs by inducing cell-cell communication.
   3.1. Assessment of the effects of acoustic patterning on cell viability, metabolic activity, and cell morphology.
   3.2. Study of the effects of acoustic patterning on cell osteogenic differentiation via ALP assay and osteocalcin signalling.

1.3 Thesis outline

Chapter 1 Provides a concise introduction and presents the rational and objectives of this study.

Chapter 2 Introduces the literature review of acoustofluidics with an emphasis on surface acoustic waves and discusses the applications of state-of-the-art surface acoustic waves for cell patterning, tissue engineering, and as functional stimuli for cells.

Chapter 3 Presents the preliminary work of this research study, including the optimization of design and experimental parameters prior to the results presented in the submitted manuscript article.

Chapter 4 Presents the original work from the author in the form of a submitted manuscript article.

Chapter 5 Provides an in-depth discussion of this study.

Chapter 6 Concludes this study and provides future perspectives of SAW-based platforms.

Chapter 7 Lists the references of this work.

CHAPTER 2: LITERATURE REVIEW

2.1. Acoustofluidics and Acoustic Cell Patterning

2.1.1 Acoustic Manipulation Phenomena

The mechanism to manipulate cells and particles using acoustic fields, often referred as acoustophoresis, consists of an alternating electric current (AC), induced to a piezoelectric material that due to the polarization of the dielectric material, causes the electrical field to be transduced into mechanical vibrations.[18] The path of propagation within the fluid medium coupled to the piezoelectric material divides acoustic waves into two general types: surface acoustic waves (SAW), which propagate at the surface of a material, and bulk acoustic waves (BAW), which travel throughout the bulk of the material and are normal to the piezo element. In the following sections, we briefly discuss the main types of acoustic waves and their mechanisms of wave propagation for cell manipulation.

2.1.1.1 Bulk Acoustic Waves

Bulk Acoustic Waves (BAWs) based microfluidic devices are generated by mechanical vibrations of piezoelectric transducers coupled to a fluid chamber. Piezoceramics, including lead zirconate titanate (PZT) or glass, are commonly used in BAW systems where BAWs resonate, upon an electrical signal, causing waves to travel throughout any intermediate medium and throughout the total fluid volume.[28] This contactless approach thus minimizes the lead toxicity as well as the heat generated to biological specimens. BAW-based devices are characterized for operational frequencies lower than 10-Megahertz (MHz), corresponding to wavelengths in the 100μm realm.[29] Since the wavelengths are often greater in magnitude than many biological samples, such as cells, biomolecules, and extracellular vesicles, the manipulation precision of individual cells and particles is limited in BAW devices. However, it is suitable for applications where bigger clusters of particles are needed and can work with higher flow rates, being suitable for scaled up applications.[30]

2.1.1.2 Surface Acoustic Waves

Conversely, surface acoustic wave (SAW) based devices are fabricated by patterning interdigitated transducers (IDTs) on piezoelectric substrates, often lithium niobate ($LiNbO_3$) wafers. Upon the

activation of an alternating current to each set of ITDs, the conducted electrical signals are translated into mechanical oscillations due to the piezoelectric effect, and propagate in the form of surface acoustic waves.[27,31] The operating frequency of SAW devices are typically in the megahertz (MHz) and lower-end gigahertz (GHz) regions. This high working frequency combined with short working wavelengths, allows the acoustic waves to be confined to the surface of the substrate. Therefore, SAWs minimize the power consumed and heat generated with a high spatial resolution for the manipulation of single cell, nanoparticles, and extracellular vesicles.[27] Furthermore, SAWs offer a higher versatility compared to BAWs since by adjusting the period of the IDTs, one can easily control the range of working frequencies, allowing for high-resolution patterning. Additionally, SAW-based platforms offer a simple design and fabrication, compact size, easy integration, low power consumption, and high biocompatibility.[24,32]

2.1.2 SAW acoustic principles

The two main forces governing the manipulation of particles and cells using acoustic fields are classified into acoustic radiation forces (ARFs) and acoustic streaming-induced drag forces.[33] Cells and particles suspended in a fluid medium that are exposed to an external acoustic field, experience hydrodynamic scattering forces that allow cells to be pushed to certain locations, often termed as acoustic pressure nodes. Acoustic radiation forces (ARFs), which are the time-averaged net force created by pressure fluctuations, govern the cell manipulation and patterning, and can be classified in primary and secondary ARFs. Primary acoustic radiation forces emerge from the direct irradiation of acoustic waves on cells/particles directing the cell/particle trajectory to defined cell/particle trajectory paths, while both secondary radiation forces and drag forces are the resultant of wave scattering on particles via indirect acoustic fields and are the main responsible for cell-cell interactions.

The primary ARF (F_r) acting on suspended, compressible, spherical particles in a liquid medium is estimated as:[34,35]

$$F_r = -\left(\frac{\pi p_0^2 V_p \beta_f}{2\lambda}\right)\phi(\beta,\rho)\sin\left(\frac{4\pi x}{\lambda}\right) \quad \textbf{(Eq. 1)}$$

$$\phi(\beta,\rho) = \frac{5\rho_p - 2\rho_f}{2\rho_p + \rho_f} - \frac{\beta_p}{\beta_f} \quad \textbf{(Eq. 2)}$$

where p_0, V_p, β_f, β_p, ρ_f, ρ_p, λ, and x are the acoustic pressure, volume of the particle, compressibility of the fluid, compressibility of the particle, density of the fluid, density of the particle, acoustic wavelength, and the distance from a pressure node, respectively. The acoustic contrast factor $\phi(\beta, \rho)$, determines the direction of the cells towards a pressure node or antinode, if ϕ is positive or negative, respectively.

Conversely, acoustic streaming-induced forces result from a secondary indirect force upon vortices in the surrounding fluid of a cell/particle. Acoustic streaming forces and the resultant drag forces on particles/cells can also determine the trajectory of suspended cells or particles in a fluid medium. Suspended particles and cells with an initial velocity ($\boldsymbol{v}_p$) that are exposed to a streaming velocity field ($\boldsymbol{v}_s$) experience a Stokes' Drag Force, which determines the direction of motion of suspended particles to the streamline of the vortices. The Stokes' Drag Force can be defined as:[36]

$$F_D = 6\pi\mu r\,(v_s - v_p) \qquad \textbf{(Eq. 3)}$$

Where μ and r are the fluid viscosity and the radius of the particle, respectively.

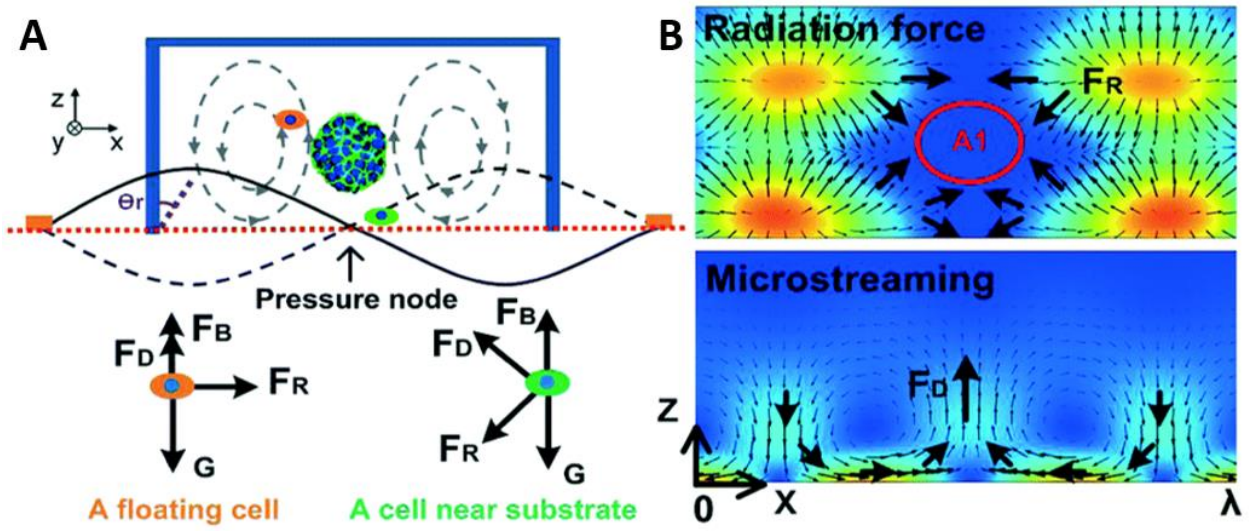

Figure 1: Acoustic schematic of forces exerted on cells upon an acoustic field. A) Acoustic mechanism of cell-cell agglomerate formation in pressure nodes showing forces experienced by a cell suspended in a medium and a cell near the piezoelectric substrate, where F_D is the drag force, F_R is the primary acoustic radiation force, F_B is the buoyant force, and G is the force of gravity. B) Simulation of the acoustic radiation pressure distribution around a pressure and microstreaming phenomena.[36] Reprinted with permission.

2.1.3 SAW operating mechanisms

Two main SAW acoustic operating mechanisms can be classified based on how ARFs interact with cells and particles, being standing-waves and traveling-waves. Travelling surface acoustic waves (TSAW) are often generated by depositing single IDTs on a piezoelectric substrate, allowing waves to propagate throughout the microchannel and form arbitrary pressure nodes to guide cells and particles.[18,26] TSAW can be divided into active and passive tweezers. Passive tweezers use predefined structures (IDTs) with a single acoustic source in order to form a pre-designed acoustic field patterning. Conversely, active TSAWs tweezers, use one or multiple transducers that can be simultaneously controlled to create an active and dynamic rotation of cells in defined 3D paths. While active TSAW are commonly used for single cell sorting and cell bioprinting, passive TSAW are more often used to manipulate and rotate cells levitated in 3D. Furthermore, in TSAW-based systems the ARF scattering force continuously pushes particles in the direction of the beam propagation, causing cells/particles to migrate from the acoustic source, *i.e.*, the IDT.

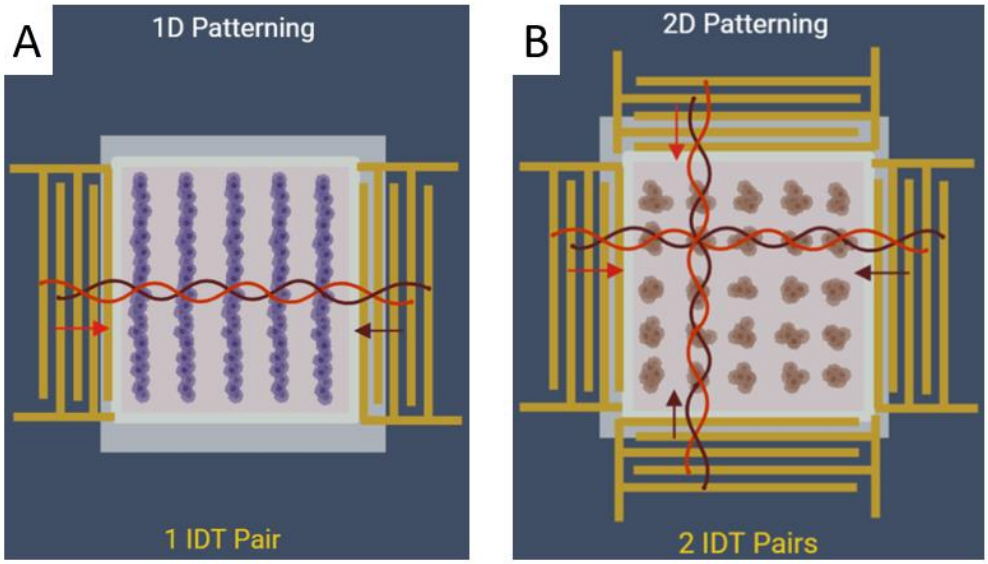

Figure 2: SSAW Patterning Schematic. A) One directional patterning using one pair of mirrored IDTs thus creating parallel linear arrangements. B) Two directional patterning using two pairs of IDTs in an orthogonal position creating cell agglomerates.

Standing Surface Acoustic Waves (SSAW), on the other hand, are formed by depositing two or more even pairs of opposite-facing interdigitated transducers (IDTs) on a piezoelectric substrate. Rayleigh, or leaky, waves leak into the liquid domain entering the liquid, where a SSAW field is formed by the interference of two travelling waves. By tuning the phase difference and the working

frequency between the two oppositely propagating acoustic waves, the position of the pressure nodes can be easily tuned. In SSAW-based mechanisms, the resonant frequency is confined to a singular frequency, dictated by the IDT design. The density of particles and fluid determines whether the particles reside in the pressure nodes (particles with positive contrast $\phi(\beta, \rho)>0$), or antinodes (particles with negative contrast $\phi(\beta, \rho)<0$), creating regions of low and high pressure that oscillate in time. In one-dimensional (1D) SSAW fields, cells are aligned in parallel pressure node patters (Figure 2A), while by having two IDTs pairs, as it is the case of two dimensional (2D) fields, particles and cells are arranged in orthogonal 2D arrays (Figure 2B). SSAW-based tweezers are often used with polydimethylsiloxane (PDMS) chambers, where the PDMS sidewalls minimize the wave attenuation to focus the cell patterning region.

2.2. SAW PATTERNING FOR TISSUE ENGINEERING AND ITS EFFECTS ON CELL FUNCTIONALITY

As discussed in Chapter 1, the high working frequency of SAWs allow them to have a high spatial resolution for cell manipulation in comparison to BAW-based devices. Moreover, SAW-based acoustic mechanisms are preferred for cell patterning as they allow for a dynamic and reconfigurable manipulation of cells by adjusting the excitation frequency, voltage, phase, and the geometry and orientation of IDTs. Furthermore, the label-free, precise, and high spatial control of cells in SAWs, coupled with its gentle and non-contact manipulating mechanism ensures high patterning efficiency with minimal effects on cell viability and functionality, making it an attractive tool for tissue engineering applications.

2.2.1 SAW Cell Manipulation at a Single Level

At a single-level cell manipulation, SSAWs have been shown to allow for a dynamically and reconfigurable manipulation of individual cells and organisms by modulating the phase, amplitude, and excitation frequencies. As an example, Ding *et al.*[37] used tunable SSAWs to guide and pattern cells and C. elegans at a single level 1D by shifting the resonance frequency in chirped IDTs. Integrating two actuating mechanisms, for instance phase-shifting and SSAW amplitude control, has also shown the ability to control both planar and vertical (normal axis) trajectories of single cells simultaneously.[38] Similarly, SSAWs can be used to precisely position cells into defined areas, such as acoustic wells. By increasing the operating frequency of SSAW, the pressure node distance was reduced to 15 μm, allowing for only one cell to reside in each individual acoustic pressure nodes, known as the 'One Cell Per acoustic Well' (OCPW) approach.[39]

Non-standing SAWs can also be used to manipulate individual organisms in a defined manner. For instance, Zhang *et al.*[40] designed a hollow-square-shaped IDT immersed in water as a sound source to generate acoustic waves, and as a micropump to pump fluid in x and y orthogonal directions to manipulate single zebrafish larvae in 2D. Wave number-spiral acoustic tweezers can be also exploited to dynamically reshape SAW fields to various pressure distributions and allow dynamic and programmable single-cell manipulation.[41] By using this configuration, IDTs can be controlled simultaneously and independently to manipulate single cells using two multitone excitation signals.

2.2.2 SAW Cell-Cell Patterning and Tissue Engineering

2.2.2.1 Cell-to-Cell Patterning

High-precision SSAWs-patterning platforms further allow to induce cell-cell interactions and study collective functional behaviors of cell-cell and cell-ECM, including network formations and neurite guidance, angiogenesis, cardiomyocyte beating, and functional 3D fibroblast networks.[41–44] SSAWs can pattern cells into 2D or 3D constructs wherein suspended cells can be actively guided and accurately organized in pressure nodes or antinodes, based on their compressibility and density properties. These pressure sites can be designed to achieve various spatial patterns, which can remain fixed or dynamically reconfigured over time by changing the frequency or by shifting the phase.[45]

For instance, Shi and colleagues proposed a SSAW-based patterning device to guide cells using one or two pairs of IDTs in an opposite and parallel or orthogonal configuration for parallel lines or node patterning, respectively.[46] In another study, SSAWs were used to control the cell spatial arrangement and evaluate the intercellular gap junctions between homotypic and heterotypic cells.[47] To exploit cell-coculture dynamics, Li *et al.*[48] patterned and cocultured epithelial cancer cells (HeLa) and endothelial cells (HMVEC-d) showing real-time monitoring of HeLa cells migration in monoculture, random co-culture, and acoustic co-culture by using a phase-shift mechanism. To further integrate cell patterning and real-time visualization, a ZnO/Si-based platform was integrated with a right-angle prism to reflect the light from the side of the microchannel into the microscope and thus record the vertical motion and location of yeast cells and particles.[49]

One limitation that should be considered with SAW devices compared to BAWs, is that their resonant frequency is typically fixed by the IDT geometry. As a solution, Ding *et al.*[50] proposed a dynamic cell mechanism patterning using slanted-finger IDTs (SFITs). SFITs allow to change the distance between the pressure nodal lines, and thus adjust the cell alignments in a more dynamic manner. Circular slanted-finger interdigital transducers (CSFITs) were also reported to dynamically manipulate particles using multi-tone excitation signals.[51] Furthermore, both surface and bulk standing waves can be integrated into one single platform. As an example, Cohen and colleagues applied standing traps for scaled neuronal patterning and demonstrated directed neuronal growth of DRG neurons due to cellular organization for up to 6 days.[52]

Table 1: Summary of published work on cell patterning and applications of cell patterning for tissue engineering using SAWs.

Application	Acoustic wave (control method, # transducers)	Acoustic Parameters	Cell/Particle (concentration) / Supporting material (culture time)
Cell Patterning	SSAW (ARF)	200 mW, λ=100µm (1D) and 141µm (2D)	1.9µm PS beads (11 760 000 beads/mL); bovine RBC; E. coli[53]
	SSAW (ARF, 2 pairs of IDTs)	13.35 MHz, 30mW (horizontal); 13.45 MHz 10mW (vertical) (λ=300µm)	10µm PS beads; HEK293T; U87; HeLa S3 (0.5-1.2x10^6 cells/mL)[47]
	SSAW (ARF phase shift, 1 pair of IDTs)	12.78 MHz (λ=300µm), 20 Vpp	HeLa, HMVEC-d (4-3 x 10^6 cells/mL)[48]
	SAW (ARF phase shift ZnO/Si thin film, 1 pair of IDTs)	42.2, 24.0 and 12.2 MHz (λ= 100, 200, and 400µm), 3500mW	0.5, 6, 10µm PS particles, Yeast cells[49]
	SSAW (ARF phase and frequency shift, 1 - 2 IDT pairs)	7.47 MHz (1D), 3.45 and 3.43 MHz (2D)	U937 cells (1.5 x 10^6 cells/mL)[41]
	SSAW (ARF, 1-2 slanted-finger IDT pairs)	12-18 MHz (λ=300-200µm) (1D), 10.5-18.5MHz (λ=400-700 µm) (2D), 23-26 dBm	PS beads, bovine RBC, HL-60[50]
	SAW (ARF frequency shift, 1 circular slanted-finger IDTs)	13.5-16.3 MHz, 8-10 Vpp	PS 10.2µm (1x10^6 beads/mL), K562 cells (1x10^7 cells/mL)[51]
	SSAW (Leaky waves, 1 pair IDTs)	12.65 MHz (λ=400µm), 1.5 W/cm^2	HeLa S3, MC3T3-E1, PC12 Adh cells (5 x 10^6 cells/mL) in PEGDA, GelMA[54]
	SSAW (ARF, 2 pairs of IDTs)	λ=300µm, 24.85 dBm, 10 min (actuation)	MCF-7 (4.68 x 10^6 cells/mL) in Collagen type I (1 day)[55]
Tissue Engineering Preservation	SSAW, slanted IDTs (2 pairs)	3.4, 4.6, 6.4 MHz, -7 to -12 dBm	Neonatal rat ventricular cardiomyocytes in GelMA, (7 days of beating activity)[44]
	SSAW (1 IDT pair)	1.0, 3.4, 5.4, 7.5 MHz (λ=1480, 435, 274, 197µm)	NIH 3T3 (fibroblast) in Fibrin gels (30 hours)[41]
	SSAW (1 IDT pair)	13.928 MHz (λ=280µm)	hADSCs, HUVECs, hiPSC-ECs (1 x 10^6 – 2 x 10^7 cells/mL) in HA-CA catechol-conjugated hyaluronic acid (28 days)[8]
	SSAW + SBAW PZT	19.4 MHz, 3-20 Vpp (SSAW) and 1.14 MHz, 10 Vpp (BAW)	DRG and PC12 in Collagen type I (6 days)[7]

Abbreviations: PS (polystyrene), RBC (Red blood cells), HEK293T (Human embryonic kidney cells), U937 cells (Human macrophages), HeLa S3 (human cervix cancer cell), HMVEC-d (Human Lung Microvascular Endothelial cells), HL-60 (promyeoloblasts), K562 (human erythroleukemic cells), PC12 (catecholamine cells), PEGDA (Poly(ethylene glycol) diacrylate), GelMA (Gelatin methacryloyl), MCF-7 (human breast cancer cells), NIH 3T3 (mouse fibroblasts), hADSCs (human adiposed derived stem cells), HUVECs (Human umbilical vein endothelial cells), hiPSC-ECs (human induced pluripotent stem cells-endothelial cells), HA-CA (Catechol-Functionalized Hyaluronic Acid), and DRGs (Dorsal Root Ganglion cells).

2.2.2.2 Cell Patterning for Tissue Engineering

Reconstructing the physical architecture of the native tissue is one of the key aspects of tissue engineering.[56] Following the initial spatial organization of cells into the desired pattern, the cell architecture preservation is crucial to establish cell-cell connections and for tissue maturation.[45] In the previous section, we discussed the role of SSAWs to induce cell-cell contacts; this next section mainly centers in the duration of exposure and the implementation of hydrogels for long-term culture and acoustic patterning preservation. Maintaining the spatial pattern architecture over the tissue development period is highly influenced by the cell type, cell-cell affinity, and cell-environment interactions. Cells with higher affinity rapidly form a strong arrangement dictated by the acoustic node design,[52] while low-affinity cells can easily migrate from their initial position and thus require a supporting matrix to retain the pattern and immobilize the cell arrangement, as it is the case of hydrogels for guided vascularization.[8,57]

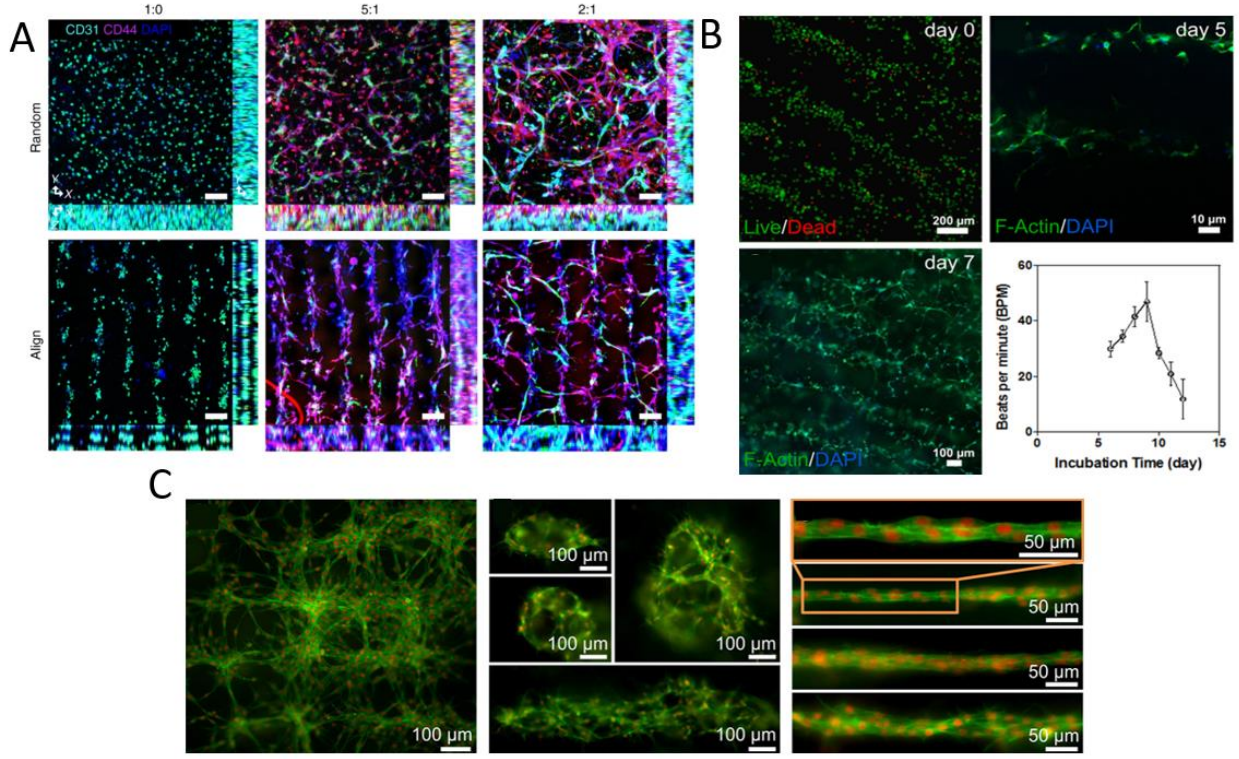

Figure 3: Acoustic linear patterning. A) SSAW-induced vascularization of HUVECs, stained with CD31 , and hADSCs, stained with CD44 at different HUVEC/hADSC ratios (1:0, 5:1, 2:1) (Scale bar = 100µm).[21] B) SSAW-patterned cardiac cells forming interconnected cellular networks after 7 days of culture with evidence of spontaneous beating rates over time.[44] C) 3D fibroblasts patterned in fibrin gels using SAWs with different cellular structures: a network, cages with different sizes, and unidirectional bundles with different diameters after 30 hours. The tissues are acoustically patterned with fibroblasts and then cultured for 30 hours.[41] Reprinted with permission.

As an example of the first method, SSAWs were used to pattern cells in parallel lines, where cells were then gently deposited by gravity on a collagen-treated surface for cells to adhere.[47] The linear arrangement of HEK293T cells was observed 40 minutes after turning off the SAWs, where acoustically patterned cells were successfully adhered to the collagen-treated surface after 1 hour. Despite the simplicity of this scaffold-free approach to preserve cell patterns, it can be very time-consuming (>1h) and the patterns can be easily deformed.[47] Hence, the use of scaffolds has increased the interest as a preserving step for patterned cell architectures. For instance, Kang *et al.*[8] demonstrated the formation of a functional collateral cylindroid transplanted in a mouse model for ischemia therapy by acoustically patterning HUVECs and hASCs cells in a catechol-conjugated hyaluronic acid scaffold. Patterned structures exhibited higher secretion of angiogenic (VEGF) and anti-inflammatory cytokines (IL-10) factors for up to 7 days (Figure 3A). Three-dimensional fibroblast tissues were also successfully formed but using fibrin gels via SSAWs. NIH3T3 fibroblasts were patterned in lines (1D) and mesh-like (2D) geometries, which showed to influence the interlink of cells. 3D networks, cell-cages with different sizes, and unidirectional bundles with different diameters were observed after 30 hours in culture for 1D and 2D patterns, where the initial fibroblast pattern influenced the post-culturing cellular architectures (Figure 3C).[41]

Another solution to retain defined acoustically patterns in a more rapid way is to use UV crosslinkable hydrogels. HeLa, MC3T3-E1, and P12 Adh cells were acoustically patterned in photocurable polymers (PEGDA700, PEGDA3400, and GelMA) using SSAWs and cultured in capillary tubes to create cellular fibers in few minutes.[58] A similar approach was used to acoustically pattern MCF-7 breast cancer cells in a 3D polymerized-collagen hydrogel. After UV-crosslinking, the scaffold could be removed from the platform and the chamber could be reused. Their results showed no significant differences in cell viability for up to 24h.[55] Moreover, nodal alignment using slanted-finger interdigital transducers (SFITs) was shown for patterning cardiomyocytes in GelMA within less than 10 seconds.[44] Patterned cardiac cells demonstrated beating activity after 5-7 days with preserved cell viability and functionality after acoustic induction (Figure 3B).

2.2.2.3 Spheroid Formation

In addition to lines, significant work on spheroid formation via standing waves has been conducted. SAWs can form spheroids by modulating pressure nodes for controlled cellular aggregation. Chen *et al.*[36] used SSAWs as a size controllable and rapid assembly method for $HepG_2$ and HEK293 aggregates, where after 24h a smooth spheroid surface was observed with high proliferation and viability for up to 7 days (Figure 4A). For its part, Hu *et al.*[59] developed an SSAW-based acoustic force assembly to engineer 3D multicellular human mononuclear leukemia spheroids (THP-1) in a photosensitive GelMA hydrogel. These spheroids showed good tumor model resemblance where the cell aggregate activity was inversely proportional to the drug concentration with a lower sensitivity to drug toxicity in comparison to monolayers.[59] Single SSAW fields have also been shown to generate mono-sized spheroids by coupling capillary tubes to the piezoelectric substrate[54,60,61] along the wave propagation direction (Figure 4C). The potential of acoustic force-directed platforms via single SSAW fields was evidenced by patterning HeLa cell spheroids suspended in polymerizable hydrogels (PEGDA and GelMA) inside capillary tubes.[54] Using this method, spheroid embedded fibers were successfully formed and could be retrieved from the capillaries after UV-crosslinking. Taking a step further, single pressure nodal lines can be exploited to form spheroids in polydimethylsiloxane (PDMS) channels perpendicular to the IDT direction (length). As an example, various cancer cell lines (Panc02, UN-KC-6141, EO771, and MCF-7) were injected into a PDMS chamber with parallel channels to cell clusters within seconds with high throughput (12,000 cell clusters) (Figure 4B).[62] After 7 days in culture, well-defined spheroids were formed and they could be used for drug (Gemcitabine) testing with an evidenced higher dose-dependent response to the drug compared to cell monolayers. Therefore, SSAWs have shown their potential for rapid patterning to create functional tissue architectures.

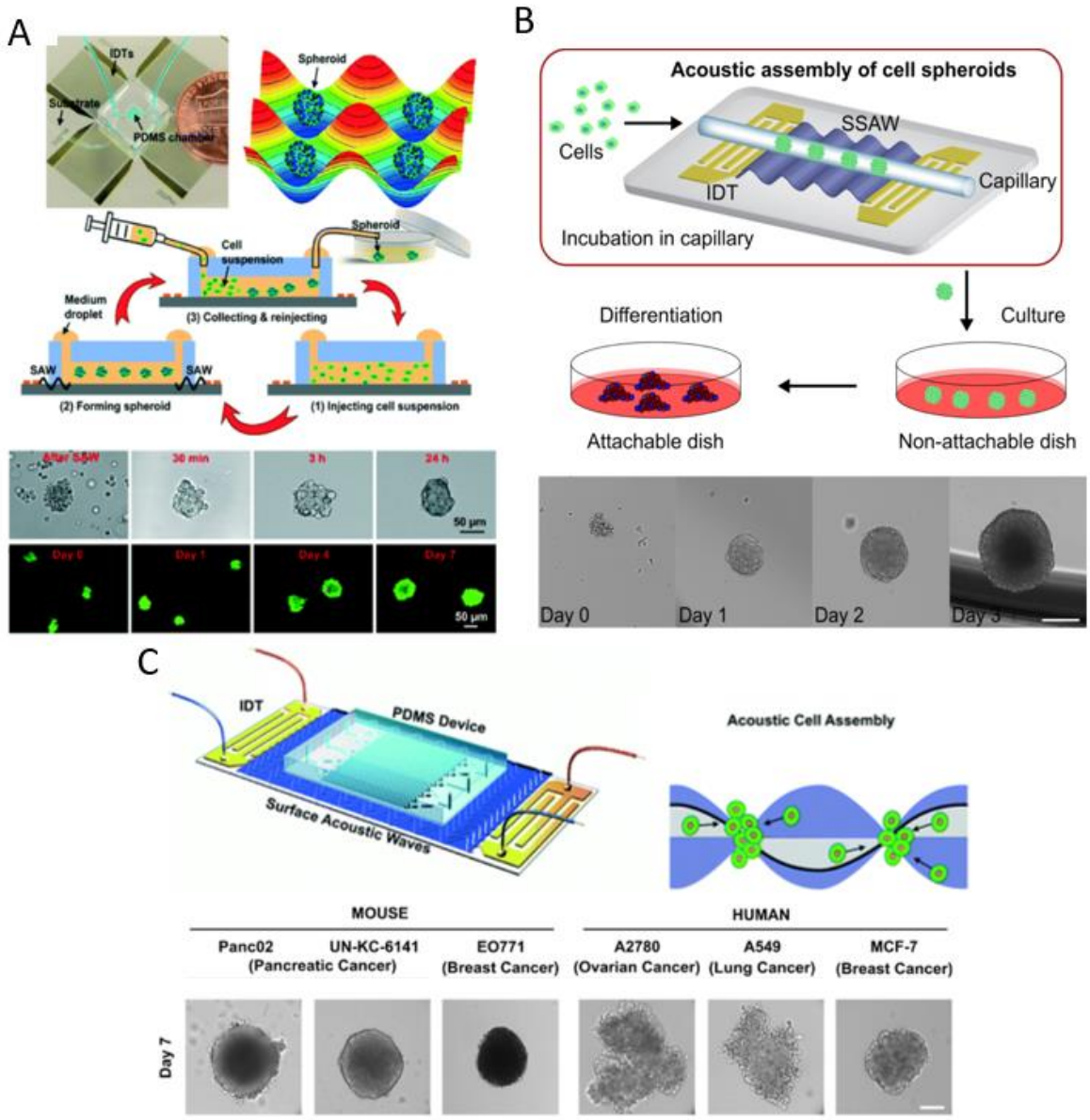

Figure 4: Cell spheroid formation using SSAWs with preserved viability over time. A) SSAW-based spheroid formation platform using orthogonal IDT configuration (top) for HepG2 cells after 7 days. Live cells were labelled with calcein AM (green) and dead cells with propidium iodide (red) (Scale bar = 50µm).[36] B) SSAW-based spheroid formation platform consisting of a capillary tube coupled to a parallel IDT setup for mouse embryonic carcinoma (P19) cells spheroid formation. Acoustically-assembled cell clusters grow into spheroids on an ultralow attachment dish after two days in culture. (Scale bar = 200µm).[60] C) High throughput SSAW-based spheroid formation platform (top) for PAnc02, UN-KC-6141, EO771, A2780, A549, MCF-7 spheroids for 7 days (bottom) (Scale bar = 100µm).[62] Adapted and reprinted with permission.

2.2.3 SAWs Modulate Cell Functionality

In addition to forming relevant tissue constructs, acoustofluidics and surface acoustic waves can be used to study their effect on cellular functionality, including cellular metabolic activity,

morphology, permeability, and wound healing. As an example, mesenchymal stromal cells, human keratinocytes, mouse osteosarcoma, and mouse fibroblasts were induced to a 48.5 MHz SAW for the study of changes in cell viability, morphology, substrate attachment, and proliferation.[63] No significant differences were reported for cell viability and nuclear morphology after exposure; however, less cell attachment and spreading in mesenchymal stromal cells and mouse osteosarcoma was reported. Moreover, SAWs have shown to increase the metabolic activity in human keratinocytes and mouse fibroblasts showing that acoustic excitation directly enhanced the cell's proliferation rate.[63] In another study using a similar frequency of 48.8MHz but with a SAW-based streaming platform on a Petri-dish, a 36% increase in the cell proliferation rate was reported due to more efficient culture media circulation.[64]

In another work, SSAW patterning was used to align primary neuron cells to study the cell growth and adhesion direction after acoustic exposure.[42] Results showed that neurite outgrowth was aligned in the direction of the SSAW pressure nodal line axes, suggesting the alignment of the cytoskeleton and ECM.[65,42] Furthermore, the nature of SSAWs, combining both mechanical stimulations and electrical triggers, can influence the cell growth and cell migration. Stamp *et al.*[21] showed a 17% increase in Saos-2 cell migration indicating a better healing rate of an *in vitro* artificial wound. The effects of frequency, amplitude, and wave modes were also used to study the proliferation rate and reactive oxygen species (ROS) levels of various cell lines. Cells exposed to piezo-mechanical SAWs showed an increased growth rate and a 135 ± 85% enhancement in the wound-healing speed, while cells exposed to electrode-generated electrical fields did not show any differences. These results would indicate that vibration and mechanical stimulation enhance wound-healing and overall proliferation.[66]

SAWs have been also reported as an efficient stimulus for wound healing by promoting tissue oxygenation in ischemic feet. Human patients treated with a commercial SAW Patch device (NanoVibronix), experienced an increase in oxygen saturation and an overall reduction in pain.[67] Neuronal activities have also been shown to change in SAW devices by altering the intensity, duration, signal continuity, and frequency of pulses. Low-intensity pulsed SAW signals were used to stimulate brain slices from epileptic patients. A reduced epileptiform activity by over 65% after 30 min exposure pled in favor of SAWs as a potential non-invasive treatment for epilepsy.[68] In another study, pulsed (10s) and continuous SAWs were induced in *C. elegans* to promote traumatic

brain injury in worms.[69] The continuous exposure, although with less acoustic pressure than that of the pulsed, caused a temporary paralysis of the worms and reduced chemotaxis learning and short-term memory loss. Therefore, acoustic fields have shown their potential as relevant methods not only to organize cells into defined patterns but to study their influence on cell and tissue functionality.

CHAPTER 3: OPTIMIZATION OF DESIGN AND EXPERIMENTAL PARAMETERS OF THE SSAW PLATFORM FOR CELL PATTERNING

3.1 Introduction

The state-of-the-art literature review presented in Chapter 2 showed the potential of acoustic cell patterning as a rapid and biocompatible method to fabricate cell spheroids, cell cages, cell fibers, and tissue patches with similar *in vivo* physiological conditions.[8,41,55,60,70,71] As discussed, cell patterning allows inducing cell-cell interactions and studying the kinetics of tissue development in order to fabricate more relevant tissue architectures.[72] Considering the findings and challenges from our literature review on acoustic patterning, in this chapter we present the design and optimization of experimental parameters of the SSAW platform for cell patterning and cell functionality studies. This section thus presents the preliminary work done prior to the submission of an original manuscript article titled "*Enhancing Metabolic Activity and Differentiation Potential in Adipose Mesenchymal Stem Cells via High-Resolution Surface Acoustic Waves Contactless Patterning*", found Chapter 4.

Different channels and interdigitated transducer (IDT) configurations were trialed for the optimization and reproducibility of pressure nodal lines, velocity and efficiency of manipulation, working frequency, working media, and cell density. This section also presents the challenges and limitations of the tested microfluidic chambers and IDTs configurations to achieve the final design for the cell patterning module and its application in tissue engineering. Two different cell pattern geometries were studied, using four sets of IDTs to create a mesh-like cell agglomerates arrangements, and two sets of opposite facing IDTs to generate parallel linear cell arrangements.

3.2 Materials and Methods

3.2.1 Materials

Dulbecco's Modified Eagle Medium (DMEM), Fetal Bovine Serum (FBS), Penicillin-Streptomycin (P/S), and microscope glass slides were purchased from Thermo Fisher Scientific (MA, USA). Dulbecco's Phosphate Buffered Saline 1X (PBS, without calcium chloride and magnesium chloride) was purchased from Sigma Aldrich (MI, USA). Trypsin-EDTA (0.25%) and Live/Dead Viability Assay Kit (L3224) were purchased from Invitrogen (MA, USA). A positive

photoresist (S1813) and a negative photoresist (SU-8 2050) were obtained from MicroChem Corp. (TX, USA). Polydimethylsiloxane (PDMS) was purchased from Dow Corning Corp. (QC, Canada). A μ-Slide 2 well co-culture chamber was purchased from ibidi GMBH (WI, USA). 4-inch 127.86° Y-cut, X-Propagating SAW grade Lithium Niobate wafers were purchased from Precision Micro-Optics (MA, USA). Human breast adenocarcinoma cells MDA-MB-231 and human breast cancer cells MCF-7 were purchased from the American Type Culture Collection (ATCC, VA, USA).

3.2.2 SSAW Device Fabrication

The SSAW device was fabricated by spin coating a 500 μm thick double-sided polished 127.86° $LiNbO_3$ piezoelectric wafer with a positive photoresist (S1813) to a 10 μm-thickness. A double layer of titanium and gold (Ti/Au 0.1/1.0 kÅ 10 nm 100 nm) was then deposited on the substrate using an e-beam evaporator (bjd1800, Airco Temescal, CA, USA). Next, the substrate was submerged in a developer (MF319, Microposit) at 70° C under sonication to lift-off the undesired coating and form the desired sets of interdigitated transducers (IDTs). The design of IDTs was comprised of 75 μm even finger and spacing gaps ($\lambda_{SAW}/2$ = 150 μm) for a total of 40 electrode pairs. For the cell agglomerate design, two orthogonal IDT pairs were deposited on the piezoelectric wafer with an offset of 45° from the X-propagation direction, allowing SAWs to share a similar resonance frequency. For the parallel cell linear design, one pair of mirrored IDTs was deposited on the piezoelectric wafer in parallel direction to the X-propagation, to allow maximum resonance frequency.

The master mold for the microfluidic chamber was fabricated by spin coating a negative photoresist (SU-8 2050) on a silicon wafer in two layers with a baking time, spin speed, and lithography dosage following the manufacturer's protocol for a 150 μm final thickness. The master mold was silanized and poured with standard 10:1 PDMS solution for replica molding with different configurations, a square chamber with a dimension of 1 cm × 1 cm × 150 μm (w × l × h) and a chamber with 10 parallel channels with a dimension of 1cm × 150 μm × 150 μm (l × w × h). The PDMS chambers were bonded, respectively, to microscope glass slides using plasma bonding treatment, and the glass slides were then coupled to the $LiNbO_3$ wafer using a drop of water to transfer the waves from the piezoelectric wafer to the chamber. A rectangle quartz capillary tube (Vitrocom Inc, NJ, USA) with a dimension of 0.3 mm x 0.4 mm x 100 mm was tested for the optimization of mesh-nodal patterning. The capillary tube was placed diagonally to the orthogonal

IDT pairs, and it was coupled to the SAW wafer using a drop of water. For the final linear cell patterning design, a commercial μ-Slide well co-culture chambered coverslip (ibidi® GmbH, MI, US) with 2 major well dimensions of 21.5 × 23.6 × 6.8 mm^3 (w × l × h) and 9 minor well dimensions of 6.1 × 6.8 × 1.3 mm^3 (w × l × h) was used.

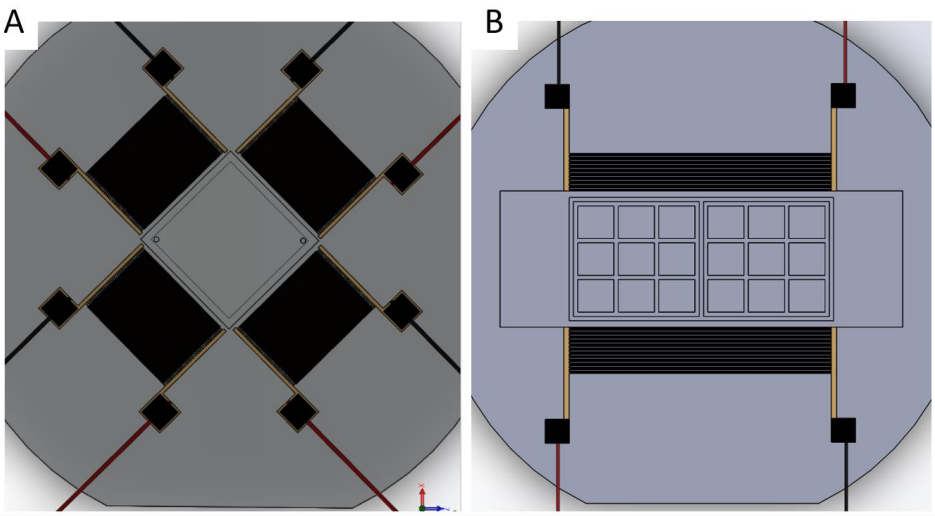

Figure 5: **SSAWs Platforms and chambers designs for cell agglomerate and linear patterning.** A) Square PDMS coupled to orthogonal IDTs pairs for cell agglomerate formation and B) Ibidi channel coupled to mirrored IDT pairs for linear patterning.

3.2.3 Cell culture and sample preparation

For the optimization of chambers and cell patterning efficiency, 9.9 μm polystyrene (PS) particles MCF-7 cells, MDA-MB-231 cells, and were used. MCF-7 and MDA-MB-231 were cultured in Dulbecco's modified Eagle medium (DMEM), supplemented with 10% fetal bovine serum (FBS) and 1% penicillin/streptomycin (P/S). Cells were cultured in a humidified incubator supplemented with 5% CO_2 at 37° C. Cell suspensions were made by detaching cells using 0.25% trypsin-EDTA (Gibco 25200, Invitrogen Co.) when reaching an 80% confluency. Dissociated cells were centrifuged at 250 g for 5 min at room temperature and re-suspended in culture media. The cell density was measured using a Countess II FL Cell Counter (Invitrogen, Thermo Fisher Scientific, MA, USA). 9.9 μm PS particles were suspended in deionized water prior to experiments.

3.2.4 Cell Agglomerate Patterning Experimental Setup

For the cell/particle agglomerate formation module, an orthogonal setup was proposed, where four sets of intersecting IDTs were deposited 45° with respect to the X-propagation direction (Y-cut) to create a mesh-like orthogonal nodal distribution (Figure 5A). A cell/particle suspension was first injected into the square PDMS microfluidic chamber. Next, two independent radiofrequency

(RF) signals of frequencies were generated via a function generator (AFG3102C, Tektronix, USA) connected to each pair of IDTs and modulated with an amplifier (25A100A, Amplified Research, USA). Cells/particles aggregated into pressure nodes by the overlap of four intersecting and travelling waves forming a mesh-like pressure nodal distribution, within seconds. The input voltage varied from 10 Vpp to 40 Vpp and the frequency range varied between of 12.5 to 13.7 MHz. The cell/particle movement was tracked and recorded using a QImaging camera (Retiga 2000R) connected to an inverted microscope (TE2000U, Nikon, USA).

3.2.5 Parallel-Lines Cell Patterning Experimental Setup

For the linear cell patterns, only one independent and controllable RF signal was generated using a function generator connected one pair of mirrored IDTs and modulated with an amplifier (Figure 5B). The working frequencies varied between 12.5 and 13.7 MHz. Different chamber configurations were tested as described in *3.2.2 SSAW Device Fabrication*, where cells were injected into the chamber and the chamber was then coupled to the lithium niobate wafer using a drop of water to transfer the SAWs. Upon a RF signal, cells aggregated into pressure nodal lines by the overlap of two opposite travelling SAWs. The cell/particle movement was tracked and recorded using a QImaging camera (Retiga 2000R) connected to an inverted microscope (TE2000U, Nikon, USA).

3.2.5 Live Dead Assay

Living cells were labeled with green fluorescence using calcein AM, while dead cells were labeled with red fluorescence using ethidium homodimer-III (Live/Dead viability kit) following the manufacturer's protocol. The cellular viability was calculated as the percentage ratio of green-fluorescent cells divided by the total fluorescent cell area using ImageJ.

$$\%\, Cell\ Viability = \frac{F(Calcein)_{494/517nm} - F(Eth\ Hom\ III)_{528/617nm}}{F(Calcein)_{494/517nm} + F(Eth\ Hom\ III)_{528/617nm}} \times 100\% \qquad \textbf{(Eq. 4)}$$

3.3 Results and Discussion

3.3.1 Cell Agglomerate Patterning using Orthogonal IDTs

To create mesh-like patterning with cells aggregated in pressure nodes, the first proposed device consisted of two orthogonal pairs of IDTs deposited at 45° from the Y-cut (X-propagating) direction of the $LiNbO_3$ substrate. A hollow PDMS square was bonded to a glass slide via plasma bonding, and it was then coupled to the piezoelectric substrate using a drop of water. Due to the

piezoelectric effect, surface vibrations in the form of SSAWs are formed at the surface of the piezoelectric substrate by applying independent RF signals to the two pairs of IDTs, creating a mesh-array of nodes and anti-nodes (Figure 6A). These waves, also known as Rayleigh waves, are then transferred to the PDMS chamber via the substrate-liquid interface where leaky waves transfer to the medium inducing cells to agglomerate into pressure nodes (Figure 6B).

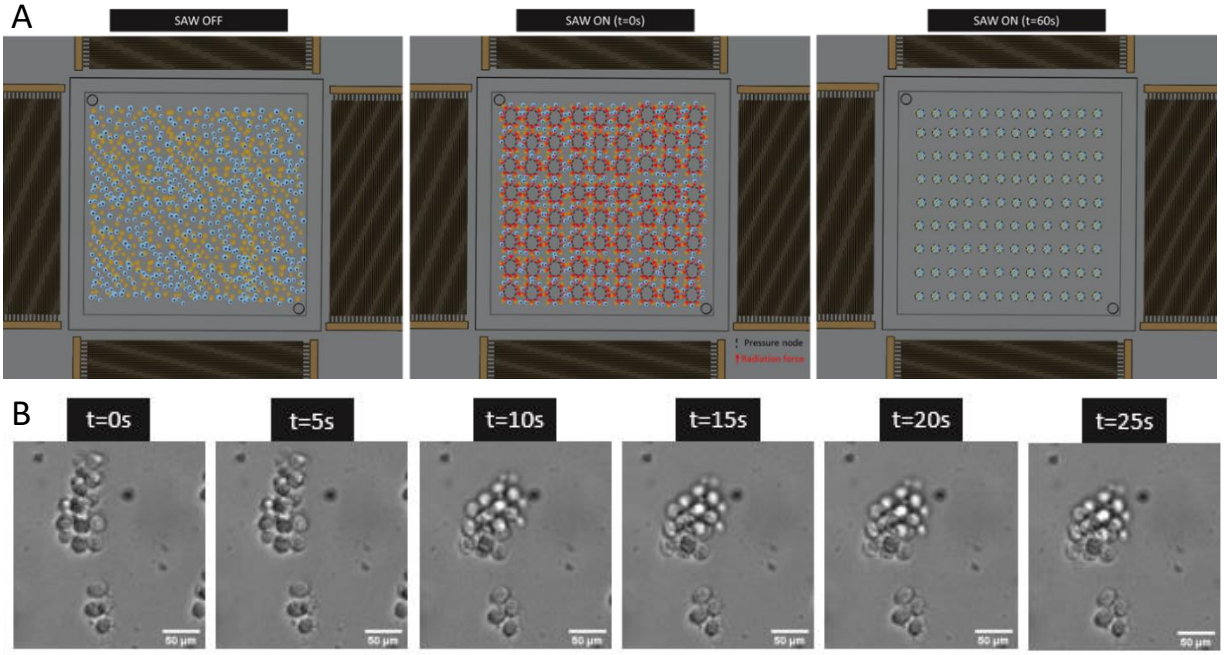

Figure 6: Cell agglomerate patterning module. A) Schematic of cell agglomerate formation upon two SAWs in orthogonal directions due to ARFs. B) Cell aggregate formation after <30s of SSAW induction. Scale bar is 50 µm.

The primary acoustic radiation force is the main responsible to guide cells towards pressure nodes areas pushing cells to aggregate and form a nodal distribution. In the acoustic standing wave field, the acoustic radiation force, acting on a cell or particle is described by **Eq. 1.**[35] The acoustic contrast factor $\phi(\beta, \rho)$ as described in **Eq. 2**[34] determines the direction of the cells towards a pressure node or antinode, if ϕ is positive or negative, respectively. For particles that are denser than the medium, $\phi(\beta, \rho)$ becomes positive and the primary ARF is directed towards the pressure nodes, which is the case for cells or particles suspended in culture media or DI water.

3.3.2 Formation of Cell Agglomerates in Different Culture Chambers

Prior to the optimization of the cell agglomerate formation module, the effects of activating one or two pairs of IDTs on PS particle aggregation were evaluated. As observed in Figure 7A, upon the activation of one pair of IDTs with a frequency of 12.51MHz and a $20V_{pp}$ amplitude, PS particles

successfully aligned to the orientation of the active IDTs, showing a consistent and well-defined linear pattern with a pressure nodal line distance of 145.48 ± 14.35 µm, matching the theoretical half-of-a-wavelength relationship, $\lambda_{SAW}/2$=150µm (or twice the IDT finger thickness, λ_{SAW}=4t).

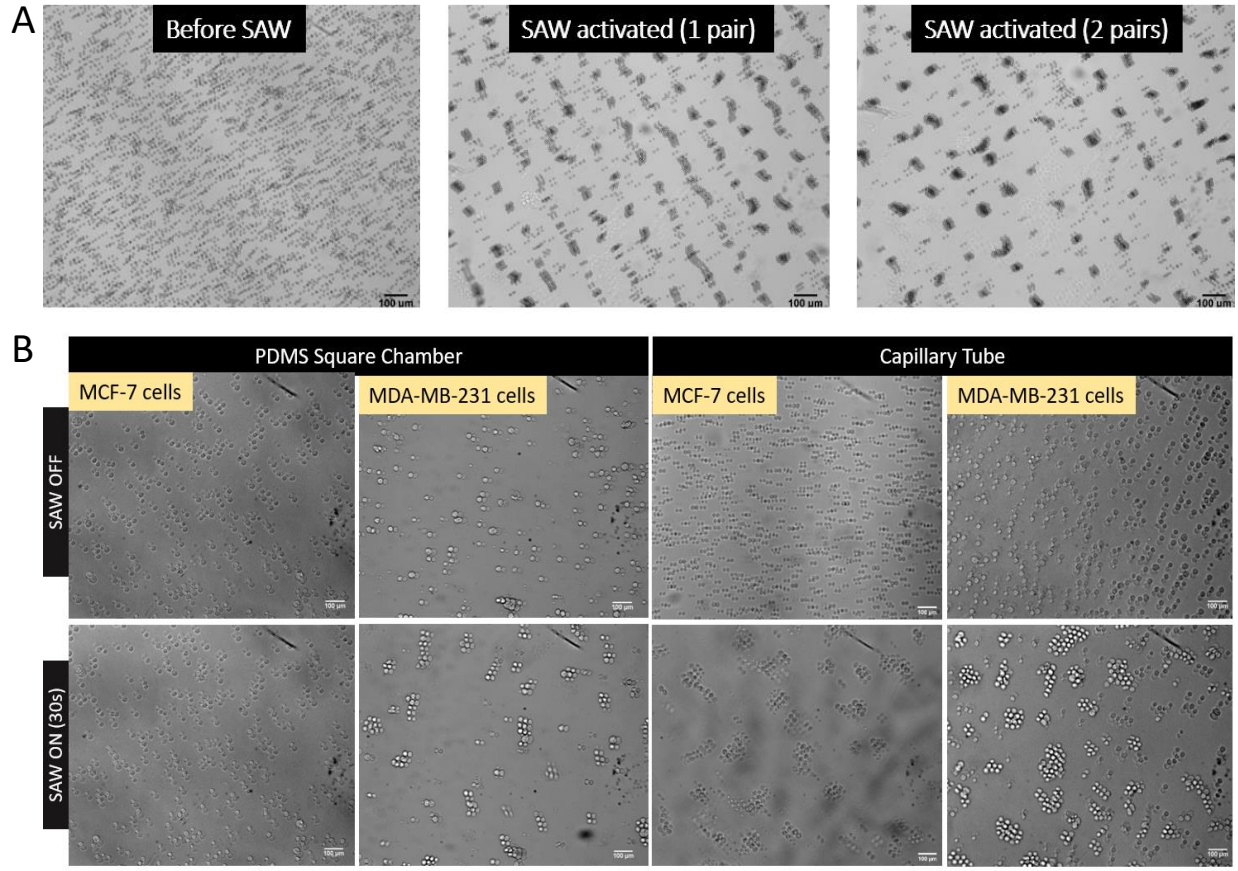

Figure 7: Particle/Cell Aggregation using two pairs of IDTs at 45° from the X-propagation direction of the $LiNbO_3$. A) Effects of one and two IDT pairs activated for PS particles aggregation. B) Cell patterning upon activation of two pairs of IDTs in a PDMS Square Chamber bonded to a glass slide for MCF-7 and MDA-MB-231 cells, and capillary tube for MCF-7 and MDA-MB-231. Scale bar is 100 µm.

Upon the activation of the second pair of IDTs using a similar frequency and voltage, particles started aggregating in a dotted-like distribution with around 52.36 ± 8.79 µm particles being aggregated, and a pressure nodal distance of 152.78 ± 11.56 µm for the opposite orientation. This mechanism was further evaluated using MCF-7 and MDA-MB-231 cells (Figure 7B). However, as noticed, poor efficiency in the cell agglomerate patterning was observed in comparison to PS particles due a reduced contrast factor ($\phi(\beta, \rho)$) between cells and culture media, thus challenging cells to move to towards pressure nodes. Despite potential solutions to improve the manipulation

efficiency of cells, increasing the working voltage, or amplitude, leads to overheating problems which can damage the piezoelectric device and can also hinder the cell viability.

Therefore, as an attempt to improve the patterning efficiency, capillary rectangular tubes were used to reduce the acoustic impedance and enhance the acoustic wave transfer throughout the liquid medium and alleviate problems with the viscous PDMS square chamber, which could dampen the waves upon reaching the chamber's walls. As observed, cells aggregated more efficiently in pressure nodes with a higher cell density per node. However, working with capillary tubes have some challenges, including non-uniformity of patterns throughout the capillary tube, as only the region enclosed by the IDTs is patterned. Moreover, streaming due to the open ends of the capillary affected the stability and efficiency of patterning, which could also bring challenges with preserving the cell viability. Additionally, retrievability was challenging after cell patterning, as the pattern was easily disrupted, which did not allow to culture the cell agglomerates for long-term.

3.3.3 Linear Cell Patterning using Parallel IDTs

In order to solve challenges with stability and efficiency of the cell agglomerate patterns and further induce cell-cell interactions for tissue development, a different approach was proposed. This configuration was comprised of one pair of opposite-facing IDTs deposited parallel to the Y-Cut (X-propagating) to maximize the wave intensity. A PDMS chamber with parallel channels was bonded to a glass slide (Figure 8A) and coupled to the piezoelectric platform using a drop of water. Upon an RF signal, opposite traveling SAWs intersect and create regions of maximum and minimum amplitude, corresponding to pressure antinodes and nodes. Particles are pushed towards pressure nodes due to acoustic radiation forces, thus creating linear and parallel particle patterns. This method was first validated using 9.9µm PS particles, where particle agglomerates were formed after 5 seconds of SSAW induction, with a consistent pressure nodal distance of 151.45 ± 4.51 µm (Figure 8B).

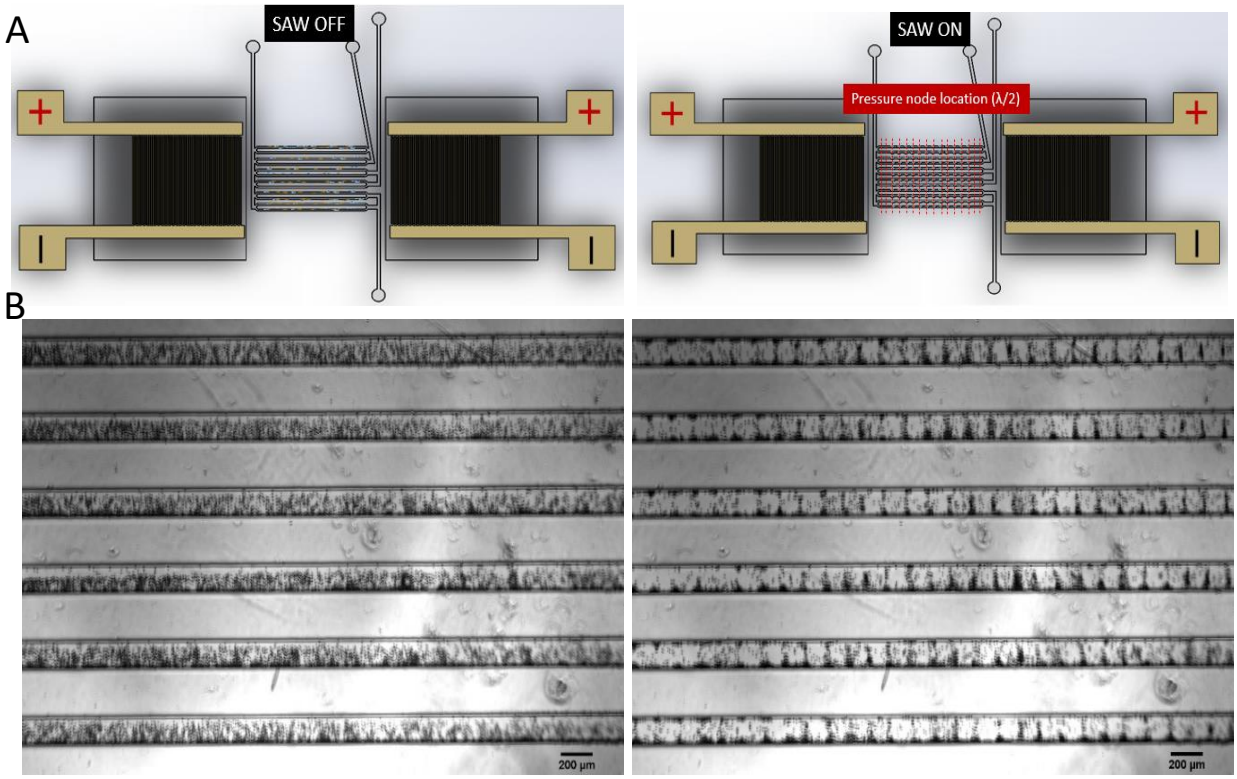

Figure 8: Linear patterning module. A) Linear-Patterning Schematic using one pair of IDTs opposite-facing each other with parallel PDMS channels. B) PS particles being patterned after SSAW was induced for 5 seconds. Scale bar is 200 µm.

To validate the platform, MCF-7 and MDA-MB-231 cells in suspension were injected into the PDMS parallel channels, separately, and the setup was subjected to SSAWs with a frequency of 13.17MHz and 40V_{pp}. When the SSAWs transmitted through the bottom glass slide bonded to the parallel PDMS channels, come in contact with the liquid medium, a linear pressure node distribution is formed inside each parallel channel. Cells aggregate to form cell clusters due to primary acoustic radiation forces pushing them to pressure nodes, and scattering forces from secondary acoustic radiation forces inducing cell-cell contacts (Figure 9A).[26] Cell clusters have a nearly uniform density as they are evently separated by the same pressure nodal distance ($\lambda_{SAW}/2$~150 µm) and the same channel boundaries (w=150 µm, h=150 µm).

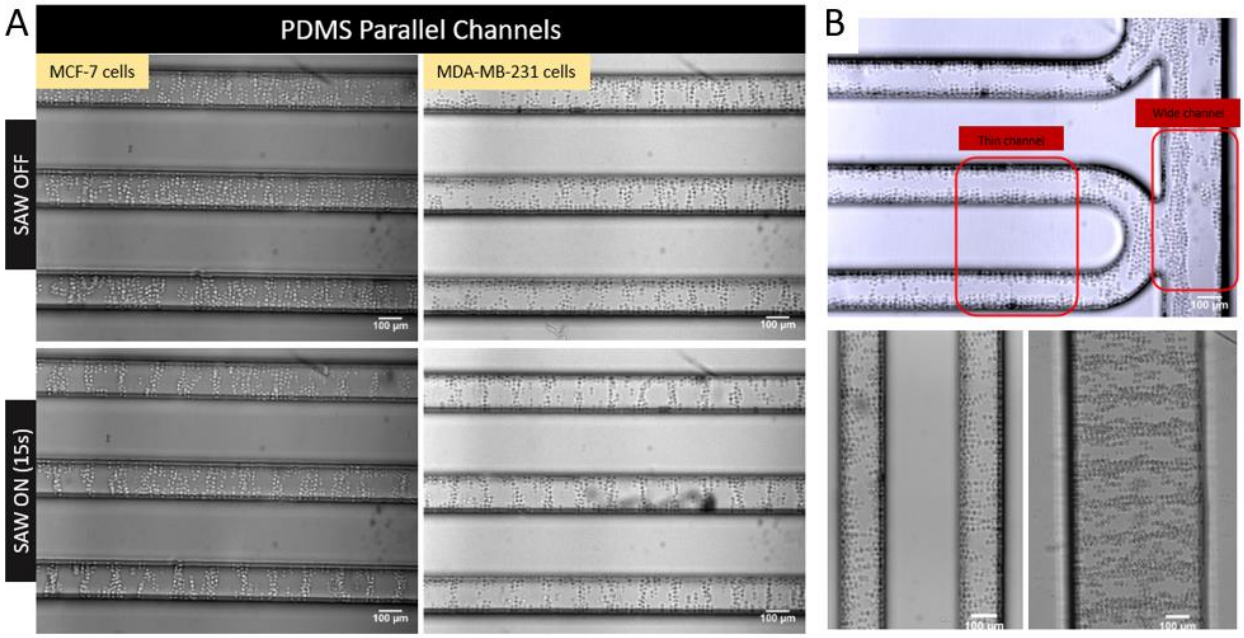

Figure 9: Linear Patterning using Parallel channels. A) Before and after SAW patterning of MCF-7 (left) and MDA-MB-231 (right) showing cell pressure lines. B) Effects of thinner and wider channels for linear node patterning with better reproducibility for wider channels.

One challenge of this method, however, is that after a few seconds of SSAW induction, microstreaming is present, causing cells to attach to the boundaries of the channels, thus disrupting the cell agglomerates. Conversely, with the induction of SSAWs for only a few seconds, cells do not form strong connections among them, thus clusters are easily disrupted. Interestingly, when observing the patterning behaviour in wider channel areas (Figure 9B, top) we observed that patterning was better mainted, leading to more uniform linear arrangements of cells, as microstreaming drag forces suggest to be reduced in wider channels (Figure 9B, bottom).[73] Another limitation of this platform is the retrievability of cell-cell patterns for long-term culture, which challenges the fabrication of relevant tissue constructs for tissue engineering applications.

Therefore, to further optimize the linear patterning module and create more reproducible cellular patterns for long term culture, while allowing waves to transfer more effectively into the fluid medium, both in-lab and commercial chambers were used with MDA-MB-231 cells suspended in DMEM. Figure 10A, B, C show three different chambers to form linear pressure node patterns, consisting of a square PDMS channel bonded to a glass slide (1.21×10^5 cells/mL), glass-PDMS bonded to a glass slide (0.97×10^5 cells/mL), and a μ-Slide 9 × 2 well (ibidi®) (1.32×10^5 cells/mL).

Poor linear patterning of cells was observed in the PDMS-glass slide configuration due to potential wave attenuation and damping of the wave once it reaches the PDMS walls. Another challenge with this setup was that often bubbles get trapped inside the channel, which can lead to undesired microstreaming causing cell patterns to get disrupted. As previously reported, bubbles exposed to an external acoustic field, are subjected to hydrodynamic forces that scatter around them thus leading to oscillations nearby the boundary of the bubble.[26,74] The glass-PDMS bonded to a glass slide allowed for a slightly better patterning of cells, however, it still remained as an inefficient and unreproducible patterning method. Another challenge of this platform was the presence of air bubbles after gravity sealing of the top glass slide to the chamber, due to surface tension, leading to problems with microstreaming.

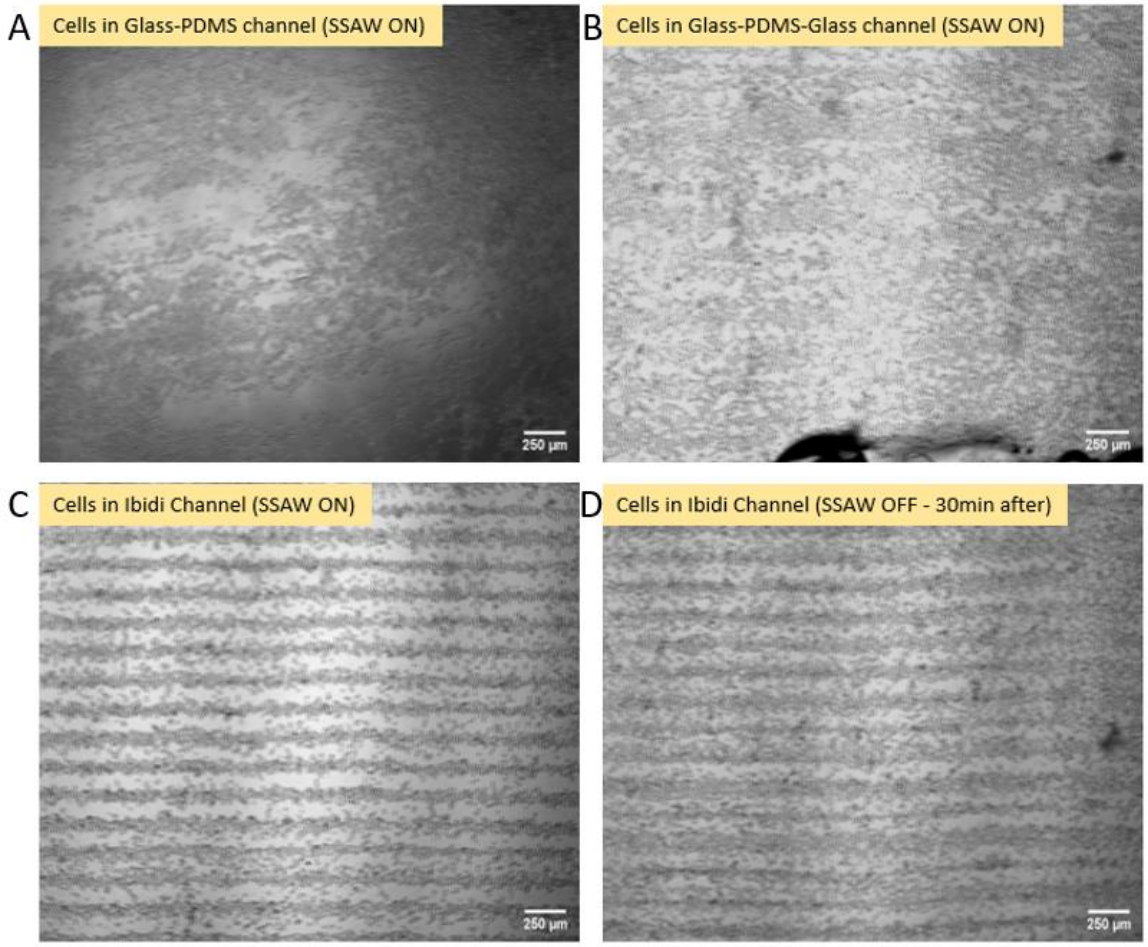

Figure 10: Linear Patterning Optimization. A) MDA-MB-231 cells contained in a square PDMS bonded to a glass slide. B) MDA-MB-231 cells contained in a hollow square PDMS bonded to two glass slides (top and bottom). C) MDA-MB-231 cells acoustically patterned in a µ-Slide channel (ibidi®). D) MDA-MB-231 cells showing pattern preservation in the µ-Slide 30 minutes after being acoustically patterned. Scale bar is 250 µm.

Conversely, a 9 × 2 well μ-Slide (ibidi®) allowed to culture and pattern cells in different wells while preserving a sterile environment with its chambered coverslip. SSAWs leaked more efficiently due to the polymer-based wells in comparison to the PDMS channel configurations, where defined pressure lines were observed after a few seconds (<30 s) of SSAW induction. As such, MDA-MB-231 cells formed linear patterns in DMEM 30 minutes after SSAWs were turned off (Figure 10D) with high reproducibility. Therefore, this platform was used for the rest of the experiments. Indeed, despite the well-established photolithography and replica molding manufacturing techniques for PDMS-based chambers, limitations including long fabrication times, single-use nature, imperfect surface wall finishing, limitations with sterility and long-term culture, and improper material bonding leading to undesired microstreaming can challenge the use of PDMS platforms for high-throughput applications in cell patterning and tissue engineering. The proposed μ-Slide well channel successfully allowed consistent and well-defined nodal lines, while proving that these lines could be preserved for up to 30 minutes in regular media after SSAWs were turned off (Figure 10D). Moreover, the simple manipulation of cells using this platform, with no need for sterilization, easy injectability of cells-media solution into the platform, compatibility with hydrogels, easy coupling to the piezoelectric wafer, and facile imaging, make this method to be more reproducible for high-throughput applications.

3.3.4 Cell viability and Co-Culture Cell Patterning

To validate the SSAW platform and study the effects of SSAW patterning on cell behaviour, we quantified the cell viability using the Live/Dead Assay kit. SSAWs were induced and fluorescent images were taken after 15 and 30 min of continuous induction of SSAWs at 40Vpp voltage and a constant frequency (13.11 MHz) (Figure 11A, B). As observed, the cell viability does not seem to be compromised (>85%) between 0 to 30 min of continuous SSAW induction, being a significantly longer time than the actual average time to aggregate cells into pressure nodes (<30 s). These results confirmed the biocompatible nature of SSAWs for cell patterning to promote cell-cell interactions, and thus would open a new avenue of opportunities in inductive tissue engineering.

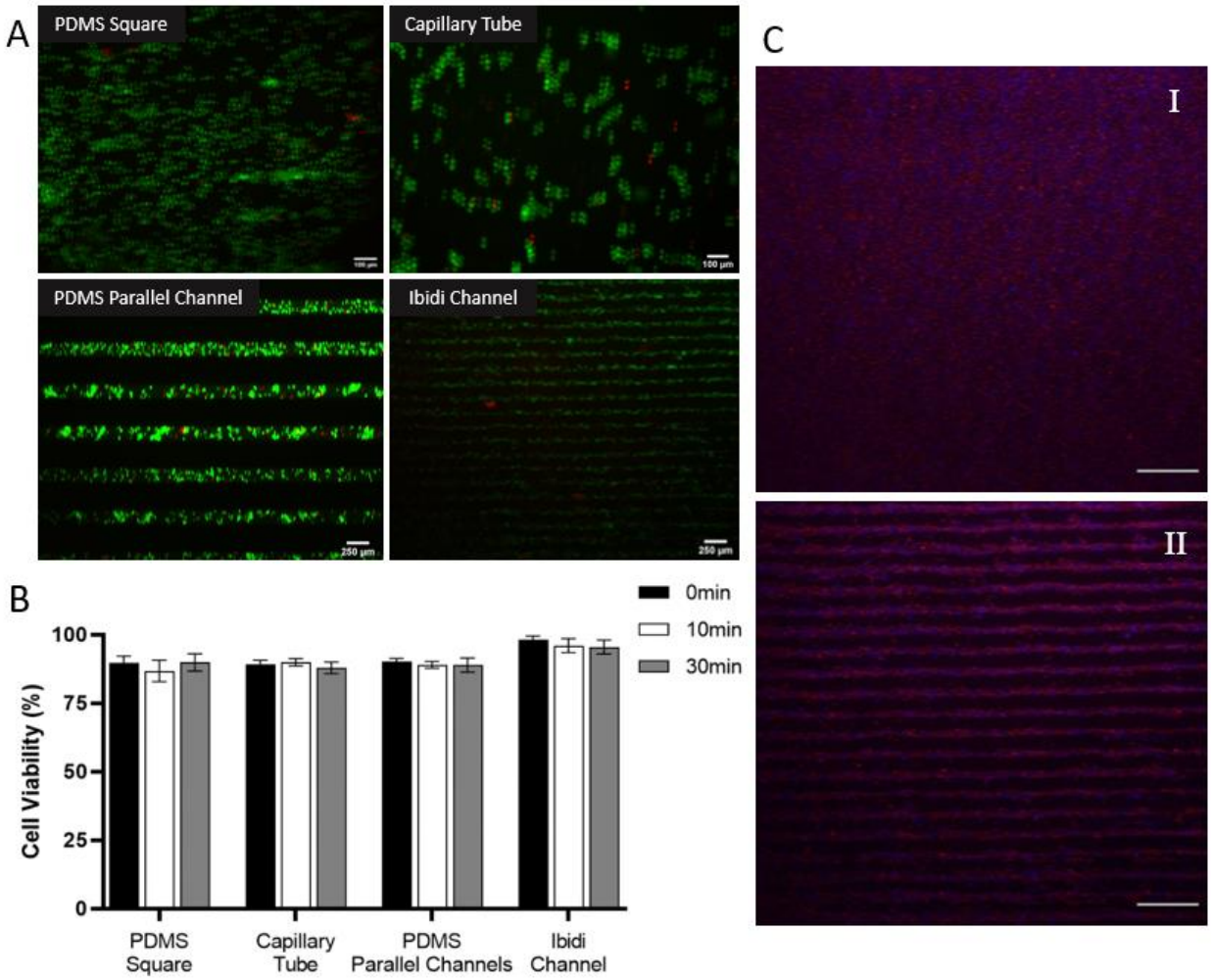

Figure 11: Platforms Validation via Cell Viability and Co-Culture Patterning. A) Calcein AM (green)/homodimer-III (red) stained MDA-MB-231 cells showing cell viability preservation after 30 min of SSAW activation at 40Vpp using a PDMS Square chamber bonded to a glass slide (Scale bar = 100µm), Capillary Tube (Scale bar = 100µm), PDMS Parallel Channel (Scale bar = 250µm), and 9 × 2 well µ-Slide (ibidi®) (Scale bar = 250µm). B) Cell viability for different chambers after 30 min of SSAW activation without significant changes in viability suggesting its high biocompatibility. C) Proof of concept of co-culture patterning prior (I) and after (II) SSAW induction using MCF-7 (blue) and MDA-MB-231 (red) (Scale bar = 500µm).

In addition to the studies of cell viability using homotypic cell-cell patterning, our SSAW platform was further used to investigate the potential of cell-cell interactions in coculture. As a proof of concept, a preliminary experiment demonstrated that two cancer cell lines MCF-7, in blue, and MDA-MB-231, in red, (Figure 11B) can be successfully patterned at defined node locations using SSAWs. The two cells were evenly distributed with defined pressure node lines and similar densities after a few seconds of SSAW induction (<15 s). Therefore, the results presented in this

preliminary work section, showed the potential of using surface acoustic waves to form linear homo- and heterotypic cell arrangements. The preserved viability during SSAW induction and its rapid and contactless operating nature motivated us to further study SSAWs for spatial and temporal patterning of multipotent cells, such as mesenchymal stem cells, allowing for cell-cell communication to potential benefit the differentiation process. Moreover, the easy manipulation using a 9 × 2 well μ-Slide (ibidi®) coupled with the theory of SSAWs may allow us to introduce hydrogels to preserve cell patterns for long term culture that can be potentially used as regenerative patches. The next chapter will discuss the role of SSAWs for adipose-derived mesenchymal stem cells patterning in hydrogels and the influence of cell-cell patterning on metabolic activity and osteogenic differentiation potential of adipose derived stem cells.

CHAPTER 4: ORIGINAL PUBLICATION – MANUSCRIPT ARTICLE

This chapter presents the original publication of the author that has been submitted to the Journal Microengineering and Nanotechnology on the 16th of February of 2022, and re-submitted after addressing the reviewers' comments on the 20th of May of 2022.

Manuscript #	MICRONANO-02120
Current Revision #	0
Submission Date	16th Feb 22 20:30:16
Current Stage	Manuscript Under Consideration
Title	Enhancing Metabolic Activity and Differentiation Potential in Adipose Mesenchymal Stem Cells via High-Resolution Surface Acoustic Waves Contactless Patterning
Running Head	Contactless Stem Cells Patterning via Surface Acoustic Waves
Manuscript Type	Article
Word Count	6334
Corresponding Author	Professor Maryam Tabrizian (maryam.tabrizian@mcgill.ca) (McGill University)
Contributing Authors	Ms Karina Martinez Villegas , Mr Reza Rasouli
Authorship	Yes
Abstract	Acoustofluidics has shown great potential for label-free bioparticle patterning with excellent biocompatibility. Acoustofluidics patterning enables inducing cell-cell interactions, which play fundamental roles in organogenesis and tissue development. One of the current challenges in tissue engineering is not only to control the spatial arrangement of cells but to preserve the cell pattern over time. In this work, we developed a standing surface acoustic wave-based platform and demonstrated its capability for well-controlled and rapid cell patterning of adipose-derived mesenchymal stem cells in a high-density homogenous collagen hydrogel. The biocompatible hydrogel is easily UV crosslinked and can be retrieved in 3 minutes. Acoustic waves successfully guided cells towards pressure nodal lines, creating a contactless alignment of cells within < 5s in culture media and <1min in the hydrogel. Acoustically patterned cells in hydrogel did not show a decrease in cell viability (>90%) 48hr after acoustic induction. Moreover, a 45.53% and 30.85% metabolic activity increase was observed in growth and differentiation media, respectively, at day 7. On day 14, the change in the metabolic activity was 32.03% using growth media, and no significant difference was observed in differentiation media. The alkaline phosphatase activity showed an increase of 80.89% and 24.90% at days 7 and 14, respectively, for acoustically patterned cells in the hydrogel. These results confirm the preservation of cellular viability and improved cellular functionality using the proposed high-resolution acoustic patterning technique and introduce unique opportunities for the application of stem cell regenerative patches for the emerging field of tissue engineering.
Subject Terms	Physical sciences/Engineering Physical sciences/Materials science
Research Square author dashboard	I understand that my manuscript and associated personal data will be shared with Research Square for the delivery of the author dashboard.
Conflict of Interest	There is no conflict of interest
Clinical Trial	No
Clinical Trial	No
Applicable Funding Source	Natural Science and Engineering Council of Canada [Tabrizian]

Manuscript Items

1. Author Cover Letter PDF (117KB)
2. Article File PDF (1097KB)
3. 0 - Video of self-standing patch Source file (1353KB)
4. Supplementary information PDF (519KB)
5. Reviewer Zip File "Zip of files for Reviewer"

Manuscript Tasks

Send Manuscript Correspondence

Check Status

Enhancing Metabolic Activity and Differentiation Potential in Adipose Mesenchymal Stem Cells via High-Resolution Surface Acoustic Waves Contactless Patterning

Running title: ASCs Patterning via High-Resolution Surface Acoustic Waves

Karina Martinez Villegas,[1] Reza Rasouli,[1] and Maryam Tabrizian[1, 2]*

[1] Department of Biological and Biomedical Engineering, [2] Faculty of Dental Medicine and Oral Health Sciences, McGill University, Montreal, QC, Canada

***Corresponding author:**

Dr. Maryam Tabrizian

3775 Rue University, Montreal, QC. H3A 2B4

Phone: (+1) 514-398-8129

Fax: (+1) 514-398-7461

Email: maryam.tabrizian@mcgill.ca

Other authors information:

Karina Martinez Villegas

E-mail: karina.martinezvillegas@mail.mcgill.ca

Reza Rasouli

E-mail: reza.rasouli@mail.mcgill.ca

4.1 Abstract

Acoustofluidics has shown great potential for label-free bioparticle patterning with excellent biocompatibility. Acoustofluidics patterning enables inducing cell-cell interactions, which play fundamental roles in organogenesis and tissue development. One of the current challenges in tissue engineering is not only to control the spatial arrangement of cells but to preserve the cell pattern over time. In this work, we developed a standing surface acoustic wave-based platform and demonstrated its capability for well-controlled and rapid cell patterning of adipose-derived mesenchymal stem cells in a high-density homogenous collagen hydrogel. The biocompatible hydrogel is easily UV crosslinked and can be retrieved in 3 minutes. Acoustic waves successfully guided cells towards pressure nodal lines, creating a contactless alignment of cells within < 5s in culture media and <1min in the hydrogel. Acoustically patterned cells in hydrogel did not show a decrease in cell viability (>90%) 48hr after acoustic induction. Moreover, a 45.53% and 30.85% metabolic activity increase was observed in growth and differentiation media, respectively, at day 7. On day 14, the change in the metabolic activity was 32.03% using growth media, and no significant difference was observed in differentiation media. The alkaline phosphatase activity showed an increase of 80.89% and 24.90% at days 7 and 14, respectively, for acoustically patterned cells in the hydrogel. These results confirm the preservation of cellular viability and improved cellular functionality using the proposed high-resolution acoustic patterning technique and introduce unique opportunities for the application of stem cell regenerative patches for the emerging field of tissue engineering.

Keywords: acoustofluidics, surface acoustic waves, cell patterning, cell differentiation, metabolic activity, adipose-derived mesenchymal stem cells, collagen, hydrogel, tissue engineering.

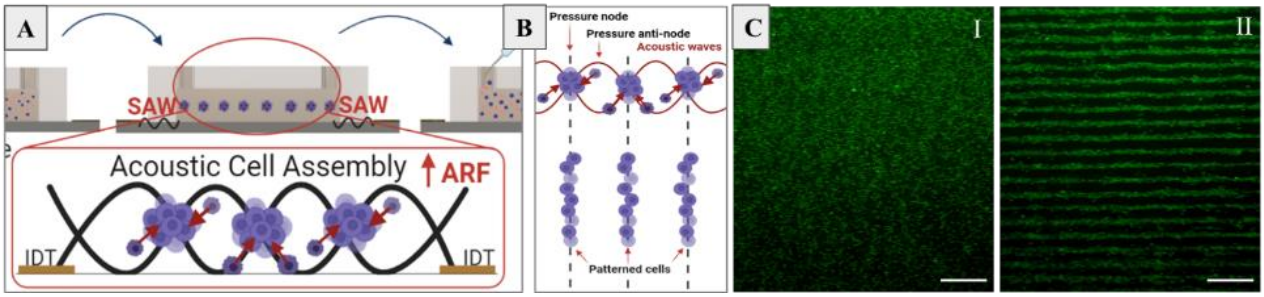

Figure 4.1: Graphical Abstract – Cell patterning working mechanism. A) Illustrative schematic of cell aggregation upon the activation of SAWs traveling in opposite directions to create standing waves. B) Working principle of cell patterning, showing cells getting guided into pressure nodes due to ARFs. C) LIVE/DEAD pictures of SSAW patterned cells (II) with defined location and high spatial resolution and control cells with no SSAW induced (I). Scale bar is 500µm.

4.2 Introduction

Biological tissues rely on microenvironmental cues, including homotypic and heterotypic cell-cell contacts, extracellular matrix (ECM) stimuli, mechanical forces, and chemical signaling. Cell-to-cell signaling is crucial in numerous biological processes, including the kinetics of aggregation in new tissues, cell migration, proliferation, differentiation, and organogenesis.[8,10,11,44,75,76] Intercellular communication is also instrumental during cell aggregation and cell assembly processes, being the first step in tissue development. Three processes are often involved in the compaction and formation of cellular patterns, including the interactions between the ECM and integrin as physical linkers to promote cellular attachment, the upregulation of cadherins upon cell-cell aggregation, and the homophilic interactions of E-cadherins to initiate strong cell adhesion.[77,78] Intercellular adhesion proteins, including connexins and pannexins, also regulate cell-cell interactions and respond to the forces experienced by the cell, which modulate the strength of adhesion, the activity of mechanosensitive signaling pathways, and contribute to the formation of cell patterns and organized structures.[78,79] By facilitating the cell-cell contacts via controlled spatial arrangements, cell signaling and communication can be enhanced improving the tissue functionality and replicating the native tissue architecture.[72]

Despite the interest in creating complex cellular constructs to mimic organized tissues, fabrication methods to control the spatial location of cells, face many limitations with efficiency and practicality. Conventional methods for cell patterning, including photolithography stamps,[13] optical tweezers,[80] magnetic patterning,[15] dielectrophoresis,[16] and 3D printing,[17] often experience long fabrication times, cell pattern heterogeneity, lack of cell density control, cell cytotoxicity, require conductive media, have low spatial resolution, and/or lack reproducibility. Furthermore, contact and high energy-based cell patterning methods can also cause alterations in the cell phenotype, which may affect the cell viability and functionality.

Acoustofluidics, the combination of acoustics and microfluidics, has been widely explored in the past two decades due to its high spatial and contactless control, coupled with its rapid operating mechanism. These characteristics together with its compatibility with hydrogels, allowing to preserve the cell pattern, render acoustofluidics as an attractive method in tissue engineering for cell spatial patterning. Typically, the first step in tissue engineering using acoustic radiation forces involves an initial organization of the cells into the desired pattern. This step is then followed by

a preservation step, in which the cell patterns are maintained over time in order for cells to establish connections and mature into tissues.[45]

While there are two main acoustic modes for cell manipulation, being Surface Acoustic Waves (SAWs) and Bulk Acoustic Waves (BAWs), SAWs offer greater advantages for cell patterning as they have higher resolution and lower power losses. The high frequency range of SSAWs in the mega-hertz to giga-hertz region allows for short wavelengths,[23] which minimizes the power consumption, making it a gentle manipulation method.[24,81] Moreover, the micron-order wavelengths in SAWs characterize them with high spatial resolution for the manipulation of single cells, where the operating frequency is confined to a singular frequency and it is dictated by the design of the interdigitated transducers (IDTs). Due to the piezoelectric effect, an electrical potential results in mechanical vibrations that propagate across the surface of the piezoelectric and through any secondary material coupled to the SAW device.[27] The configuration and location of the IDTs also determines the type of SAW, which can generate traveling or standing waves. Particularly, standing surface acoustic waves (SSAWs) are formed by placing opposite-facing pairs of IDTs on a piezoelectric substrate. Upon a radio frequency signal to the pair of IDTs, the opposite travelling waves create regions of low and high acoustic pressure, namely pressure nodes and antinodes, respectively. Therefore, cells can be guided towards the pressure nodes to create defined patterns.

Different biomaterials for cell-patterning preservation have been proposed to help build the tissue architecture. For instance, 3D fibroblast tissues were formed using NIH 3T3 fibroblasts in a solution of thrombin mixed with fibrinogen at an adjustable concentration where structures were crosslinked in 10 minutes.[41] Cage-like structures were shown after 30 hours due to cell migration, growth, and interactions with F-actin alignment. Conversely, in a collagen type I hydrogel, MCF-7 cells were patterned and polymerized after 10 min at neutral pH and 37°C by heat transferred from the IDTs, thus preserving cell viability.[55] In another study, co-aligned HUVECs and hASCs were patterned and preserved in a catechol-conjugated hyaluronic acid scaffold, and further implanted in a mouse model to create a functional collateral vascularized cylindroid for ischemia therapy.[8]

One limitation of these biomaterials, however, is the crosslinking time and uniformity of the scaffolds. As a solution, hydrogels that polymerize rapidly, such as photocurable polymers, can combine SSAW rapid patterning and crosslinking within a few minutes. Using different concentrations of PEGDA and GelMA® it allowed to rapidly crosslink HeLa, MC3T3-E1, and P12Adh cells via UV light to form cell-hydrogel patterns in capillary tubes in less than 5 minutes.[54] In a similar way, cardiomyocytes were mixed with a GelMA® solution followed by SSAW-patterning and UV crosslinking, where cardiomyocytes showed beating activity for up to 7 days.[44] Despite the similarity of the working methods for linear SSAW patterning, the effects of acoustic patterning of adipose-derived stem cells in a 3D environment for the preservation of cell viability, the improvement of the metabolic activity on patterned cells, and the differentiation of patterned stem cells into an osteogenic lineage as a proof-of-concept of a regenerative tissue patch, has not yet been reported to our knowledge.

Therefore, in this work we propose a SSAW-based cell patterning platform to fabricate rapid cell-laden hydrogel constructs using a methracylated collagen type I hydrogel (PhotoCol®-LAP) with the capability of being retrieved from the platform <3 min of photo crosslinking. Collagen is the most abundant component of the ECM and it is commonly used in tissue engineering as it recapitulates the native tissue microenvironment.[30] Furthermore, the flexibility of PhotoCol®-LAP as a UV sensitive hydrogel can preserve the high resolution of SSAWs by rapidly crosslinking the aligned cells. A systematic experimental plan was used to demonstrate that the proposed acoustic force-based microfluidics platform has the capability to rapidly control the spatial alignment of cells in a 3D matrix, while preserving the viability and improving the functionality of patterned cells. Bright-field and confocal microscopy techniques were used to study the linear arrangements of adipose-derived stem cells and their structural preservation over time. Live/dead cell assay, alamarBlue™ assay, and alkaline phosphatase enzymatic activity were assessed to investigate the effects of SSAWs on viability, metabolic activity, and osteogenic differentiation, respectively, of patterned cells in the hydrogel matrix for up to 14 days. Furthermore, the expression of osteocalcin in patterned cells in comparison to control cells was imaged using confocal fluorescence microscopy to confirm the potential of this SSAW-based platform for tissue engineering by creating an *in vitro* biomimetic tissue construct.

4.3 Results and Discussion

4.3.1 Parameters Optimization of SSAW Platform Using PS particles and MC3T3-E1 Cells

4.3.1.1 SSAW Working Mechanism and Device Fabrication and Working Principles

Figure 4.2A illustrates the SSAW patterning device, which is comprised of one pair of mirrored IDTs deposited on a $LiNbO_3$ substrate. Standing surface acoustic waves (SSAWs) are generated upon a radio frequency (RF) signal is being applied to each set of IDTs, where two identical but opposite traveling waves propagate on the surface of the $LiNbO_3$. The interference between the two traveling SAWs forms a periodic distribution of pressure nodes and antinodes with minimum and maximum pressure amplitudes, respectively. Each set of IDTs consisted of 40 pairs of electrodes with a finger thickness (t_{IDT}) and periodic spacing of 75µm. The wavelength (λ) of the SSAW is 300µm, defined as twice the pitch (d) of the IDT ($d=2t_{IDT}$), and thus the distance between each pressure node is 150µm, or half a SSAW wavelength. Prior to the optimization of the platform, the theoretical resonant frequency, was approximated calculated as $f = c_s/\lambda \approx 13.27MHz$, where c_s and λ are the speed of sound in $LiNbO_3$ (*3980m/s*) and the theoretical SSAW wavelength ($300\mu m$), respectively. The working frequency was, however, experimentally optimized and determined to be 13.11MHz based on both the efficiency of manipulation, *i.e.*, how rapid the cells were guided towards the pressure nodes, and the stability of the pressure lines over time.

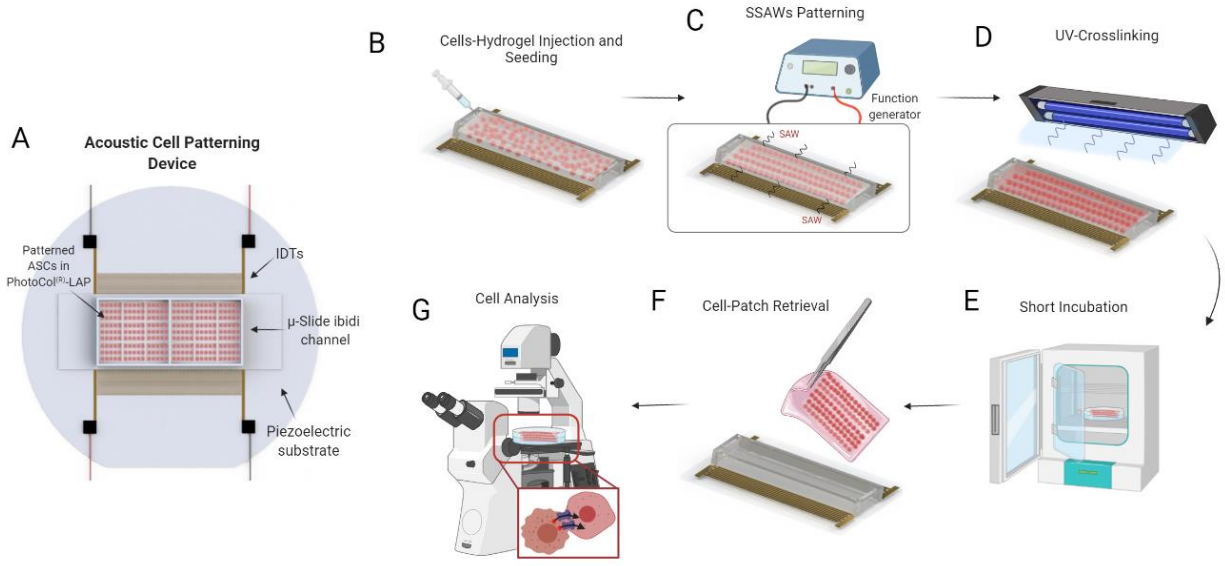

Figure 4.2: SSAW patterning platform and workflow of patterning mechanism and retrievability. A) Schematic of SSAW platform. B) Cells-Hydrogel solution is seeded into the platform. B) SSAW waves are induced to the IDTs via a function generator to create cell patterns.

D) UV light is applied to the patterned cells in the hydrogel to crosslink the scaffold. E) Short incubation of UV-crosslinked cells-hydrogel scaffold is done to complete the gelation of the cell-patch. F) Cell-Patch is retrieved from the platform for potential implantation. G) Cell analysis is performed at days 1, 7, and 14.

The governing force for cell patterning is the acoustic radiation force (ARF), or the time-averaged net force created by pressure fluctuations, and it can be classified in primary and secondary ARF. Primary acoustic radiation forces emerge from the direct irradiation of acoustic waves on cells, which in turn directs the cell trajectory to the defined pressure nodes; while both secondary radiation forces and drag forces induce and promote cell-cell interactions.[82] The primary ARF (F_r) acting on suspended, compressible, spherical particles in a liquid medium can be estimated as:[34]

$$F_r = -\left(\frac{\pi p_0^2 V_p \beta_f}{2\lambda}\right)\phi(\beta,\rho)\sin\left(\frac{4\pi x}{\lambda}\right) \quad \textbf{(Eq. 1)}$$

$$\phi(\beta,\rho) = \frac{5\rho_p - 2\rho_f}{2\rho_p + \rho_f} - \frac{\beta_p}{\beta_f} \quad \textbf{(Eq. 2)}$$

where p_0, V_p, β_f, βp, ρ_f, ρ_p, λ, and x are the acoustic pressure, volume of the particle, compressibility of the fluid, compressibility of the particle, density of the fluid, density of the particle, acoustic wavelength, and the distance from a pressure node, respectively. The acoustic contrast factor $\phi(\beta,\rho)$, determines the direction of the cells towards a pressure node or antinode, if ϕ is positive or negative, respectively. Therefore, for particles that are denser than the medium, $\phi(\beta,\rho)$ becomes positive and the primary ARF is directed towards the pressure nodes.

Rayleigh waves, also known as leaky waves, are often used in SSAW devices to pattern cells, as they can efficiently leak into the fluid medium in contact with the fluid path.[83] When the resonating Rayleigh wave encounters the liquid medium, it generates longitudinal-mode leaky waves, leading to pressure fluctuations within the medium.[38,84] By coupling the channel to the piezoelectric substrate via a drop of water, the waves can efficiently leak and create pressure nodal lines with defined boundaries. Polyimide tape was used in the proposed platform to enclose the SSAW working region, and thus improve the intensity of the ARF to pattern cells more efficiently.

For the cell-laden hydrogel constructs, the cells suspended in media were mixed with PhotoCol®-LAP to a 1:3 ratio. In the proposed design, a commercial ibidi μ-Slide channel was used due to its excellent optical quality and low acoustic damping. After activating an RF to each of the IDT pairs simultaneously, cells in PhotoCol®-LAP were patterned in parallel lines in less than 1 minute. In order to preserve the pattern of the cell-laden hydrogel constructs, UV light was applied at 10 cm

from the ibidi® coverlid for <3 minutes to induce gradual crosslinking while minimizing detrimental effects on cells. The samples were then placed in an incubator for less than 30 minutes to complete the gelation process. Retrievability of patterned cell-laden hydrogel constructs was achieved using conventional tweezers for potential implantation.

4.3.1.2 Device and Experimental Parameter Optimization

For the optimization of the patterning module, parameters including the cell tracking velocity, frequency, and voltage were carried out using MC3T3-E1 cells in growth media (alpha-MEM). Figure 4.3A shows the efficient patterning of SSAWs, prior (i) and after (ii) RF activation, revealing that the proposed SSAW platform is suitable as a high-resolution cell patterning method. For its part, the velocity was calculated using the ImageJ TrackMate plugin,[85] where videos were pre-processed to track individual cells at a 50 fps rate. Ten different voltages were used to capture the displacement of MC3T3-E1 cells where, as expected, the velocity of manipulation with the working voltage increases linearly (Figure 4.3B). Furthermore, Figure 4.3C shows the velocity distribution of MC3T3-E1 cells following a nearly normal distribution where the majority of cells are moving with an average velocity of ~50μm/s in αMEM media.

One challenge of using high voltages (>40V_{pp}) that should be considered in the design of an SSAW platform, is the proportional square increase of the heat generated on the piezoelectric substrate. In our platform, the working time in which the function generator is activated to translate electrical potentials into surface acoustic waves is very short (< than 30 seconds). Due to this short exposure time, even at high voltages (20 V_{pp} or 0.1 W ~ 20 dBm, for an impedance of 3.7kΩ at the IDT resonant frequency measured using an Agilent Precision Impedance Analyzer) no cell survival hindering is expected. Working with this input voltages and setup (including the coupling layer) did not lead to a significant increase in the temperature for the short time exposure. This was confirmed by the absence of crosslinking in the PhotoCol® hydrogel which is a temperature sensitive biomaterial, when the SAW was activated but UV light was absent. The biocompatible and low heat generation in controlled working conditions, for instance for the manipulation of HeLa cells, was previously shown using SAWs.[37] This work showed that even after a high-power exposure (23 dBm) for up to 10 minutes, no significant physiological damages were found to the cell viability and proliferation, where the temperature of the piezoelectric substrate increased less than 3 degrees (25°C to 27.9°C). It was also reported by the same group that even at a higher input

power of 25 dBm for the manipulation of larger organisms, such as C. elegans, the temperature reached a maximum temperature of 31°C after 10 minutes, thus not being detrimental to cell viability.[37] In another work, U-937 monocyte cells were induced to high-power SAWs (26.7 dBm) and cultured for up to 48hrs. These authors showed no detrimental effects on cell viability with maximum heating of the culture medium of only 0.5 +/- 0.2°C even in the presence of acoustic streaming.[86] It is important to note that for applications in biological research, a temperature under 40°C prevents protein denaturation and physiological damage to cells, which is significantly greater than the values that have been reported in the literature using SSAW devices for cell manipulation.[87] Another important design feature of our setup is the use of a non-elastomeric ibidi chamber which allows us to reduce the absorption of acoustic radiation, resulting in less heat being absorbed and as well as limiting the high-power consumption improving the efficiency of the device.[88]

Furthermore, parameters including the patterning time, the pressure node distance, the pattern preservation criteria, and cell viability were determined using different media conditions, including αDMEM complete media, serum-free αDMEM media, PBS 1X, PhotoCol® 2.0mg/mL, PhotoCol® 2.5mg/mL, and PhotoCol® 3.0mg/mL (Table 1). The time to guide cells towards the pressure nodes was very rapid in αDMEM complete media, serum-free αDMEM media, and PBS (1X) (<5 seconds). However, the cell pattern was not preserved over time, and it was easily disrupted few seconds after the SSAW signal was ceased. For the PhotoCol® samples, the time to guide cells was longer but still within seconds (<1 min). One other advantage of PhotoCol®-embedded samples is that the cell pattern was maintained over time by rapidly gelling the cell-laden hydrogel using UV light in less than 3 minutes.

Pressure nodal lines, which serves as an indicator of how reproducible our acoustic patterning method is, were calculated by averaging 100 different pressure nodal lines using ImageJ. The average distance between pressure lines for MC3T3-E1 suspended in growth media was 149.56 ± 5.03 µm. For serum-free media and PBS 1X solutions, the nodal location corresponded to 156 ± 1.21 µm and 149.24 ± 3.21 µm, respectively. Finally, for the cell-laden PhotoCol® samples the pressure node distance was measured for 3, 2.5, and 2 mg/mL (initial PhotoCol® concentration) to be 130.04 ± 8.53, 140.02 ± 10.41, and 152.02 ± 11.21 µm, respectively. All samples were

consistent and matched the theoretical value of 150 μm, or half a SSAW wavelength, suggesting the reproducibility of this method.

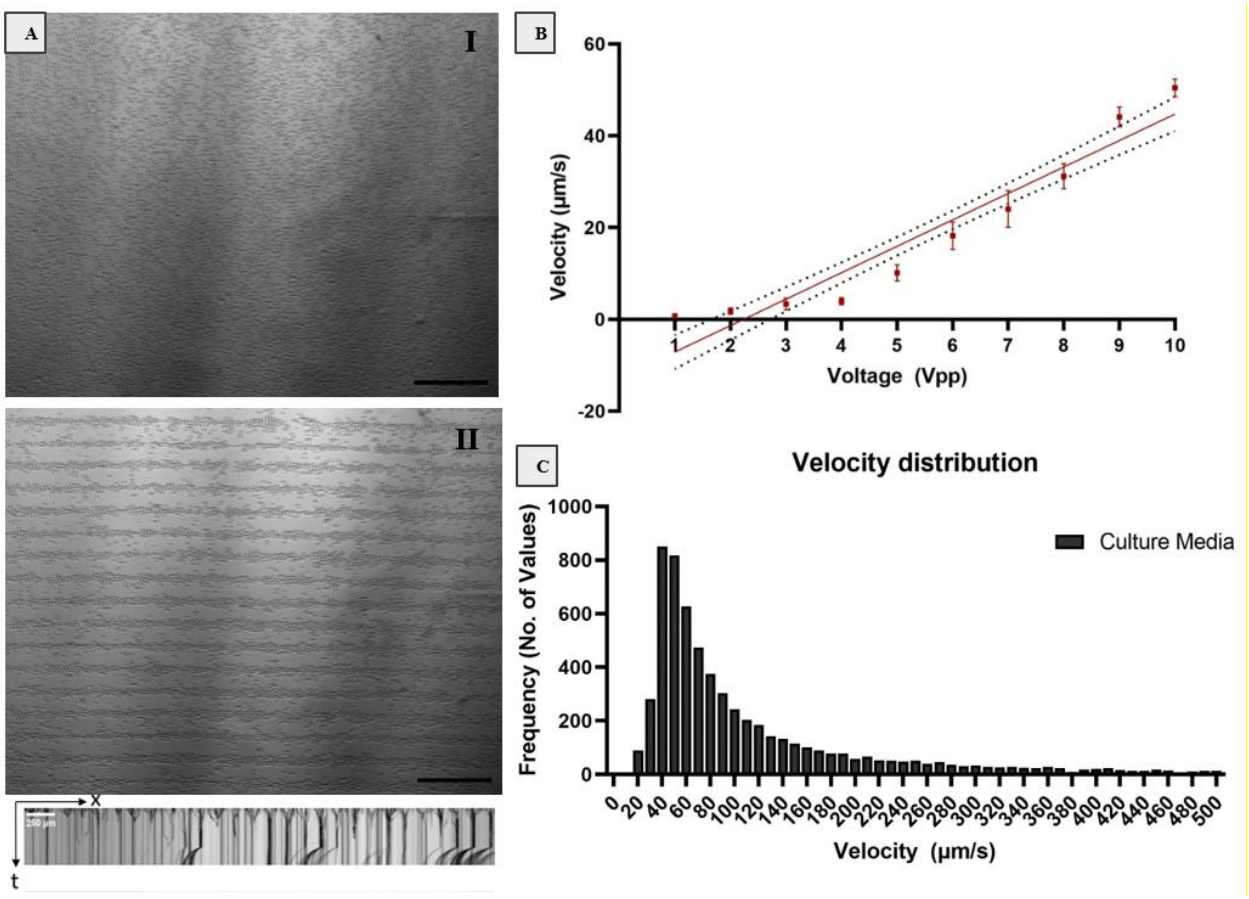

Figure 4.3: A) Cells prior SSAW activation and after SSAW activation with kymograph image showing nodal line distribution and distance. B) Velocity vs voltage plot. C) Velocity distribution of cells in culture media. Scale Bar is 500μm.

Interestingly, cell viability of >90% was shown for both regular growth media and serum-free media samples, proving the gentle nature and stress-free mechanism of SSAWs. However, for samples suspended in PBS 1X, cells were compromised 24hr after SSAW exposure (<60% cell viability), due to potential insufficient nutrients in the culture media. In addition, PhotoCol®-embedded samples showed lower viability for 2 mg/mL initial collagen concentration after 24 hrs, which can be attributed to the higher acetic acid content of the PhotoCol® solution at this lower concentration. In contrast, high viability (>90%) was observed for both 3 and 2.5 mg/mL collagen concentrations after 24 hrs. Therefore, a collagen concentration of 2.5 mg/mL was found to be not only highly biocompatible but also have a lower viscosity, reducing the patterning time with higher patterning flexibility.

Table 2: Parameter selection for SSAW-patterning optimization

Parameter/ Condition	Cell density (cells/mL)	Time to Guide Cells to Nodes (s)	Pressure Node Location (µm)	Cell viability (24hr)	Cell pattern preserved (24hr)
Culture Media	1.25×10^6	1.14 ± 0.03	149.56 ± 5.03	93.12 ± 3.23	×
Serum-Free Media	1.53×10^6	1.94 ± 0.26	156.02 ± 1.21	90.51 ± 2.01	×
PBS 1X	1.23×10^6	0.94 ± 0.26	149.24 ± 3.21	81.09 ± 2.11	×
Collagen 3mg/mL	9.45×10^5	25.09 ± 1.26	130.04 ± 8.53	93.23 ± 4.34	✓
Collagen 2.5mg/mL	1.02×10^6	18.94 ± 1.46	140.02 ± 10.41	90.07 ± 3.25	✓
Collagen 2mg/mL	9.91×10^5	16.45 ± 2.42	152.02 ± 11.21	76.18 ± 4.36	✓

Different cell conditions were also used to optimize the acoustic patterning module using culture media. Samples with different cell concentrations (2.5×10^6, 1.3×10^6, and 0.6×10^6 cells/mL) were injected into the ibidi chamber and were acoustically patterned. For these three different cell concentrations, the node distance and velocity of manipulation were very similar, indicating that the cell density has a negligible influence on the acoustic patterning using our platform (Figure 4.4C).

In addition to the initial organization of the cells into the desired pattern, a preservation step is fundamental to establish cell-cell connections and induce tissue maturation.[45] To preserve the cell pattern, ECM-based hydrogels are commonly used due to their high biocompatibility and tunable gelation, allowing to maintain cellular arrangements over time. For our platform, a UV-sensitive collagen-based matrix (PhotoCol®-LAP) was used to form cell-laden hydrogel constructs that can be retrievable after gelation. This dose allowed the hydrogel to crosslink in less than 3 minutes. As seen in Figure 4.4A, the retrievability of the cell-laden hydrogel constructs from the mini well is shown, after being exposed to UV light for 3 minutes. The easy manufacturing steps and easy retrievability using conventional tweezers suggest the great potential of our acoustic patterned cell-laden hydrogel as a regenerative tissue patch for transplantation.

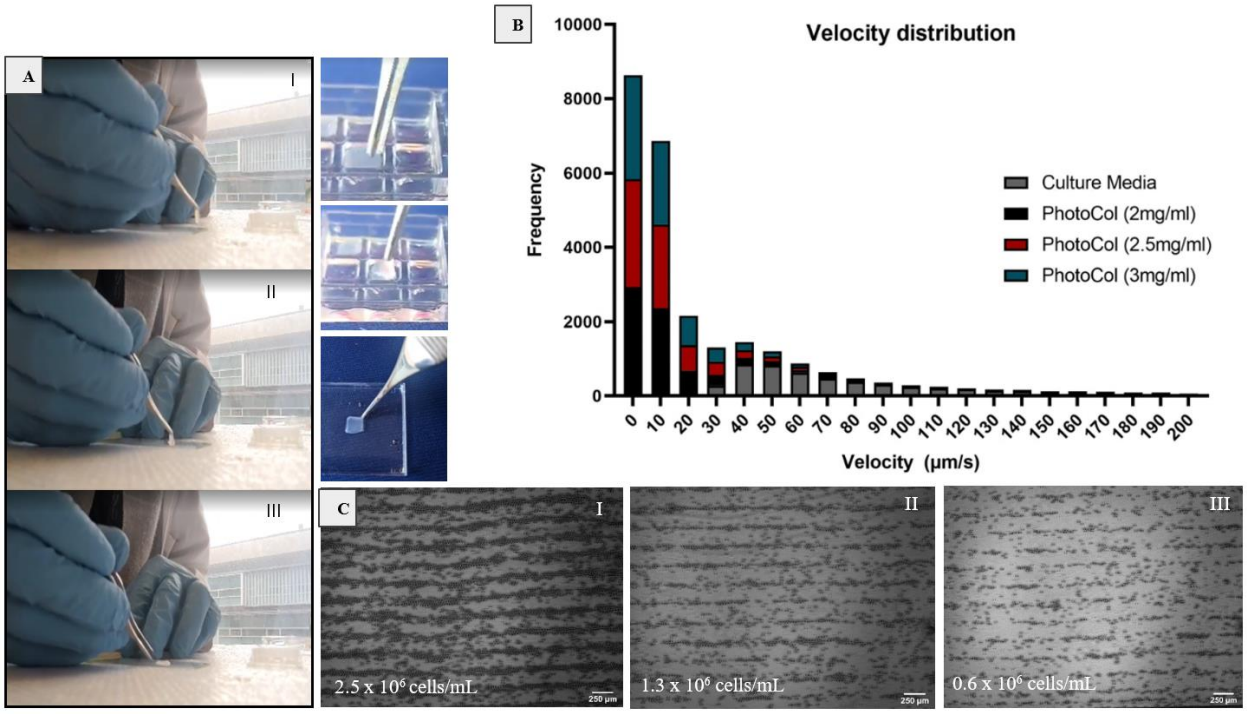

Figure 4.4: Cell Patterning Sample Optimization. A) Retrievability of cell-hydrogel construct after 3 min of UV-exposure. B) Velocity distribution of different cell-suspension conditions. C) Cell patterning for various cell densities (I)2.5 x 10^6, (II) 1.3 x 10^6, and (III) 0.6 x 10^6 cells/mL showing defined patterned lines. Scale bar is 250µm.

Furthermore, three different PhotoCol® initial concentrations were trialed, being 2, 2.5, and 3mg/mL, and compared to the velocity distribution results obtained using regular growth media. As observed in Figure 4.4B, the velocity of MC3T3-E1 cells being acoustically patterned is significantly faster in cells suspended in growth media due to a lower viscosity in comparison to cell-laden PhotoCol® samples. As expected, the higher the viscosity of the suspension medium is, the longer and less efficient becomes the cell manipulation. The velocity of patterning was reduced to nearly 50% when cells were suspended in PhotoCol® solution (Figure 4.4B). However, the average time to guide the cells towards the pressure nodes and form the linear patterns was still less than 1 minute.

4.3.2 SSAW patterning of Stem Cells Enhances Cell Viability, Metabolic Activity and Osteogenic Differentiation

4.3.2.1 SSAW-Patterning Improves ASCs Cell Viability and Metabolic Activity

To validate the biocompatibility of our proposed SSAW platform, we evaluated the cell viability over time using a Live/Dead cell kit. ASCs and MC3T3-E1 were stained and mixed with media or hydrogel solution before injecting them into the channel for acoustic patterning. Three test groups were prepared, including ASCs suspended in PhotoCol®-LAP (3.3×10^4 cells/mL), ASCs suspended in DMEM/F-12 (5.1×10^5 cells/mL), and MC3T3-E1 suspended in αMEM (5.5×10^5 cells/mL). Fluorescent images were taken at 0hr (control), 24, and 48hrs after SSAW was activated. Our results confirm that high cell viability (>90%) was preserved for all groups 48hrs after being exposed to SSAWs (Figure 4.5A). There is no significant difference between the control (0hr) and the acoustically patterned groups MC3T3 in αMEM and ASCs in PhotoCol®-LAP for 24hr and 48hr after SSAW induction ($p<0.0001$, Anova Two-Factor with Replication, n=3), which proves the gentle nature of SSAWs that suggests to not affect the cell viability. A difference in cell viability was observed between 24 and 48hrs for the ASC-DMEM/F12 (media) group, nonetheless with over 85% cell survival.

One of the challenges of tissue engineering, in addition to preserving the cell viability, is to maintain the cellular spatial arrangement over time.[89] By using a methacrylated collagen hydrogel, we could preserve the linear patterns after UV crosslinking, which could also prevent the early degradation of tissues prior to cell differentiation and migration. Figure 4.5B confirms the preservation of the cell pattern in PhotoCol®-LAP 48hrs after of SSAW activation, where dense and defined lines are observed. No significant differences in cell viability were observed between the control and acoustically patterned group.

The effects of UV light on cell-hydrogel photopolymerization and cell viability have been widely reported.[44,90–93] For instance, Lin *et al.*[92] showed that endothelial colony-forming cells (ECFCs) and mesenchymal stem cells (MSCs) remain viable (>93%) for up to 120s of UV, and were only negatively affected beyond 300s of UV light exposure ($7.5 mW/cm^2$). Moreover, this group demonstrated that by increasing the UV exposure time, the spreading capacity of cells inside their hydrogel (GelMA) diminished, which is directly correlated to the degree of GelMA polymerization, as expected. In another study, the effects of UV light on human MSCs photo-

encapsulated in GelMA were studied. Results showed that upon the induction of UV light (490–510 nm) with an intensity of 20mW/cm^2, good cell viability (>75%) was maintained after 4 minutes of light exposure with a 3% reduction after 10 minutes.[93] Our results confirmed this similar behaviour as cell viability was preserved for UV-exposed samples exposed < 3 min to an intensity of 1 mW/cm^2 at 10 cm from the source based on the Live/Dead assay. After 48 hrs of incubation, high viability >90% is shown, with no significant differences observed after crosslinking cells with UV light.

To further investigate the effects of acoustic cell patterning on cell functionality, we quantified the metabolic activity of acoustically patterned ASCs in hydrogel solution (PhotoCol®-LAP) and non-patterned ASCs (control) in PhotoCol®-LAP via alamarBlue™. After sample fabrication, the control and the acoustically patterned group were cultured in growth and differentiation media, where alamarBlue™ assay was performed at days 1, 7, and 14. As seen in Figure 4.5E, both control and acoustically patterned cells-hydrogel groups cultured in growth media showed a continuous proliferation between days 1 to 14. Acoustically patterned cells-hydrogel constructs cultured in growth media showed a 45.53% and 32.03% increase in metabolic activity after day 7 and day 14, respectively. Interestingly, a different behavior was observed for the acoustically patterned and control groups cultured in differentiation media after day 7, where a constant metabolic activity was noticed. This null change in the cell-laden hydrogel metabolic activity from day 7 to day 14, suggests that cells start differentiating upon the induction of differentiation media, with a similar behavior for both the control and the acoustically patterned groups.

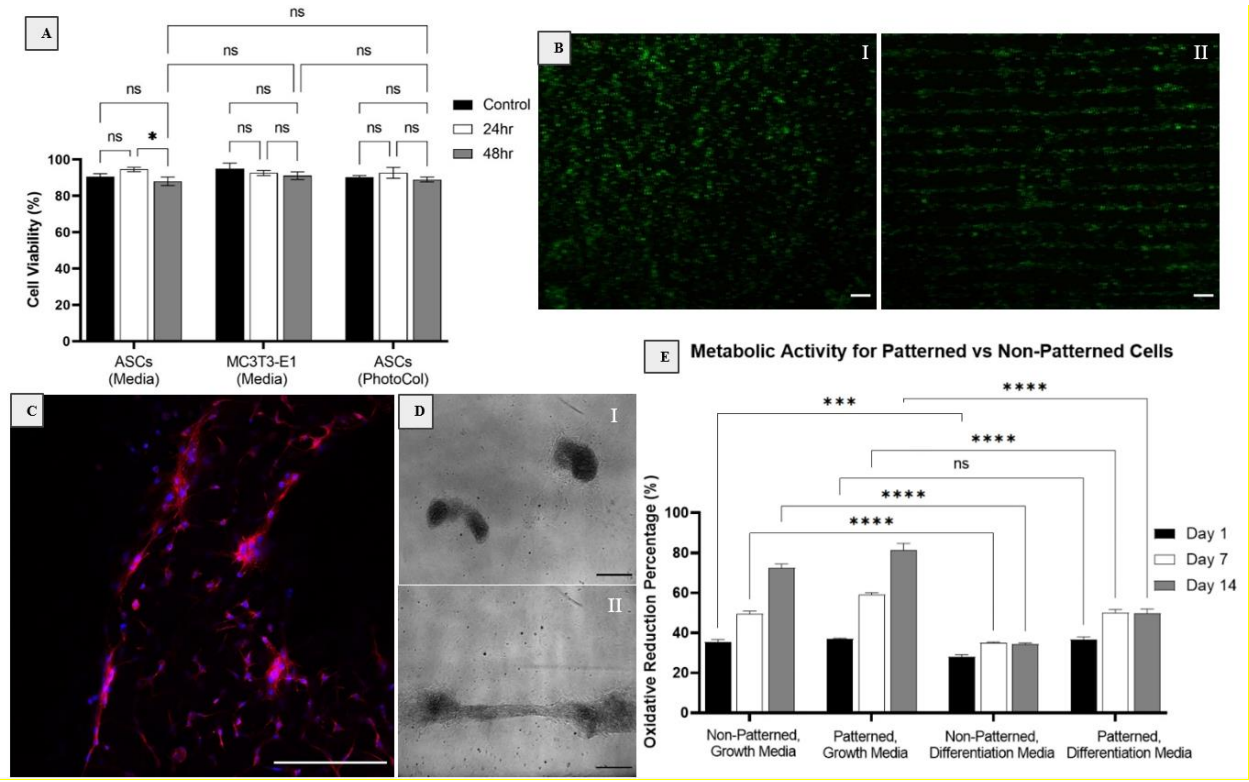

Figure 4.5: Cell viability and metabolic activity for patterned and non-patterned cells. A) Cell viability for patterned ASCs and MC3T3-E1 with and without PhotoCol® for up to 48hr after SSAW induction (n=3; *: $p < 0.05$; **: $p < 0.01$; ***: $p < 0.001$; ****: $p < 0.0001$). B) Live/Dead showing high cell viability after (I) 0hr and (II) 48hrs of SSAW induction. C) Acoustically patterned ASCs showing aligned nucleus (Hoechst 33342) and actin (Phalloidin-iFluor 594) fibers aligned after one week in growth media. D) ASCs cells-cell structure alignment of non-patterned (I) and patterned (II) cells in PhotoCol® at day 14. E) Metabolic activity of acoustically patterned and non-patterned ASCs cultured in growth media and differentiation media. Scale bar is 250 μm.

More interestingly, the acoustically patterned group cultured in growth media showed an enhancement in metabolic activity at days 7 (17.43%) and 14 (11.44%) compared to that of the control group ($p<0.0001$, Anova Two-Factor with Replication, n=3) (Supplementary Figure 1A). In a similar manner, the acoustically patterned group cultured in differentiation media showed a significant increase in metabolic activity compared to that of the control group at days 1 (28.82%), 7 (35.36%), and 14 (36.43%) (Supplementary Figure 1B).

In addition, Figure 4.5C shows acoustically patterned cells within PhotoCol®-LAP, where the cell nucleus and actin fibers are shown to be aligned with a predominant unidirectional orientation after 1 week in culture. For its part, Figure 4.5D shows the cell-cell arrangement and the multicellular structure of the control group and acoustically patterned samples after 14 days in culture using

differentiation media. As observed, the cell-cell structural morphology and directional alignment is different between the control (Figure 4.5D(I)) and acoustically patterned (Figure 4.5D(II)) groups. Non patterned cells, show a lack of cellular interconnections with a non-spreading cell-cell morphology. Acoustically patterned samples, in contrast, show the extension of elongated protrusions at the end of the cell membrane, which suggests to guide the cellular migration and interconnection.[94,95] This geometrical difference could be a result of better cell-cell junctions due to patterning, which suggests the improvement of cell communication due to an upregulation of cadherins, receptors, integrins, and signaling proteins.[96] It has been also previously reported, that the extension of pseudopodia and tissue branching increases the strength of intercellular connectivity, which facilitates rapid, long-range communication between cells throughout the organism. Therefore, these qualitative results coupled to the metabolic activity data discussed, indicate that cadherin-mediated connections from cell-cell contacts could influence the cell behavior, including the metabolic rate, as previously reported.[97]

4.3.2.2 SSAW-Patterning Enhances ASCs Cell Osteogenic Differentiation

To further validate our SSAW platform and investigate the effects of acoustic patterning on cell functionality, we assessed the differentiation potential of acoustically patterned ASCs in PhotoCol®-LAP cultured in differentiation media via ALP activity and osteocalcin signaling. ALP is a membrane-bound enzyme present in osteoblasts and involved in bone mineralization, that has been widely used as an early marker of osteogenic differentiation.[98,99] As seen in Figure 4.6A, both acoustically patterned and control groups cultured in differentiation media showed an increase in ALP activity between days 7 and 14, coinciding with the results obtained for the metabolic activity. As ASCs start their differentiation process and change their phenotype, they stop proliferating.[100] Acoustically patterned samples enhanced their ALP activity by 80.62% between days 1 and 7 and by 53.71% between days 7 and 14. Furthemore, SSAW-based patterning shows to enhance the differentiation potential of ASCs, where Figure 4.6A confirms an increase difference percentage in ALP activity of 88.89% at day 7 and 24.90% at day 14 for the acoustically patterned samples in comparison to the control group. Therefore, acoustically patterned cells experience an higher ALP activity due to cell-cell and cell-matrix junctions which modulate the strength of adhesion and activate mechanosensitive signaling pathways that can influence the cell differentiation process.[2]

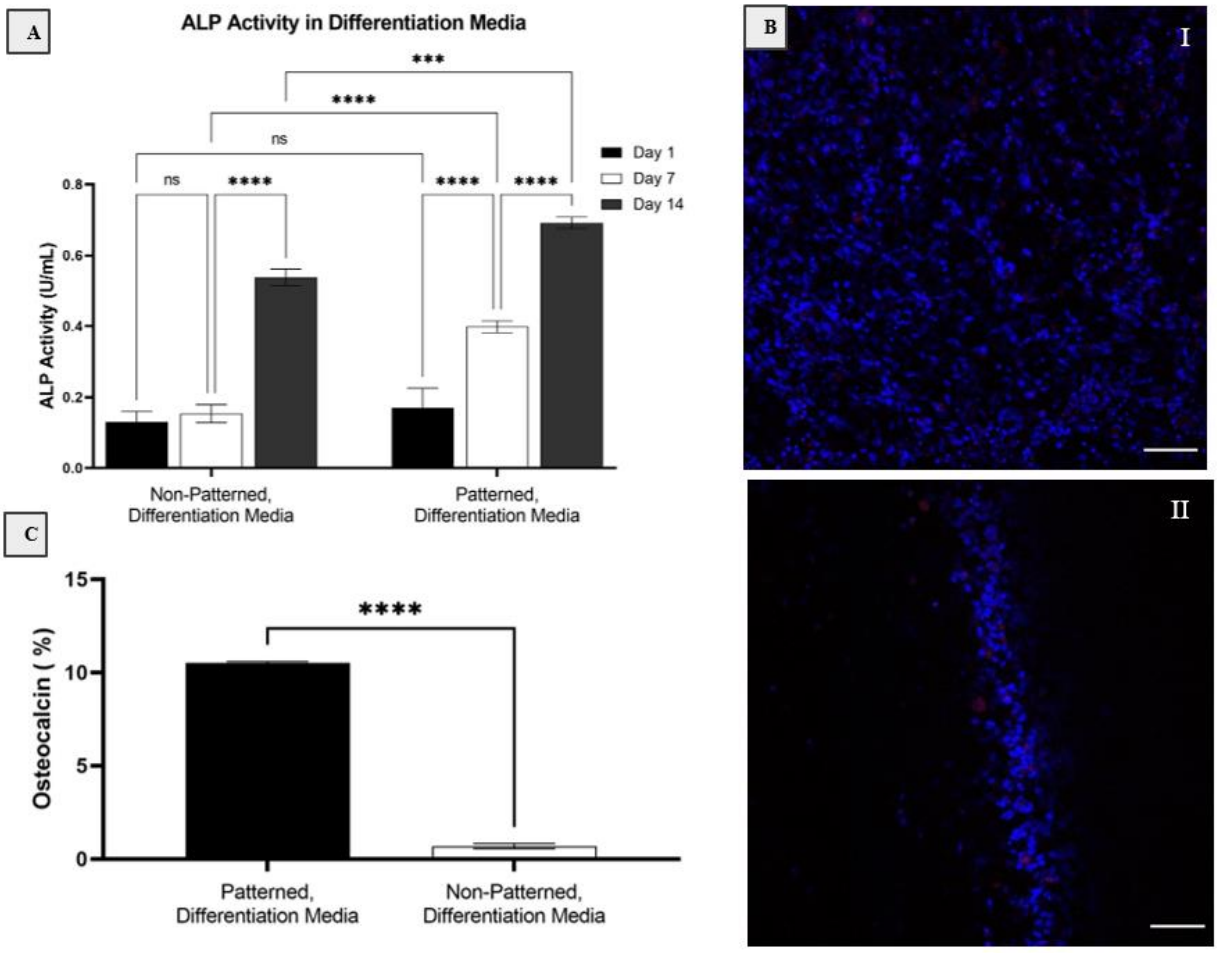

Figure 4.6: Osteogenic Differentiation Potential of Acoustically Patterned Cells. A) ALP Activity for non-patterned and patterned cells encapsulated in PhotoCol®-LAP hydrogel at days 1, 7 and 14 (n=3; *: $p < 0.05$; **: $p < 0.01$; ***: $p < 0.001$; ****: $p < 0.0001$). B). Confocal images of non-patterned (control) cells (I) and acoustically patterned cells (II) with an equal density of 2.5 x 10^6 cells/mL after 14 days of culture in differentiation media, where osteocalcin is shown in red and the nuclei in blue. C) Osteocalcin percentage difference between acoustically patterned and non patterned groups. Confocal images were analyzed using ImageJ to quantify the ratio of the osteocalcin signal area percentage versus the total stained area, (n=3; ****: $p < 0.0001$). Scale bar is 250 μm.

Confocal fluorescent images of acoustically patterned and control groups at day 14 (Figure 4.6B) were in concordance with the ALP activity results. Acoustically patterned ASCs-PhotoCol®-LAP constructs cultured in differentiation media for up to 14 days had a 10 times higher osteogenic signal (Figure 4.6C), quantified as the ratio of osteocalcin area, divided by the total stained area. Osteocalcin is a bone-specific protein synthesized by osteoblasts, that is typically used as an early marker for osteogenic differentiation in rat mesenchymal stem cells.[101] Therefore, we can observe

from Figure 4.6B that rat adipose-derived stem cells differentiate into osteoblasts more efficiently for the acoustically patterned group, due to improved cell-cell microenvironments that can efficiently coordinate cellular functions,[102] such as cellular differentiation and proliferation for regenerative medicine applications.

Furthermore, our culture platform consisting of major well dimensions of 21.5 × 23.6 × 6.8 mm^3 and minor well dimensions of 6.1 × 6.8 × 1.3 mm^3, allowed us to study the effects of cell patterning in 3D. Cells-PhotoCol®-LAP solution was evenly divided between control and acoustically patterned groups with an even density of 2.5 x 10^6 cells/mL. Therefore, Figure 4.6B suggests that acoustically patterned cells are aligned throughout the z-direction as ASCs are localized and condensed at the pressure nodal line. Previous work, however, has shown that the cell-cell nodal alignment slightly changes with respect to the height of the channel, where a higher acoustic force is experienced at the surface of the piezoelectric element.[44] We imaged acoustically patterned cells after 1 week in culture in vertical cross-sections (z-stacks) using confocal microscopy. As shown in Supplementary Figure 6, cells aligned into pressure nodes more efficiently closer to the surface of the piezoelectric substrate and disperse at the surface of the hydrogel, though, still maintaining their general pattern. This work thus allowed us to study the structural changes of acoustic patterning coupled to insightful information about the cell-cell behaviour, including enhanced proliferation and differentiation of stem cells.

4.4 Conclusion

In this work, we implemented an SSAW-based contactless cell patterning platform to rapidly fabricate high-resolution cell-hydrogel linear arrangements of adipose-derived mesenchymal stem cells with the capability of being retrieved from the SSAW platform after UV crosslinking. The fast arrangement of cells in linear patterns with a reproducible linear nodal separation of ~150μm was successfully shown in <5 seconds for culture media and <1 minute in PhotoCol®-LAP hydrogel. We demonstrated the capability of creating multiple biomimetic tissue patches from aligned adipose-derived stem cells in a UV-crosslinkable PhotoCol®-LAP hydrogel that can be easily retrievable from the platform as a proof-of-concept of tissue regeneration. We studied the effects of acoustic cell patterning for enhanced cellular proliferation and osteogenic differentiation, which has never been directly correlated to SSAW-patterning using adipose-derived stem cells. The acoustically patterned cells remained viable with an increased metabolic activity and enhanced

osteogenic differentiation potential, as revealed by the quantification of alamarBlue™, ALP activity, and osteocalcin signaling for up to 14 days. Cell-cell interconnection was also improved in acoustically patterned cells, which is critical for cell communication, cell migration, and tissue development. Together, these results confer to the proposed acoustofluidics platform a great avenue of opportunities to construct tissue patches with induced cell-cell contacts for their application in tissue regeneration and wound healing.

4.5 Materials and Methods

4.5.1 Materials

Methacrylated Type I Collagen with LAP photoinitiator kit (PhotoCol®-LAP) was purchased from Advanced Biomatrix (CA, USA). StemXVivo® Osteogenic/Adipogenic Base Media and StemXVivo® Osteogenic Supplement were purchased from R&D Systems (MN, USA). Dulbecco's Modified Eagle Medium/Nutrient Mixture F-12 (DMEM/F12), Minimum Essential Medium (MEM-Alpha/α-MEM), Fetal Bovine Serum (FBS), Penicillin-Streptomycin (P/S), Antibiotic-Antimycotic, Formaldehyde solution, and TrypLE™ Express Enzyme were all purchased from Thermo Fisher Scientific (MA, USA). Bovine Serum Albumin (BSA) and Dulbecco's Phosphate Buffered Saline 1X (PBS, without calcium chloride and magnesium chloride) were purchased from Sigma Aldrich (MI, USA). AlamarBlue™ Cell Viability Reagent, Live/Dead Viability Assay Kit (L3224), and Hoechst 33342 (Trihydrochloride, trihydrate – 10 mg/mL solution in water) were purchased from Invitrogen (MA, USA). Alkaline Phosphatase (ALP) Assay Kit (Colorimetric) and the antibody Phalloidin iFluor 594 conjugate (ab176757) were purchased from Abcam (Cambridge, MA). Osteocalcin Rabbit Polyclonal Antibody (primary antibody) was purchased from Proteintech (IL, USA) and Alexa Fluor Plus 647-Goat anti-Rabbit IgG (H+L) High Cross-Absorbed Secondary Antibody was purchased from Thermo Fisher Scientific (MA, USA). A μ-Slide 2 well co-culture chamber was purchased from ibidi GMBH (WI, USA). 4-inch 127.86° Y-cut, X-Propagating SAW grade Lithium Niobate wafers were purchased from Precision Micro-Optics (MA, USA). Murine pre-osteoblasts (MC3T3-E1) were purchased from the American Type Culture Collection (ATCC, Virginia, USA). Subcutaneous adipose tissue was harvested by Dr. Hadil Al-Jallad and Antoine Karoichan from two 3-4 months old Wistar rats provided by the Research Institute of McGill University's Health Centre's (RI-MUHC) animal facility, as described previously.[100]

4.5.2 Fabrication of the SSAW platform

The SAW device was fabricated using standard soft-lithography, e-beam evaporation, and lift-off methods. A 7 μm-thick photoresist layer (S1813, MicroChem, TX, USA) was spin-coated on a 500 μm thick double-sided polished 127.86° $LiNbO_3$ piezoelectric wafer. A double layer of titanium and gold (Ti/Au 0.1/1.0kȦ 10nm 100 nm) was deposited on the substrate using an e-beam evaporator (bjd1800, Airco Temescal, CA, USA). Next, the substrate was submerged in a developer (MF319, Microposit) at 70° under sonication to lift-off the undesired coating and form a pair of interdigitated transducers (IDT). The design of IDT is comprised of finger and spacing gaps of 75μm (or a period of 300μm) for a total of 40 electrode pairs. A commercial μ-slide well co-culture channel with major well dimensions: 21.5 × 23.6 × 6.8 mm^3 (w× l × h) and minor well dimensions 6.1 × 6.8 × 1.3 mm^3 (w× l × h) was used to chamber the cells by coupling it to the piezoelectric substrate using a drop of water. Polyimide tape was used to delimit the SSAW working area and eliminate any interactions of SSAWs with the outer substrate region.

4.5.3 Cell Culture

ASCs were seeded in 0.1% gelatin coated T75 flasks and cultured in growth medium Dulbecco's modified Eagle medium (DMEM/F-12), supplemented with 10% fetal bovine serum (FBS), 1% penicillin/streptomycin (P/S), and 1% antibiotic-antimycotic (AA). At a 70-80% confluency cells were trypsinized using TrypLE Express Enzyme (1X), where cells were used before passage 7 for all experiments. MC3T3-E1 were cultured in alpha-DMEM, supplemented with 10% fetal bovine serum (FBS) and 1% penicillin/streptomycin (P/S, GIBCO, USA) in T-75 flasks. Before the experiments, cells were detached to flasks using 0.25% trypsin-EDTA. The cell density was measured using a Countess II FL Cell Counter (Invitrogen, Thermo Fisher Scientific, MA, USA).

4.5.4 Experimental setup for cell patterning platform

For the optimization of the cell patterning parameters, including the amplitude, working frequency, velocity, and cell density, both 9.9 μm polystyrene (PS) particles and MC3T3-E1 cells were used. PS particles and MC3T3-E1 cells were suspended in deionized water and growth media (αDMEM), respectively. At passages 20-30, MC3T3-E1 were retrieved using 0.25% trypsin-EDTA. For Live/Dead, alamarBlue™, and ALP activity quantification, ASCs were used. At passage 4, ASCs were retrieved using TrypLE 1X for a final cell concentration of 500,000 cells in 200μL DMEM/F-12 media.

PhotoCol®-LAP was prepared following the manufacturer's protocol. Briefly, methacrylated type I collagen (PhotoCol®), diluted in acetic acid to a concentration of 3 mg/mL, was neutralized and mixed with 2% LAP (photoinitiator, 17 mg/mL in PBS 1X). ASCs cells in 200μL media were further diluted with the PhotoCol®-LAP solution at a ratio of 1:3.

Cell-laden hydrogel constructs without SSAWs activation, *i.e.*, no cell patterning (control) group, were compared to cell-laden hydrogel constructs subjected to SSAWs, *i.e.*, acoustic cell patterning. For the control group, cells-hydrogel solution (50μL) was evenly injected into the minor wells of an ibidi μ-Slide channel with a random cell distribution. No acoustic force was applied.

Conversely, for the acoustically patterned group, the same density of cell-hydrogel solution was injected into the minor wells of an ibidi μ-Slide channel. Two pieces of polyimide tape (3M, Maplewood, MN, USA) were placed on the $LiNbO_3$ substrate to delimit the SSAW working region and to create a space for the coupling liquid between the piezoelectric substrate and the channel. The ibidi channel was then coupled to the piezoelectric substrate using a drop of water. One independent and controllable AC radiofrequency (RF) signal was generated using a function generator (AFG3022C, Tektronix, OR, USA) connected to an amplifier (25A250A, Amplifier Research, PA, USA). The input voltage was set between 10-40Vpp and working frequencies varied between 12.5-13.11MHz. The cell movement was tracked and recorded using a QImaging camera (Retiga 2000R, ARI, USA) connected to an inverted microscope (TE2000U, Nikon Eclipse, MA, USA).

Once the patterns were formed (< 1 min), the function generator was turned off and both control and acoustically patterned cells-hydrogel constructs were exposed to UV light (405nm, ~1mW/cm^2) at a distance of 10 cm from the surface of the ibidi® coverlid for <3 minutes to induce gradual crosslinking. The photo-crosslinked constructs were then placed in a 37°C incubator for 30 minutes. After short incubation, 1mL DMEM/F-12 media (growth media) or StemXVivo® Osteogenic Base Media (differentiation media) was added to each of the 2 major wells. Growth or differentiation media was changed every 3-4 days for up to 14 days.

4.5.5 Live Dead Cell Evaluation

For this set of experiments, three test groups were analyzed, ASCs suspended in PhotoCol®-LAP, ASCs suspended in DMEM/F12, and MC3T3-E1 suspended in αMEM. Briefly, 50μL of ASCs-PhotoCol®-LAP (3.3×10^4 cells/mL), ASCs-DMEM/F12 (5.1×10^5 cells/mL), or MC3T3-E1-αMEM (5.5×10^5 cells/mL) were injected into the mini-wells of the ibidi channel. The channel was

coupled to the $LiNbO_3$ wafer and an RF signal of 13.11MHz at 40Vpp was exerted to induce SSAWs for <1 min. SSAWs were turned off, and fluorescent images were captured after 0hr, 24hr, and 48hr. Living cells were labeled with green fluorescence using calcein AM, while dead cells were labeled with red fluorescence using ethidium homodimer-III (Live/Dead viability kit) following the manufacturer's protocol. The cellular viability was calculated as the percentage ratio of green-fluorescent cells (Live) divided by the total fluorescent cell area (both Live and Dead) using ImageJ. A replicate of three samples were used for the analysis.

4.5.6 Metabolic activity of encapsulated ASCs

To study the effects of acoustic cell patterning on cell metabolic activity, we compared both non-patterned (control) and acoustically patterned cell-hydrogel constructs. Both groups were cultured in growth media (DMEM/F12) and differentiation media (StemXVivo® Osteogenic Base Media) to further investigate the impact of acoustic cell patterning on osteogenic differentiation. AlamarBlue™ assay was used to measure the metabolic activity of ASCs-PhotoCol®-LAP constructs following the manufacturer's protocol. At days 1, 7, and 14, media was removed, and the cell-hydrogel constructs were washed twice with PBS. The samples were then covered with a 10% alamarBlue™ reagent solution in complete growth medium and incubated for 4 hours at 37°C and 5% CO_2. After incubation, the supernatant was collected in a 96 well plate and the absorbance was measured at 570 nm (excitation) and 600 nm (emission) wavelengths using spectrophotometry (SpectraMax i3, SoftMax Pro 6.3, Molecular Devices, CA, USA). The samples were prepared in triplicates and the absorbance from each replicate was also measured in triplicates. The measurements were averaged and used to calculate the percent reduction of alamarBlue™ following the equation:

$$\frac{(\varepsilon ox)600 \times A570 - (\varepsilon ox)570 \times A600}{(\varepsilon red)570 \times A°600 - (\varepsilon red)600 \times A570} \times 100$$

where A is the absorbance value of the experimental sample, $A°$ is the absorbance value of the control, $(\varepsilon ox)570 = 80{,}586$, $(\varepsilon ox)600 = 117{,}216$, $(\varepsilon red)570 = 155{,}677$, and $(\varepsilon red)600 = 14{,}652$.

4.5.8 Alkaline phosphatase (ALP) activity for osteogenic differentiation

The supernatant of acoustically patterned and control ASCs-PhotoCol®-LAP constructs was collected in 1.5 mL microcentrifuge tubes and snap frozen in liquid nitrogen at days 1, 7, and 14.

Samples were then stored at -80°C until the assay was performed. The ALP activity was quantified using a commercial ALP kit (colorimetric), following the manufacturer's protocol.

4.5.9 Immunofluorescence

At day 14, the supernatant was removed from the ibidi channel and cells-hydrogel constructs were washed twice with PBS 1X. Cells were fixed in 4% paraformaldehyde for 30 minutes and permeabilized with 0.1% Triton-X in PBS for 10 minutes and blocked with 2% BSA solution in PBS for 30 minutes. After blocking, the samples were incubated with osteocalcin rabbit polyclonal antibody (1:100) in 0.2% BSA solution and were incubated overnight at 4°C. The next day, the samples were incubated with the secondary antibody, Alexa Fluor Plus 647-Goat anti-Rabbit IgG at a 1:500 dilution in 0.2% BSA for 1 hour at room temperature. The cellular nuclei and actin were stained with Hoechst 33342 (1:1000) and Phalloidin iFluor 594 (1:1000), respectively, in 0.2% BSA solution for 1 hour at room temperature. Samples were stored at 4°C until imaging. Fluorescent images were captured using confocal laser scanning microscopy (LSM 710, Zeiss AxioObserver).

4.5.10 TrackMate Analysis

The TrackMate plugin was used to evaluate the cell-patterning velocity. A Laplacian of Gaussian (LoG) filter was used with Blob diameter and intensity threshold inputs. The Bright field videos were processed by first inverting the contrast using the Invert LUT from the Lookup Tables and applying a Variance filter to give a fluorescent-like image appearance to detect individual cells. The Blob diameter was estimated as the cell diameter (15μm). These spots were then linked into trajectories using the Linear Assignment Problem (LAP) tracker. The velocity was then calculated from the Spots data for a 50fps, such as:

$$v = \frac{\sqrt{(x^2 + y^2)}}{\left(\frac{frame}{50fps}\right)}$$

4.5.11 Statistical analysis

Three independent replicates (n=3) of each group were performed for each experiment. Data were presented as mean ± SD. Two-way analysis of variance (ANOVA) with Tukey's test was used to assess the statistical significance of the data at 95% confidence. Graphs were prepared using GraphPad Prism.

Data availability

The data that support the findings of this study are available from the corresponding authors upon reasonable request.

Acknowledgements

The authors would like to acknowledge the financial support from the Natural Sciences and Engineering Research Council of Canada (NSERC) through the Discovery Grant and the Biomedical Engineering Department for their support through the Graduate Excellence Award. The authors would also like to thank Dr. Hadil Al-Jallad and Antoine Karoichan for harvesting adipose tissue from rats to obtain adipose-derived mesenchymal stem cells.

Conflict of interest

The authors declare that they have no known competing financial interests or personal relationships that could have appeared to influence the work reported in this paper.

Permission to reproduce material from other sources

No material was reproduced from other sources.

Contribution of Authors

All work and experiments conducted in this thesis were done by the authors. All experimental figures and data analysis presented herein were completed by the authors. Harvesting of adipose tissue from rats was performed by Antoine Karoichan and Dr. Hadil Al-Jallad.

4.6 References

1. Wang, Z. et al. Single-cell patterning technology for biological applications. Biomicrofluidics vol. 13 61502 (2019).
2. Kang, B. et al. High-resolution acoustophoretic 3D cell patterning to construct functional collateral cylindroids for ischemia therapy. Nat. Commun. 9, (2018).
3. Naseer, S. M. et al. Surface acoustic waves induced micropatterning of cells in gelatin methacryloyl (GelMA) hydrogels. Biofabrication 9, 015020 (2017).
4. Armstrong, J. P. K. et al. Engineering Anisotropic Muscle Tissue using Acoustic Cell Patterning. Adv. Mater. 30, 1802649 (2018).
5. Dias, A. D., Unser, A. M., Kruger, U., Xie, Y. & Corr, D. T. Laser direct-write patterning influences early embryonic stem cell differentiation. 2015 41st Annu. Northeast Biomed. Eng. Conf. NEBEC 2015 (2015) doi:10.1109/NEBEC.2015.7117042.
6. McBeath, R., Pirone, D. M., Nelson, C. M., Bhadriraju, K. & Chen, C. S. Cell Shape, Cytoskeletal Tension, and RhoA Regulate Stem Cell Lineage Commitment. Dev. Cell 6, 483–495 (2004).
7. Weber, G. F., Bjerke, M. A. & DeSimone, D. W. Integrins and cadherins join forces to form adhesive networks. J. Cell Sci. 124, 1183 (2011).
8. Vadivelu, R. K., Kamble, H., Shiddiky, M. J. A. & Nguyen, N. T. Microfluidic Technology for the Generation of Cell Spheroids and Their Applications. Micromachines 2017, Vol. 8, Page 94 8, 94 (2017).
9. Scemes, E., Suadicani, S. O., Dahl, G. & Spray, D. C. Connexin and pannexin mediated cell—cell communication. Neuron Glia Biol. 3, 199 (2007).
10. Heller, E. & Fuchs, E. Tissue patterning and cellular mechanics. J. Cell Biol. 211, 219 (2015).
11. Otsuka, H. Micropatterning of cell aggregate in three dimension for in vivo mimicking cell culture. Colloid Interface Sci. Pharm. Res. Dev. 223–241 (2014) doi:10.1016/B978-0-444-62614-1.00011-9.
12. Jing, P. et al. Optical tweezers system for live stem cell organization at the single-cell level. Biomed. Opt. Express 9, 771 (2018).
13. Grogan, S. P. et al. In Situ Tissue Engineering Using Magnetically Guided Three-Dimensional Cell Patterning. Tissue Eng. Part C. Methods 18, 496 (2012).

14. Suzuki, M., Yasukawa, T., Shiku, H. & Matsue, T. Negative dielectrophoretic patterning with different cell types. Biosens. Bioelectron. 24, 1043–1047 (2008).

15. Xu, T., Jin, J., Gregory, C., Hickman, J. J. & Boland, T. Inkjet printing of viable mammalian cells. Biomaterials 26, 93–99 (2005).

16. Olofsson, K., Hammarström, B. & Wiklund, M. Ultrasonic based tissue modelling and engineering. Micromachines 9, (2018).

17. Ahmed, H., Ramesan, S., Lee, L., Rezk, A. R. & Yeo, L. Y. On-Chip Generation of Vortical Flows for Microfluidic Centrifugation. Small 1903605 (2019) doi:10.1002/smll.201903605.

18. Meng, L. et al. Acoustic tweezers. J Phys D Appl Phys 52, 273001 (2019).

19. Ozcelik, A. et al. Acoustic tweezers for the life sciences. Nat. Methods 15, 1021–1028 (2018).

20. Gao, Y., Fajrial, A. K., Yang, T. & Ding, X. Emerging on-chip surface acoustic wave technology for small biomaterials manipulation and characterization. Biomater. Sci. 9, 1574–1582 (2021).

21. Tian, Z. et al. Generating multifunctional acoustic tweezers in Petri dishes for contactless, precise manipulation of bioparticles. Sci. Adv. 6, (2020).

22. Nguyen, T. D. et al. Large-Scale Fabrication of 3D Scaffold-Based Patterns of Microparticles and Breast Cancer Cells using Reusable Acoustofluidic Device. Adv. Eng. Mater. 2001377 (2021) doi:10.1002/adem.202001377.

23. Lata, J. P. et al. Surface Acoustic Waves Grant Superior Spatial Control of Cells Embedded in Hydrogel Fibers. (2016) doi:10.1002/adma.201602947.

24. Rasouli, R. & Tabrizian, M. Rapid Formation of Multicellular Spheroids in Boundary-Driven Acoustic Microstreams. Small 2101931 (2021) doi:10.1002/SMLL.202101931.

25. Ding, X. et al. Surface acoustic wave microfluidics. Lab Chip 13, 3626–3649 (2013).

26. Doinikov, A. A. Acoustic radiation pressure on a compressible sphere in a viscous fluid. J. Fluid Mech. 267, 1–22 (1994).

27. Hess, P. Surface Acoustic Waves in Materials Science. Phys. Today 55, 42 (2007).

28. Vanneste, J. & Bühler, O. Streaming by leaky surface acoustic waves. Proc. R. Soc. A Math. Phys. Eng. Sci. 467, 1779–1800 (2011).

29. Guo, F. et al. Three-dimensional manipulation of single cells using surface acoustic waves. Proc. Natl. Acad. Sci. U. S. A. 113, 1522–1527 (2016).

30. Tinevez, J. Y. et al. TrackMate: An open and extensible platform for single-particle tracking. Methods 115, 80–90 (2017).

31. Ding, X. et al. On-chip manipulation of single microparticles, cells, and organisms using surface acoustic waves. Proc. Natl. Acad. Sci. U. S. A. 109, 11105–11109 (2012).

32. Greco, G. et al. Surface-Acoustic-Wave (SAW)-Driven Device for Dynamic Cell Cultures. Anal. Chem. 90, 7450–7457 (2018).

33. Yarmolenko, P. S. et al. Thresholds for thermal damage to normal tissues: An update. Int. J. Hyperth. 27, 320–343 (2011).

34. Ding, X. et al. Surface acoustic wave microfluidics. Lab Chip 13, 3626 (2013).

35. Ikada, Y. Challenges in tissue engineering. J. R. Soc. Interface 3, 589–601 (2006).

36. Wang, Y., Han, C. & Mei, D. Standing Surface Acoustic Wave-Assisted Fabrication of Region-Selective Microstructures via User-Defined Waveguides. Langmuir 35, 11225–11231 (2019).

37. Zamanian, B. et al. Interface-Directed Self-Assembly of Cell-Laden Microgels. Small 6, 937–944 (2010).

38. Lin, R. Z., Chen, Y. C., Moreno-Luna, R., Khademhosseini, A. & Melero-Martin, J. M. Transdermal regulation of vascular network bioengineering using a photopolymerizable methacrylated gelatin hydrogel. Biomaterials 34, 6785–6796 (2013).

39. Sharifi, S., Sharifi, H., Akbari, A. & Chodosh, J. Systematic optimization of visible light-induced crosslinking conditions of gelatin methacryloyl (GelMA). Sci. Reports 2021 111 11, 1–12 (2021).

40. Abbott, R. et al. The effects of substrate morphology by regulating pseudopods formation on cell directional alignment and migration. J. Phys. D. Appl. Phys. 55, 105401 (2021).

41. Spurlin, J. W. & Nelson, C. M. Building branched tissue structures: from single cell guidance to coordinated construction. Philos. Trans. R. Soc. B Biol. Sci. 372, (2017).

42. Friedl, P. & Mayor, R. Tuning Collective Cell Migration by Cell–Cell Junction Regulation. Cold Spring Harb. Perspect. Biol. 9, (2017).

43. Nelson, C. M. et al. From the Cover: Emergent patterns of growth controlled by multicellular form and mechanics. Proc. Natl. Acad. Sci. U. S. A. 102, 11594 (2005).

44. Jahan, K., Manickam, G., Tabrizian, M. & Murshed, M. In vitro and in vivo investigation of osteogenic properties of self-contained phosphate-releasing injectable purine-crosslinked chitosan-hydroxyapatite constructs. Sci. Reports 2020 101 10, 1–17 (2020).

45. Hessle, L. et al. Tissue-nonspecific alkaline phosphatase and plasma cell membrane glycoprotein-1 are central antagonistic regulators of bone mineralization. Proc. Natl. Acad. Sci. 99, 9445–9449 (2002).

46. Karoichan, A., Baudequin, T., Al-Jallad, H. & Tabrizian, M. Encapsulation and differentiation of adipose-derived mesenchymal stem cells in a biomimetic purine cross-linked chitosan sponge. J. Biomed. Mater. Res. Part A 110, 585–594 (2022).

47. Heller, E. & Fuchs, E. Tissue patterning and cellular mechanics. J. Cell Biol. 211, 219 (2015).

48. Nakamura, A. et al. Osteocalcin Secretion as an Early Marker of In Vitro Osteogenic Differentiation of Rat Mesenchymal Stem Cells. https://home.liebertpub.com/tec 15, 169–180 (2009).

49. Shen, C. J., Fu, J. & Chen, C. S. Patterning Cell and Tissue Function. Cell. Mol. Bioeng. 2008 11 1, 15–23 (2008).

4.7 Supplementary Information

Enhancing Metabolic Activity and Differentiation Potential in Adipose Mesenchymal Stem Cells via High-Resolution Surface Acoustic Waves Contactless Patterning

Karina Martinez Villegas,[1] Reza Rasouli,[1] and Maryam Tabrizian [1, 2]*

[1] Department of Biological and Biomedical Engineering, [2] Faculty of Dental Medicine and Oral Health Sciences, McGill University, Montreal, QC, Canada

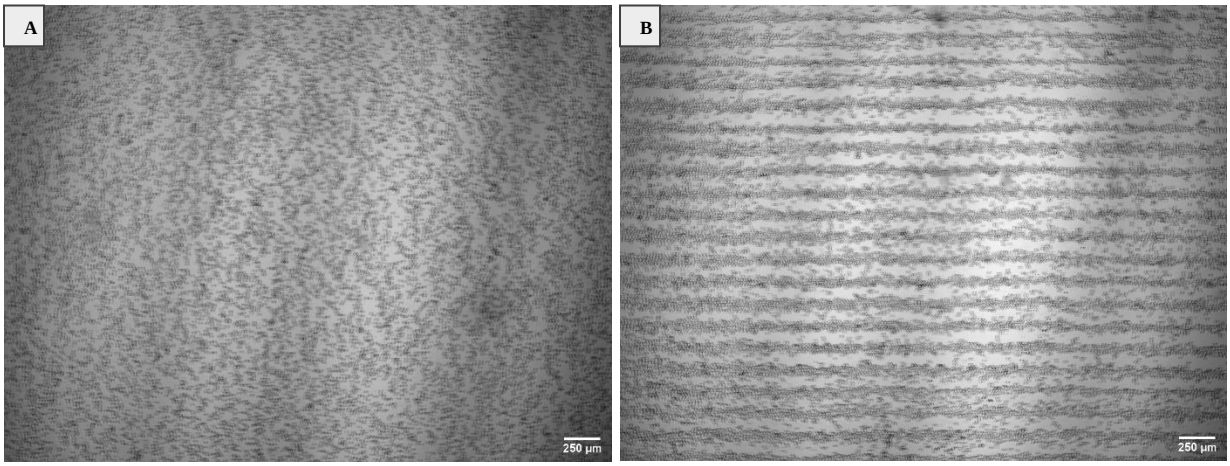

Supplementary Figure 1: Brightfield images of high-resolution standing surface acoustic wave patterning of MC3T3-E1 cells showing 20 well-defined pressure nodal lines. A) Non-patterned cells showing random distribution of cells. B) Acoustically patterned cells showing defined lines of high-density cells (1.5 x10^6 cells/mL) in growth media. Scale bar is 250µm.

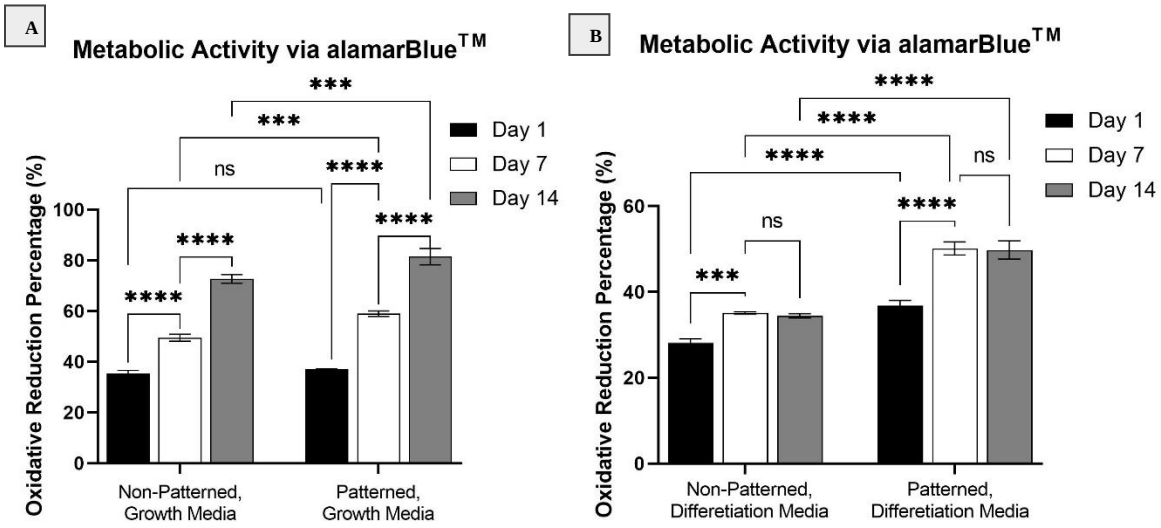

Supplementary Figure 2: Metabolic activity as an indicator of cell proliferation of acoustically patterned and non-patterned (control) cells in PhotoCol®-LAP hydrogel cultured in growth and differentiation media. A) Acoustically patterned cells in PhotoCol®-LAP cultured in growth media show a significantly different increase in metabolic activity

compared to control samples for days 7 and 14 (n=3; ****: $p < 0.001$). B) Metabolic activity of patterned and control samples, where acoustically patterned samples have an increase in showing a sign increase for acoustically patterned cells in PhotoCol®-LAP cultured in differentiation media with statistical significance for days 7 and 14 (n=3; ****: $p < 0.0001$).

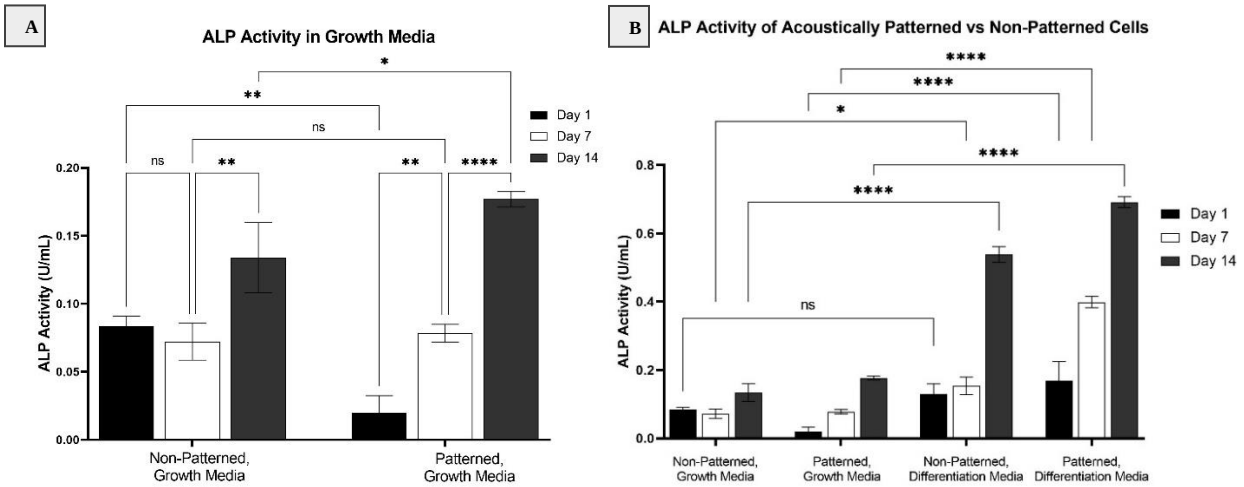

Supplementary Figure 3: Alkaline Phosphatase Activity of acoustically patterned cells in PhotoCol®-LAP hydrogel cultured in growth and differentiation media. A) Alkaline Phosphatase activity showing slight upregulation of ALP activity at day 14 of acoustically patterned samples cultured in growth media with statistically significance for days 1 and 14 (n=3; *: $p < 0.05$; **: $p < 0.01$; ***: $p < 0.001$;****: $p < 0.0001$). B) Alkaline Phosphatase Activity of all groups combined showing significant difference between growth and differentiation media with an increase in ALP for cell-laden hydrogels cultured in differentiation media after days 1, 7, and 14 (n=3; *: $p < 0.05$; **: $p < 0.01$; ***: $p < 0.001$;****: $p < 0.0001$).

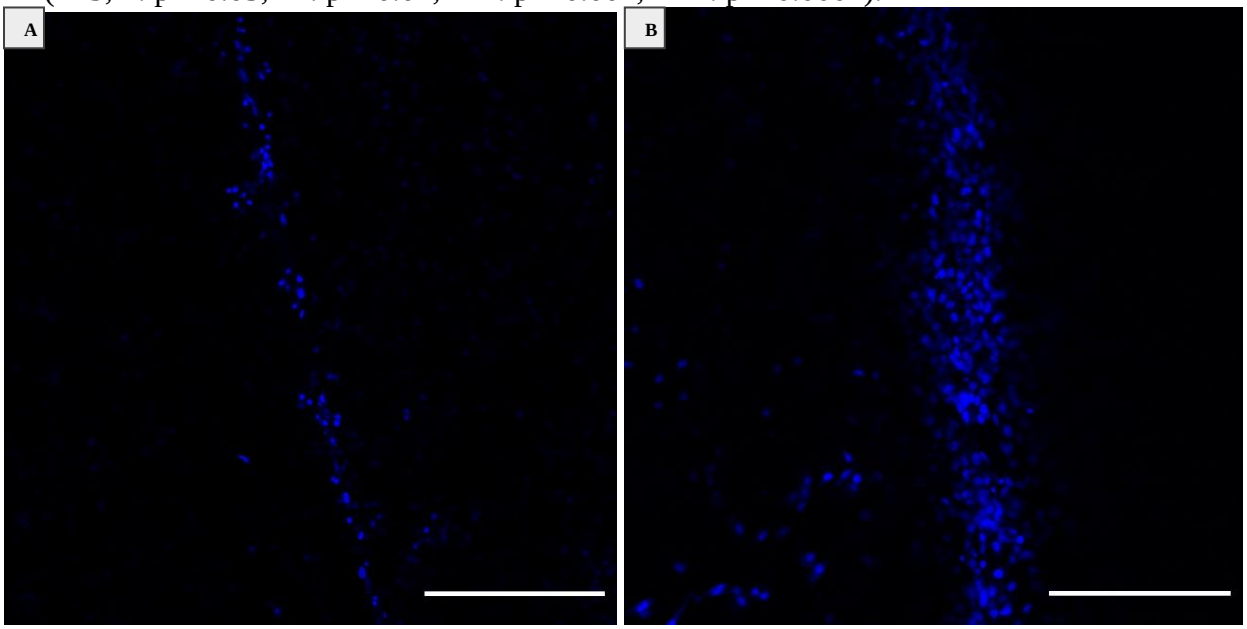

Supplementary Figure 4: Acoustically patterned adipose-derived stem cells (ASCs) showing nucleus (Hoechst 33342) in single pressure node cultured in growth media after (A) one week of culture and (B) two weeks of culture. Scale bar is 250μm.

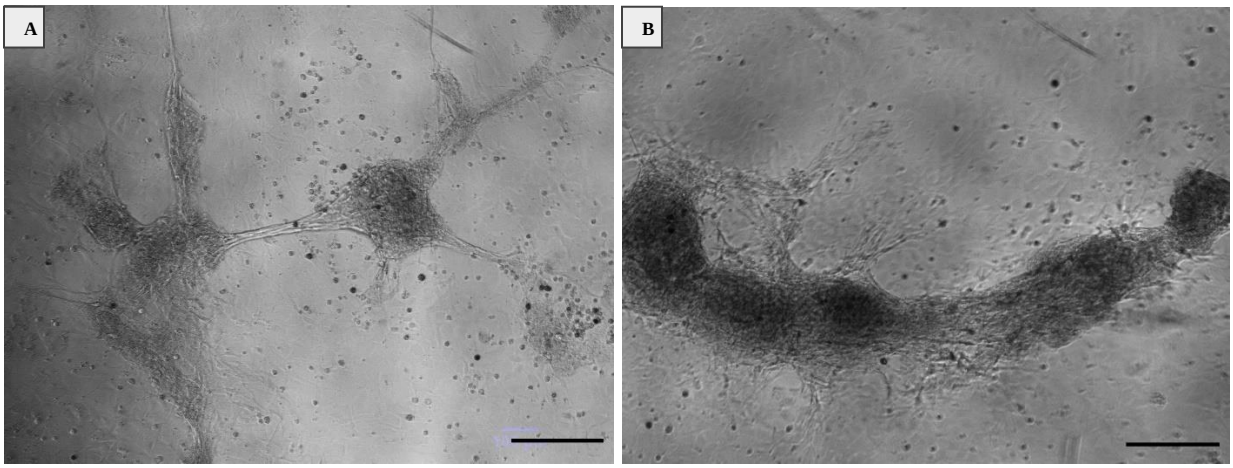

Supplementary Figure 5: Cell morphology for control and acoustically patterned adipose-derived stem cells in PhotoCol®-LAP hydrogel after 14 days cultured in differentiation media. A) Random distribution of ASCs led to poor cellular interconnections with few cell membrane protrusions. B) Acoustically patterned cells showed high-levels of cellular interconnections with a dense spreading-like morphology suggesting strong cell-cell interconnections. Scale bar is 250µm.

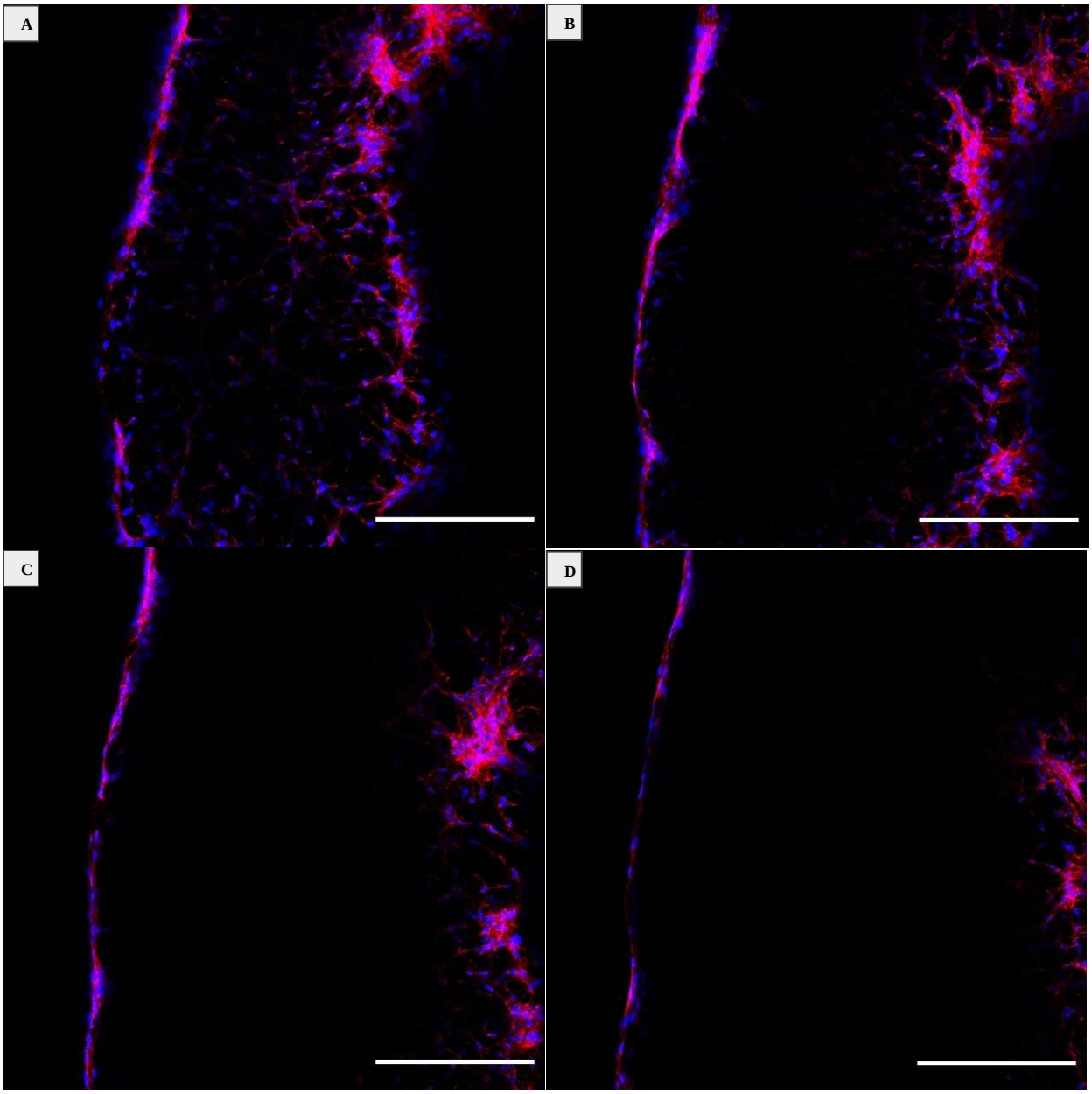

Supplementary Figure 6: Z-stack projection of acoustically patterned adipose-derived stem cells (ASCs) showing aligned nucleus (Hoechst 33342) and actin fibers (Phalloidin-iFluor 594) cultured in growth media after one week of culture from closer point to the piezoelectric substrate (A) to furthest point from the substrate (D). Scale bar is 250μm.

CHAPTER 5: GENERAL DISCUSSION

Acoustofluidics has shown a great potential for the manipulation of bioparticles and cells, from cell separation, cell sorting and cell patterning to biosensing.[26,27] The nature of piezoelectric materials in converting electrical potentials into mechanical vibrations, provide several advantages for acoustic tweezers including preserved biocompatibility due to their contactless and gentle handling nature. Moreover, the principles of acoustic tweezers relying on acoustic radiation forces for particle and cell manipulation rather than changing the media configuration, *e.g.,* in dielectrophoresis, allow cells to maintain their biological environment and better preserve their viability. The versatility of acoustofluidics and acoustic tweezers rely on different factors including the ability to manipulate particles regardless of their geometrical, electrical, magnetic, or optical properties in different suspension media (*e.g.*, complete growth medium, serum-free medium, differentiation medium, DI water, and hydrogels), and the simple, reusable, and easy integrability nature of these platforms, being compatible with well-established microfabrication techniques. As outlined in Chapter 2, the goal of this study is to demonstrate that acoustofluidics-based platforms can be used as a safe and effective method for manipulating and patterning cells in different media conditions.

This study therefore proposes a Standing Surface Acoustic Wave (SSAW)-platform for high-resolution and contactless cell manipulation in culture media and a hydrogel solution. A methacrylated collagen type I (PhotoCol®-LAP) hydrogel was selected to preserve the cell patterns due to its capability of being UV-crosslinked within minutes and being retrievable from the culture channel as a tissue patch. To fulfill the first objective of this study, the design and fabrication of an acoustofluidics platform for cell patterning, we proposed and tested different culture chambers and interdigitated transducer configurations using both polystyrene particles and cells. We experimentally optimized the design of the acoustofluidics platform using two configurations of IDTs creating pressure nodes for cells to orientate and aggregate. The first design included two pairs of orthogonal IDTs deposited at 45° from the X-propagating direction to form a mesh-like pressure nodal distribution, while the second configuration comprised of one pair of mirrored IDTs parallel to the X-propagating direction, thus generating parallel pressure nodal lines. The orientation of the IDTs on the piezoelectric substrate highly influenced the efficiency of

patterning as evidenced by the number of cells guided towards the pressure node lines instead of resting in the antinode regions, where IDTs deposited in the same direction of the X-propagating direction led to stronger, more reproducible, and uniform cell linear patterns.[40] Therefore, by shifting the IDTs 45° to the X-propagating direction, waves propagated with less intensity as evidenced by a poor alignment of cells. Despite the preliminary results using polystyrene particles suspended in deionized water and the orthogonal IDT configuration for cell nodal agglomerates, the lower acoustic contrast factor of cells in growth media, did not lead to consistent cell aggregates that could be maintained over time. In contrast, when we placed the IDTs parallel to the X-propagating direction, SAWs transferred stronger and more efficiently through the piezoelectric substrate, thus leading to better and more reproducible results, where most cells that are initially in a random distribution are aligned more uniformly. Moreover, the effects of the acoustic working frequency and voltage on cell patterning optimization were also evaluated. The working frequency was experimentally selected based on both the speed of patterning and the stability of patterns over time. The theoretical frequency differed from the experimental working frequency due to physical phenomena in the culture medium, including microstreaming. The voltage was also experimentally selected based on how fast the particles are guided towards the pressure nodes, while limiting overheating problems in the platform. As expected, the velocity of cell patterning increased linearly with increasing voltage, where acoustic radiation forces (ARFs) push cells towards the pressure nodes more strongly. However, one of the challenges of using high voltages (>40V_{pp}), is the proportional square increase of the heat generated on the piezoelectric substrate, which can hinder cell viability. Another constraint of using high voltages is the presence of undesired microstreaming which prevented us from preserving pressure nodal lines for cells to aggregate and form strong cell-cell connections. However, we successfully demonstrated that heat effects on cell viability are negligible in our setup due to short SSAW exposure time which preserves high cell viabilities.

As part of our second objective, the evaluation of the platform for reproducible and stable cell patterns, different culture chambers were experimentally tested. These chambers included a square PDMS on a glass slide, a square glass-PDMS on a glass slide, a glass rectangular capillary tube, and a 9 × 2 well polymer μ-Slide (ibidi®). Standing waves leaked through the glass slide efficiently using a drop of water as our coupling layer; however, the high-viscosity of PDMS caused waves to dampen and did not allow SAWs to efficiently propagate inside the chamber. Glass capillary

tubes transferred waves more efficiently due to the low acoustic impedance of glass; however, long-term culture using this setup was challenging and retrievability of the patterns was not successful. Conversely, the μ-Slide (ibidi®) channel was simple, could pattern multiple cells in different wells, and could be maintained sterile throughout the experiment due to the chambered coverslip setup. Moreover, this setup enabled a rapid formation of linear patterns in <5 seconds for culture media and <1 min in a hydrogel solution with well-defined and reproducible linear nodes at a spacing of ~150μm ($\lambda_{SAW}/2$). The retrievability of the photo-cured cell patterns in hydrogel was also demonstrated using the μ-Slide channel, suggesting its potential to fabricate biomimetic tissue patches. Therefore, this channel was chosen to validate our platform for adipose-derived mesenchymal stem cells (ASCs) patterning and to study the effects of acoustic patterning on cell viability, metabolic activity, and differentiation potential of stem cells as part as our third objective.

With SSAWs being induced for <1 min, the viability of acoustically patterned ASCs in the methacrylated collagen type I hydrogel assayed for up to 48 hours, was preserved (>90% live cells). Cell-cell contacts were also improved in acoustically patterned cells, evidenced by elongated protrusions at the end of the cell membrane with a spreading-like morphology, being critical for cell communication, cell migration, and ultimately, tissue development.[94] Moreover, the metabolic activity of acoustically patterned cells in the hydrogel and the control group (random distribution of cells within the hydrogel) was assessed using growth media and differentiation media. Acoustically patterned cells in hydrogel cultured in growth media showed a statistically significant enhancement of their metabolic activity compared to the control group for days 7 and 14. These results thus suggest that by inducing cell-cell contacts, a higher cell proliferation is evidenced. However, acoustically patterned cells in hydrogel and the control group cultured in differentiation media, showed a different behavior. After day 7, both acoustically patterned cells and control groups cultured in differentiation media stopped their proliferation process, as evidenced by a constant metabolic activity via alamarBlue™, which has been previously reported to be correlated to the differentiation of stem cells.[100] Therefore, SSAWs do not seem to limit the functionality of stem cells with a similar trend for both control and patterned cells.

To confirm these results, the alkaline phosphatase activity, an early marker of osteogenic differentiation, was compared for both groups. Acoustically patterned cells and control groups

cultured in differentiation media showed a significant increase in the ALP activity after day 7, coinciding with the results obtained for metabolic activity. As ASCs start their differentiation process and change their phenotype, they stop proliferating. More interestingly, acoustically patterned samples significantly enhanced the ALP activity in comparison to the control group for days 7 and 14. These results thus suggest that acoustically patterned cells could experience a higher ALP activity due to induced cell-cell and cell-matrix contacts, which modulate the strength of adhesion and activate mechanosensitive signaling pathways that can influence the cell differentiation process.[2] Confocal fluorescent images were used to confirm the upregulation of osteocalcin, a bone-specific protein synthesized by osteoblasts, as a differentiation marker. At day 14, acoustically patterned cells showed a higher osteocalcin percentage signal than that of to the control group. These results thus evidenced the relevance of spatial patterning cells to study cell-cell behavior and functionality changes *in vitro*.

CHAPTER 6: CONCLUSIONS AND FUTURE PERSPECTIVE

This study presented the design and fabrication of a SSAW-based platform, its optimization for cell patterning in pressure nodes and pressure nodal lines, its validation using different cell lines suspended in media and hydrogel solutions, and finally the use of adipose-derived mesenchymal stem cells to study the effects of acoustic patterning on cell viability, metabolic activity, and osteogenic differentiation. The introduction of the working principles of surface acoustic waves for cell manipulation and cell patterning and its use in tissue engineering and cell functionality studies led to the hypothesis of this work, the fabrication of a rapid and contactless cell patterning method for the study of adipose-derived stem cells' proliferation and osteogenic differentiation. The preliminary work presented in this study helped us optimize the design and configuration of IDTs and culture chambers for the effective and reproducible patterning of different cell lines with proven preservation of cell viability after SSAW induction. These results led to the submitted manuscript article on ASCs patterning within a hydrogel solution that can be rapidly photo-cured to create tissue patches as a proof of concept of tissue regeneration.

It would be of interest, however, to further study the unique capabilities of acoustofluidics, and ultrasonic waves, for the reorganization of the native tissue architecture of heterotypic cell co-cultures, cell-cell interactions for organogenesis, changes in cell adhesion and migration over time, and the influence of SAWs on cellular phenotypes. We reported on the role of acoustic patterning for cell co-cultures using MDA-MB-231 and MCF-7. Therefore, by acoustically patterning two or more cell types in a controlled manner, for instance, adipose-derived stem cells and endothelial cells (HUVECS), angiogenesis could be induced. This platform would allow to better preserve the tissue constructs for long-term culture with a minimal interference to the cellular environment. Moreover, the miniaturization and flexibility of SAWs, acting as both actuators and sensors, could also allow to integrate manipulation and characterization modules in a single chip as a lab-on-a-chip device.[27] An ideal platform may be able to use SAW acoustophoresis to pattern endothelial cells and stem cells, where the detection of biomolecules (*e.g.,* VEGF proteins) could be detected by immobilizing corresponding binding-molecules on the substrate of a SAW sensing module.[103]

Conversely, most applications using SAWs only rely on a small range of operating frequencies, typically in the MHz region, therefore, it could be of interest to explore the effects of GHz,

particularly on cell phenotype changes. High-frequency (GHz) ultrasound waves have been reported to induce changes in neurite outgrowth and to accelerate the delivery of growth factors into cells,[104] ion channel stimulation for human neuromodulation,[105] nanoparticle enrichment for biosensing,[106] and the delivery of plasmid DNA through cell permeabilization (sonoporation).[107] Therefore, it would be of interest to use new methods and materials to explore higher frequencies, for example, implementing complementary oriented piezoelectric thin films.[108] Finally, research in the field of acoustofluidics should also focus on the standardization of fabrication methods for easy adaptation to fields such as biology and medicine, as they can significantly benefit from acoustic tweezers for single-cell analysis, cell-cell interactions, and cell migration studies, which are critical applications in biomedicine. Current limitations of acoustofluidics platforms, that should be addressed by miniaturizing these devices, include the integration of function generators, amplifiers, piezoelectric wafers, transducers, and signal processors into a compact all-in-one system. Owing to the biocompatible and flexible materials of acoustofluidics, it could be of interest to implant these devices inside the body or as wearable devices to deliver continuous, localized and high-frequency acoustic waves with minimal energy. New trends advocate for the integration of low-cost and portable imaging systems, such as smartphones, with acoustic micro-imaging techniques to revolutionize the field of PoC sensing.[109] As an example, smartphones can be integrated to acoustofluidics platforms for point of care testing,[110] where the digital input and output of acoustic biosensors facilitate both the activation and the electronic readout. Hence, a plethora of applications and opportunities in tissue engineering remains yet to be explored and to be developed.

CHAPTER 7: REFERENCES FROM MASTER'S THESIS

1. Guillotin, B. & Guillemot, F. Cell patterning technologies for organotypic tissue fabrication. *Trends Biotechnol.* **29**, 183–190 (2011).

2. Heller, E. & Fuchs, E. Tissue patterning and cellular mechanics. *J. Cell Biol.* **211**, 219 (2015).

3. Peerani, R. *et al.* Niche-mediated control of human embryonic stem cell self-renewal and differentiation. *EMBO J.* **26**, 4744–4755 (2007).

4. Nelson, C. M. Geometric control of tissue morphogenesis. *Biochim. Biophys. Acta - Mol. Cell Res.* **1793**, 903–910 (2009).

5. Wang, Z. *et al.* Single-cell patterning technology for biological applications. *Biomicrofluidics* **13**, (2019).

6. Jeger-Madiot, N. *et al.* Self-organization and culture of Mesenchymal Stem Cell spheroids in acoustic levitation. *Sci. Reports 2021 111* **11**, 1–8 (2021).

7. Cohen, S. *et al.* Large-scale acoustic-driven neuronal patterning and directed outgrowth. *Sci. Rep.* **10**, 1–11 (2020).

8. Kang, B. *et al.* High-resolution acoustophoretic 3D cell patterning to construct functional collateral cylindroids for ischemia therapy. *Nat. Commun.* **9**, (2018).

9. Friedl, P. & Mayor, R. Tuning Collective Cell Migration by Cell–Cell Junction Regulation. *Cold Spring Harb. Perspect. Biol.* **9**, (2017).

10. Dias, A. D., Unser, A. M., Kruger, U., Xie, Y. & Corr, D. T. Laser direct-write patterning influences early embryonic stem cell differentiation. *2015 41st Annu. Northeast Biomed. Eng. Conf. NEBEC 2015* (2015) doi:10.1109/NEBEC.2015.7117042.

11. McBeath, R., Pirone, D. M., Nelson, C. M., Bhadriraju, K. & Chen, C. S. Cell Shape, Cytoskeletal Tension, and RhoA Regulate Stem Cell Lineage Commitment. *Dev. Cell* **6**, 483–495 (2004).

12. Uto, K., Tsui, J. H., DeForest, C. A. & Kim, D. H. Dynamically Tunable Cell Culture

Platforms for Tissue Engineering and Mechanobiology. *Prog. Polym. Sci.* **65**, 53 (2017).

13. Otsuka, H. Micropatterning of cell aggregate in three dimension for in vivo mimicking cell culture. *Colloid Interface Sci. Pharm. Res. Dev.* 223–241 (2014) doi:10.1016/B978-0-444-62614-1.00011-9.

14. Nahmias, Y., Schwartz, R. E., Verfaillie, C. M. & Odde, D. J. Laser-guided direct writing for three-dimensional tissue engineering. *Biotechnol. Bioeng.* **92**, 129–136 (2005).

15. Grogan, S. P. *et al.* In Situ Tissue Engineering Using Magnetically Guided Three-Dimensional Cell Patterning. *Tissue Eng. Part C. Methods* **18**, 496 (2012).

16. Suzuki, M., Yasukawa, T., Shiku, H. & Matsue, T. Negative dielectrophoretic patterning with different cell types. *Biosens. Bioelectron.* **24**, 1043–1047 (2008).

17. Xu, T., Jin, J., Gregory, C., Hickman, J. J. & Boland, T. Inkjet printing of viable mammalian cells. *Biomaterials* **26**, 93–99 (2005).

18. Ozcelik, A. *et al.* Acoustic tweezers for the life sciences. *Nature Methods* vol. 15 1021–1028 (2018).

19. Tian, Z. *et al.* Generating multifunctional acoustic tweezers in Petri dishes for contactless, precise manipulation of bioparticles. *Sci. Adv.* **6**, (2020).

20. Xie, Y., Bachman, H. & Huang, T. Acoustofluidic methods in cell analysis. **117**, 280–290 (2019).

21. Stamp, M. E. M., Brugger, M. S., Wixforth, A. & Westerhausen, C. Acoustotaxis-: In vitro stimulation in a wound healing assay employing surface acoustic waves. *Biomater. Sci.* **4**, 1092–1099 (2016).

22. Ramesan, S., Rezk, A. R., Dekiwadia, C., Cortez-Jugo, C. & Yeo, L. Y. Acoustically-mediated intracellular delivery. *Nanoscale* **10**, 13165–13178 (2018).

23. Ahmed, H., Ramesan, S., Lee, L., Rezk, A. R. & Yeo, L. Y. On-Chip Generation of Vortical Flows for Microfluidic Centrifugation. *Small* 1903605 (2019) doi:10.1002/smll.201903605.

24. Meng, L. *et al.* Acoustic tweezers. *J Phys D Appl Phys* **52**, 273001 (2019).

25. Ozcelik, A. *et al.* Acoustic tweezers for the life sciences. *Nat. Methods* **15**, 1021–1028 (2018).

26. Ozcelik, A. & Huang, T. J. Acoustic Tweezers for Single-Cell Manipulation. *Handb. Single-Cell Technol.* 1051–1077 (2022) doi:10.1007/978-981-10-8953-4_40.

27. Gao, Y., Fajrial, A. K., Yang, T. & Ding, X. Emerging on-chip surface acoustic wave technology for small biomaterials manipulation and characterization. *Biomater. Sci.* **9**, 1574–1582 (2021).

28. Özer, M. B. & Çetin, B. An extended view for acoustofluidic particle manipulation: Scenarios for actuation modes and device resonance phenomenon for bulk-acoustic-wave devicesa). *J. Acoust. Soc. Am.* **149**, 2802 (2021).

29. Liu, Y. *et al.* Materials, Design, and Characteristics of Bulk Acoustic Wave Resonator: A Review. *Micromachines 2020, Vol. 11, Page 630* **11**, 630 (2020).

30. Rasouli, R. & Tabrizian, M. Rapid Formation of Multicellular Spheroids in Boundary-Driven Acoustic Microstreams. *Small* 2101931 (2021) doi:10.1002/SMLL.202101931.

31. Yeo, L. Y. & Friend, J. R. Surface acoustic wave microfluidics. *Annu. Rev. Fluid Mech.* **46**, 379–406 (2014).

32. Gao, Y., Li, Y. & Ding, X. Acoustofluidic technology for cell biophysics. *Micro Nano Syst. Biophys. Stud. Cells Small Org.* 153–171 (2021) doi:10.1016/B978-0-12-823990-2.00007-6.

33. Liu, S. *et al.* Investigation into the Effect of Acoustic Radiation Force and Acoustic Streaming on Particle Patterning in Acoustic Standing Wave Fields. *Sensors (Basel).* **17**, (2017).

34. Doinikov, A. A. Acoustic radiation pressure on a compressible sphere in a viscous fluid. *J. Fluid Mech.* **267**, 1–22 (1994).

35. Bruus, H. Acoustofluidics 7: The acoustic radiation force on small particles. *Lab Chip* **12**, 1014–1021 (2012).

36. Chen, K. *et al.* Rapid formation of size-controllable multicellular spheroids via {3D}

acoustic tweezers. *Lab Chip* 2636–2643 (2016) doi:10.1039/C6LC00444J.

37. Ding, X. *et al.* On-chip manipulation of single microparticles, cells, and organisms using surface acoustic waves. *Proc. Natl. Acad. Sci. U. S. A.* **109**, 11105–11109 (2012).

38. Guo, F. *et al.* Three-dimensional manipulation of single cells using surface acoustic waves. *Proc. Natl. Acad. Sci. U. S. A.* **113**, 1522–1527 (2016).

39. Collins, D. J. *et al.* Two-dimensional single-cell patterning with one cell per well driven by surface acoustic waves. *Nat. Commun.* **6**, 8686 (2015).

40. Zhang, P. *et al.* Contactless, programmable acoustofluidic manipulation of objects on water. *Lab Chip* **19**, 3397–3404 (2019).

41. Tian, Z. *et al.* Generating multifunctional acoustic tweezers in Petri dishes for contactless, precise manipulation of bioparticles. *Sci. Adv.* **6**, (2020).

42. Brugger, M. S. *et al.* Orchestrating cells on a chip: Employing surface acoustic waves towards the formation of neural networks. *Phys. Rev. E* **98**, 1–6 (2018).

43. Kang, B. *et al.* High-resolution acoustophoretic 3D cell patterning to construct functional collateral cylindroids for ischemia therapy. doi:10.1038/s41467-018-07823-5.

44. Naseer, S. M. *et al.* Surface acoustic waves induced micropatterning of cells in gelatin methacryloyl (GelMA) hydrogels. *Biofabrication* **9**, 015020 (2017).

45. Olofsson, K., Hammarström, B. & Wiklund, M. Ultrasonic based tissue modelling and engineering. *Micromachines* **9**, (2018).

46. Shi, J. *et al.* Acoustic tweezers: patterning cells and microparticles using standing surface acoustic waves (SSAW). *Lab Chip* **9**, 2890 (2009).

47. Guo, F. *et al.* Controlling cell-cell interactions using surface acoustic waves. doi:10.1073/pnas.1422068112.

48. Li, S. *et al.* Standing surface acoustic wave based cell coculture. *Anal. Chem.* **86**, 9853–9859 (2014).

49. Tao, X. *et al.* 3D patterning/manipulating microparticles and yeast cells using ZnO/Si thin

film surface acoustic waves. *Sensors Actuators, B Chem.* **299**, 126991 (2019).

50. Ding, X. *et al.* Tunable patterning of microparticles and cells using standing surface acoustic waves. *Lab Chip* **12**, 2491–2497 (2012).

51. Kang, P. *et al.* Acoustic tweezers based on circular, slanted-finger interdigital transducers for dynamic manipulation of micro-objects. *Lab Chip* **20**, 987–994 (2020).

52. cohen, S. *et al.* Large-scale acoustic-driven neuronal patterning and directed outgrowth. doi:10.1038/s41598-020-60748-2.

53. Shi, J. *et al.* Acoustic tweezers: patterning cells and microparticles using standing surface acoustic waves (SSAW). *Lab Chip* (2009) doi:10.1039/B910595F.

54. Lata, J. P. *et al.* Surface Acoustic Waves Grant Superior Spatial Control of Cells Embedded in Hydrogel Fibers. (2016) doi:10.1002/adma.201602947.

55. Nguyen, T. D. *et al.* Large-Scale Fabrication of 3D Scaffold-Based Patterns of Microparticles and Breast Cancer Cells using Reusable Acoustofluidic Device. *Adv. Eng. Mater.* 2001377 (2021) doi:10.1002/adem.202001377.

56. Dalecki, D. & Hocking, D. C. Advancing Ultrasound Technologies for Tissue Engineering. doi:10.1007/978-981-287-470-2_28-1.

57. Olofsson, K., Carannante, V., Ohlin, M., Frisk, T. & on a Chip, K.-K. Acoustic formation of multicellular tumor spheroids enabling on-chip functional and structural imaging. *Lab Chip* (2018) doi:10.1039/C8LC00537K.

58. Lata, J. P. *et al.* Surface Acoustic Waves Grant Superior Spatial Control of Cells Embedded in Hydrogel Fibers. *Adv. Mater.* **28**, 8632–8638 (2016).

59. Hu, X. *et al.* On-chip hydrogel arrays individually encapsulating acoustic formed multicellular aggregates for high throughput drug testing. *Lab Chip* **20**, 2228–2236 (2020).

60. Wu, Y. *et al.* Acoustic assembly of cell spheroids in disposable capillaries. *Nanotechnology* **29**, 504006 (2018).

61. Guo, F. *et al.* Precise Manipulation and Patterning of Protein Crystals for Macromolecular

Crystallography Using Surface Acoustic Waves. *Small* **11**, 2733–2737 (2015).

62. Chen, B. *et al.* High-throughput acoustofluidic fabrication of tumor spheroids. *Lab Chip* **19**, 1755–1763 (2019).

63. Devendran, C., Carthew, J., Frith, J. E. & Neild, A. Cell Adhesion, Morphology, and Metabolism Variation via Acoustic Exposure within Microfluidic Cell Handling Systems. *Adv. Sci.* **6**, 1902326 (2019).

64. Greco, G. *et al.* Surface-Acoustic-Wave (SAW)-Driven Device for Dynamic Cell Cultures. (2018) doi:10.1021/acs.analchem.8b00972.

65. Peng, D. *et al.* Mechanisms and Applications of Neuromodulation Using Surface Acoustic Waves—A Mini-Review. *Frontiers in Neuroscience* vol. 15 27 (2021).

66. Brugger, M. S. *et al.* Vibration enhanced cell growth induced by surface acoustic waves as in vitro wound-healing model. *Proc. Natl. Acad. Sci. U. S. A.* **117**, 31603–31613 (2020).

67. Rosenblum, J. I., Gazes, M. I. & Greenberg, N. Surface acoustic wave patch therapy affects tissue oxygenation in ischemic feet. *Wounds* **26**, 301–305 (2014).

68. Lin, Z. *et al.* Non-invasive ultrasonic neuromodulation of neuronal excitability for treatment of epilepsy. *Issue 12 Theranostics* **10**, 5514–5526 (2020).

69. Miansari, M. *et al.* Inducing Mild Traumatic Brain Injury in C. elegans via Cavitation-Free Surface Acoustic Wave-Driven Ultrasonic Irradiation. *Sci. Rep.* **9**, 12775 (2019).

70. Sriphutkiat, Y., Kasetsirikul, S. & Zhou, Y. Formation of cell spheroids using Standing Surface Acoustic Wave (SSAW). *Int. J. Bioprinting* **4**, (2018).

71. Chen, B. *et al.* High-throughput acoustofluidic fabrication of tumor spheroids. *Lab Chip* (2019) doi:10.1039/C9LC00135B.

72. Heller, E. & Fuchs, E. Tissue patterning and cellular mechanics. *J. Cell Biol.* **211**, 219 (2015).

73. Devendran, C., Collins, D. J. & Neild, A. The role of channel height and actuation method on particle manipulation in surface acoustic wave (SAW)-driven microfluidic devices. *Microfluid. Nanofluidics* **26**, 1–14 (2022).

74. Jalal, J. & Leong, T. S. H. Microstreaming and Its Role in Applications: A Mini-Review. *Fluids 2018, Vol. 3, Page 93* **3**, 93 (2018).

75. Wang, Z. *et al.* Single-cell patterning technology for biological applications. *Biomicrofluidics* vol. 13 61502 (2019).

76. Armstrong, J. P. K. *et al.* Engineering Anisotropic Muscle Tissue using Acoustic Cell Patterning. *Adv. Mater.* **30**, 1802649 (2018).

77. Weber, G. F., Bjerke, M. A. & DeSimone, D. W. Integrins and cadherins join forces to form adhesive networks. *J. Cell Sci.* **124**, 1183 (2011).

78. Vadivelu, R. K., Kamble, H., Shiddiky, M. J. A. & Nguyen, N. T. Microfluidic Technology for the Generation of Cell Spheroids and Their Applications. *Micromachines 2017, Vol. 8, Page 94* **8**, 94 (2017).

79. Scemes, E., Suadicani, S. O., Dahl, G. & Spray, D. C. Connexin and pannexin mediated cell—cell communication. *Neuron Glia Biol.* **3**, 199 (2007).

80. Jing, P. *et al.* Optical tweezers system for live stem cell organization at the single-cell level. *Biomed. Opt. Express* **9**, 771 (2018).

81. Ozcelik, A. *et al.* Acoustic tweezers for the life sciences. *Nat. Methods* **15**, 1021–1028 (2018).

82. Ding, X. *et al.* Surface acoustic wave microfluidics. *Lab Chip* **13**, 3626–3649 (2013).

83. Hess, P. Surface Acoustic Waves in Materials Science. *Phys. Today* **55**, 42 (2007).

84. Vanneste, J. & Bühler, O. Streaming by leaky surface acoustic waves. *Proc. R. Soc. A Math. Phys. Eng. Sci.* **467**, 1779–1800 (2011).

85. Tinevez, J. Y. *et al.* TrackMate: An open and extensible platform for single-particle tracking. *Methods* **115**, 80–90 (2017).

86. Greco, G. *et al.* Surface-Acoustic-Wave (SAW)-Driven Device for Dynamic Cell Cultures. *Anal. Chem.* **90**, 7450–7457 (2018).

87. Yarmolenko, P. S. *et al.* Thresholds for thermal damage to normal tissues: An update. *Int.*

J. Hyperth. **27**, 320–343 (2011).

88. Ding, X. *et al.* Surface acoustic wave microfluidics. *Lab Chip* **13**, 3626 (2013).

89. Ikada, Y. Challenges in tissue engineering. *J. R. Soc. Interface* **3**, 589–601 (2006).

90. Zamanian, B. *et al.* Interface-Directed Self-Assembly of Cell-Laden Microgels. *Small* **6**, 937–944 (2010).

91. Wang, Y., Han, C. & Mei, D. Standing Surface Acoustic Wave-Assisted Fabrication of Region-Selective Microstructures via User-Defined Waveguides. *Langmuir* **35**, 11225–11231 (2019).

92. Lin, R. Z., Chen, Y. C., Moreno-Luna, R., Khademhosseini, A. & Melero-Martin, J. M. Transdermal regulation of vascular network bioengineering using a photopolymerizable methacrylated gelatin hydrogel. *Biomaterials* **34**, 6785–6796 (2013).

93. Sharifi, S., Sharifi, H., Akbari, A. & Chodosh, J. Systematic optimization of visible light-induced crosslinking conditions of gelatin methacryloyl (GelMA). *Sci. Reports 2021 111* **11**, 1–12 (2021).

94. Abbott, R. *et al.* The effects of substrate morphology by regulating pseudopods formation on cell directional alignment and migration. *J. Phys. D. Appl. Phys.* **55**, 105401 (2021).

95. Spurlin, J. W. & Nelson, C. M. Building branched tissue structures: from single cell guidance to coordinated construction. *Philos. Trans. R. Soc. B Biol. Sci.* **372**, (2017).

96. Friedl, P. & Mayor, R. Tuning Collective Cell Migration by Cell–Cell Junction Regulation. *Cold Spring Harb. Perspect. Biol.* **9**, (2017).

97. Nelson, C. M. *et al.* From the Cover: Emergent patterns of growth controlled by multicellular form and mechanics. *Proc. Natl. Acad. Sci. U. S. A.* **102**, 11594 (2005).

98. Jahan, K., Manickam, G., Tabrizian, M. & Murshed, M. In vitro and in vivo investigation of osteogenic properties of self-contained phosphate-releasing injectable purine-crosslinked chitosan-hydroxyapatite constructs. *Sci. Reports 2020 101* **10**, 1–17 (2020).

99. Hessle, L. *et al.* Tissue-nonspecific alkaline phosphatase and plasma cell membrane glycoprotein-1 are central antagonistic regulators of bone mineralization. *Proc. Natl.*

Acad. Sci. **99**, 9445–9449 (2002).

100. Karoichan, A., Baudequin, T., Al-Jallad, H. & Tabrizian, M. Encapsulation and differentiation of adipose-derived mesenchymal stem cells in a biomimetic purine cross-linked chitosan sponge. *J. Biomed. Mater. Res. Part A* **110**, 585–594 (2022).

101. Nakamura, A. *et al.* Osteocalcin Secretion as an Early Marker of In Vitro Osteogenic Differentiation of Rat Mesenchymal Stem Cells. *https://home.liebertpub.com/tec* **15**, 169–180 (2009).

102. Shen, C. J., Fu, J. & Chen, C. S. Patterning Cell and Tissue Function. *Cell. Mol. Bioeng. 2008 11* **1**, 15–23 (2008).

103. Kim, M., Iezzi, R., Shim, B. S. & Martin, D. C. Impedimetric biosensors for detecting vascular endothelial growth factor (VEGF) based on poly(3,4-ethylene dioxythiophene) (PEDOT)/gold nanoparticle (Au NP) composites. *Front. Chem.* **7**, 234 (2019).

104. He, S. *et al.* Ultra-rapid modulation of neurite outgrowth in a gigahertz acoustic streaming system. *Lab Chip* **21**, 1948–1955 (2021).

105. Balasubramanian, P. S., Singh, A., Xu, C. & Lal, A. GHz Ultrasonic Chip-Scale Device Induces Ion Channel Stimulation in Human Neural Cells. *Sci. Reports 2020 101* **10**, 1–20 (2020).

106. Cui, W., Mu, L., Duan, X., Pang, W. & Reed, M. A. Trapping of sub-100 nm nanoparticles using gigahertz acoustofluidic tweezers for biosensing applications. *Nanoscale* **11**, 14625–14634 (2019).

107. Zhang, Z. *et al.* Hypersonic Poration: A New Versatile Cell Poration Method to Enhance Cellular Uptake Using a Piezoelectric Nano-Electromechanical Device. *Small* **13**, 1–10 (2017).

108. Lu, R., Yang, Y., Link, S. & Gong, S. Enabling Higher Order Lamb Wave Acoustic Devices with Complementarily Oriented Piezoelectric Thin Films. *J. Microelectromechanical Syst.* **29**, 1332–1346 (2020).

109. Ozcan, A. Mobile phones democratize and cultivate next-generation imaging, diagnostics

and measurement tools. *Lab Chip* **14**, 3187–3194 (2014).

110. Zhang, L., Tian, Z., Bachman, H., Zhang, P. & Huang, T. J. A Cell-Phone-Based Acoustofluidic Platform for Quantitative Point-of-Care Testing. *ACS Nano* **14**, 3159–3169 (2020).

APPENDIX THESIS

Permission for using submitted manuscript in thesis/dissertations

(https://www.nature.com/nature-portfolio/reprints-and-permissions/permissions-requests).

Author reuse

Authors have the right to reuse their article's Version of Record, in whole or in part, in their own thesis. Additionally, they may reproduce and make available their thesis, including Springer Nature content, as required by their awarding academic institution.

Authors must properly cite the published article in their thesis according to current citation standards.

Material from: 'AUTHOR, TITLE, JOURNAL TITLE, published [YEAR], [publisher - as it appears on our copyright page]'

If you are any doubt about whether your intended re-use is covered, please contact journalpermissions@springernature.com for confirmation.